Institute of Thermoelectricity, Academy of Sciences and Ministry of Education and Science of Ukraine

Journal of THERMOELECTRICITY

International Research

Founded in December, 1993

published 6 times a year

No. 2 *2016*

Editorial Board

International Editorial Board

Founders – National Academy of Sciences, Ukraine
Institute of Thermoelectricity of National Academy of Sciences and Ministry of Education and Science of Ukraine

Certificate of state registration № КВ 15496-4068 ПР

Editorial office manager N. Kharbaka

Approved for printing by the Academic Council of Institute of Thermoelectricity of the National Academy of Sciences and Ministry of Education and Science, Ukraine

Address of editorial office:
Ukraine, 58002, Chernivtsi, General Post Office, P.O. Box 86.
Phone: +(380-372) 90 31 65.
Fax: +(380-3722) 4 19 17.
E-mail: jt@inst.cv.ua
http://www.jt.inst.cv.ua

Signed for publication 25.03.16. Format 70×108/16. Offset paper №1. Offset printing.
Printer's sheet 11.5. Publisher's signature 9.2. Circulation 400 copies. Order 5.

Printed from the layout original made by "Journal of Thermoelectricity" editorial board
in the printing house of "Bukrek" publishers,
10, Radischev Str., Chernivtsi, 58000, Ukraine

CONTENTS

O.N. Manyk, T.O. Manyk, V.R. Bilinsky-Slotylo

Yu.Fedkovych Chernivtsi National University
2, Kotsyubinsky str., Chernivtsi, 58012 Ukraine

ON THE CHEMICAL BOND OF POLYMORPHOUS IRON MODIFICATIONS

An integrated approach to studying new skutterudite-based thermoelectric materials which include iron was proposed. The operating model was chosen with regard to experimental information on the thermodynamic properties of the system, calculations of structural changes of polymorphous modifications, the force and energy characteristics of iron chemical bond which allows performance optimization of the resulting material.
Key words: chemical bond, force and energy characteristics, material science.

Introduction

The subject of creating new thermoelectric materials with a given complex of physical and chemical properties sets for material science a task of development of a theory which opens up an opportunity of well-founded solution of this problem from the standpoint of chemical bond.

Such materials must possess high electric conductivity and low thermal conductivity, as well as a complex of physical and chemical properties restricting the choice of initial components for their synthesis. On the one hand, the resulting materials must have a periodic structure for electronic waves whose wavelength is factors of ten greater than interatomic distances ($\lambda_{el} \sim 10^{-6}$ cm), while lattice vibrations have the wavelength ($\lambda_{sp} \sim 10^{-8}$ cm). This difference between λ_{el} and λ_{sp} allows creating in crystal lattice such inhomogeneities which would be efficient for phonon scattering and almost would not scatter electronic waves (would not reduce current carrier mobility). Such inhomogeneities are created by introduction of impurity atoms into the lattice or by formation of solid solutions based on chemical compounds which are crystallized in similar lattices, forming superlattices, i.e. periodic semiconductor structures.

Of key importance is development of methods for research of substances characterized by several polymorphous modifications, as well as semiconductor materials based on transient group elements of the periodic table to which iron refers. Skutterudite-based thermoelectric materials are crystallized in the structure of deformed perovskite AB_3 with a void in the centre of cluster of body-centered cubic lattice. One of the methods for optimization of thermoelectric characteristics of such material is to arrange metal atoms in these voids in order to form filled skutterudites. Atoms which fill the voids can act as donors or acceptors, as well as strong phonon scattering centres. Semiconductor materials of *n*- and *p*-type were obtained on the basis of $La_{0.9}Fe_3CoSb_{12}$, $Ce_{0.9}Fe_3CoSb_{12}$, $Ce_3Fe_xCo_{4-x}Sb_{12}$ antimonides [1 – 5]. How to perform optimization of thermoelectric properties in such materials? What is the dynamics of chemical bond formation? What is the nature of polymorphous transformations? How does valence change? The answers to these and the related questions can be found in the present paper which is dedicated to integrated consideration of structural peculiarities of iron chemical bond as the basic component of new materials. To solve this problem, the formalism of chemical bond theory must be combined with the models of melting theory, thermodynamics and statistical physics, elasticity theory and microscopic theory of crystal lattice. Such an approach allows explaining the nature of polymorphous transformations, the

dynamics of chemical bond formation, hence the properties of materials obtained on the basis of iron.

Models being developed must take into account different kinds of motion and interaction between atoms forming chemical bonds, which reflect dependence of thermodynamic functions on the kinds of motion and interaction, as well as the dynamics of chemical bonds formation in transition from liquid into solid state and vice versa (first-order phase transitions), reflect the dynamics of polymorphous transformations both in liquid and solid state (second-order phase transitions).

In this connection, the present paper is a generalization of the methods of vibrational melting theory with regard to vibrational and precession-rotational kinds of motion of atoms forming chemical bonds in the approximation of anharmonic oscillator model. The contribution of precession-rotational motion was estimated by solving the inverse problem through comparison of calculated results to the experimental values of the temperature dependence of heat capacity and generalization of statistical models.

Chemical bond and statistical models

Analyzing the properties of iron, it is noteworthy to mention the polymorphism of this element responsible for its thermal treatment in the absence of which iron as the basis for steel and many other materials would not have gained such a wide acceptance. Up to temperature 912 °C iron exists in α - modification with body-centered cubic crystal lattice, at higher temperature – in γ – modification with face-centered cubic crystal lattice, above 1394 °C the lattice type again changes for body-centered cubic one.

The mechanism and speed of polymorphous transformations are determined by the energy characteristics of the initial and final structures which depend on the type of chemical bond and the way of atoms arrangement in the structure.

Such representation of the element gives a chance to explain a number of its properties. However, creation of new materials on the basis of iron calls for additional information on the mechanisms of chemical bond formation, since it can result in creation of both *n*- and *p*-type material.

Unlike common methods of structural chemistry [6], when first the electron structure of atoms is considered, hybridization type is chosen, and then the results are compared to the experiment, here the inverse problem was solved, namely from the experimental data of x-ray structural analysis the coordinates of unit cell atoms were determined and spatial angles between the bond directions of atoms were found [7 – 9]. Hybrid functions of atoms, for instance, in the approximation of simplest *sp*-hybridization [7] were written in the form of a system of linear combinations of *s*- and p_x, p_y, p_z- orbitals, respectively:

$$\varphi_i = a_i + b_i p_x + c_i p_y + d_i p_z \,, \tag{1}$$

where a_i, b_i, c_i, d_i are expansion coefficients of hybrid orbitals.

If hybrid orbitals are represented in the general form (1), the angle between them Θ_{ij} is determined (as the angle between two vectors φ_i and φ_j) by condition [8]:

$$\cos\Theta_{ij} = -\frac{a_i \cdot a_j}{\sqrt{1-a_i^2}\cdot\sqrt{1-a_j^2}} \,. \tag{2}$$

The notation is the same as that in formula (1). By substituting numerical values of spatial angles Θ_{ij} into formula (2) and writing (2) for all possible values of *i* and *j* admitted by the task symmetry, we obtained a system of equations to find coefficients a_i. To find coefficients b_i, c_i, d_i, we used conditions for orthonormalization of functions:

$$\begin{cases} \left|\varphi_i\right|^2 = 1, \\ \left(\varphi_i \cdot \varphi_j\right) = 0. \end{cases} \tag{3}$$

By substituting into (3) all possible values of i and j and the earlier found values of coefficients a_i, a system of equations was obtained to find the unknown coefficients b_j, c_j, d_j, which in turn allowed finding the electron density distribution between atoms corresponding to real interatomic distances and the angles between bond directions. This information allows reducing the degree of secular equations in the calculation of band structure of substance under study. In a similar way, *p*-, *d*-, *f*-shells are taken into account. The thus constructed real model of iron made it possible to take account of the shortest interatomic distances of iron which do not correspond to the shortest interatomic distances of ideal lattices. The schematic of interatomic distances and chemical bonds of ideal and real BBC lattice of α-*Fe* and FCC lattice of γ-*Fe* is given in Fig. 1, 2.

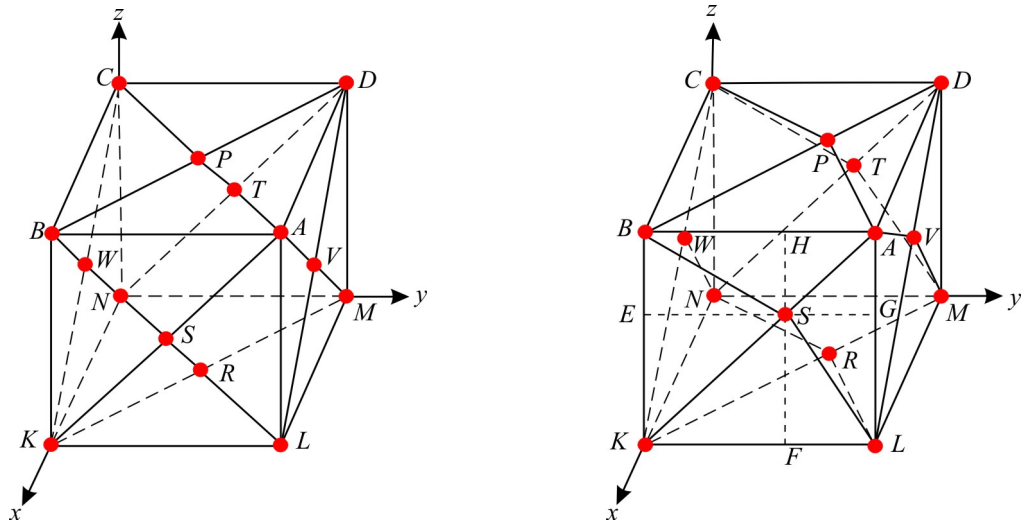

a) *b*)

Fig. 1. Schematic of interatomic distances and chemical bonds of the first and second neighbours: a) ideal FCC lattice of iron; b) real FCC lattice of iron (first neighbours – $r_1 = SA$, $r_2 = SB$, $r_3 = SL$, $r_4 = SK$ and second neighbours, $r_5 = 2{\cdot}SH$, $r_6 = 2{\cdot}SG$, $r_7 = AB$, $r_8 = 2{\cdot}SE$, $r_9 = 2{\cdot}SF$).

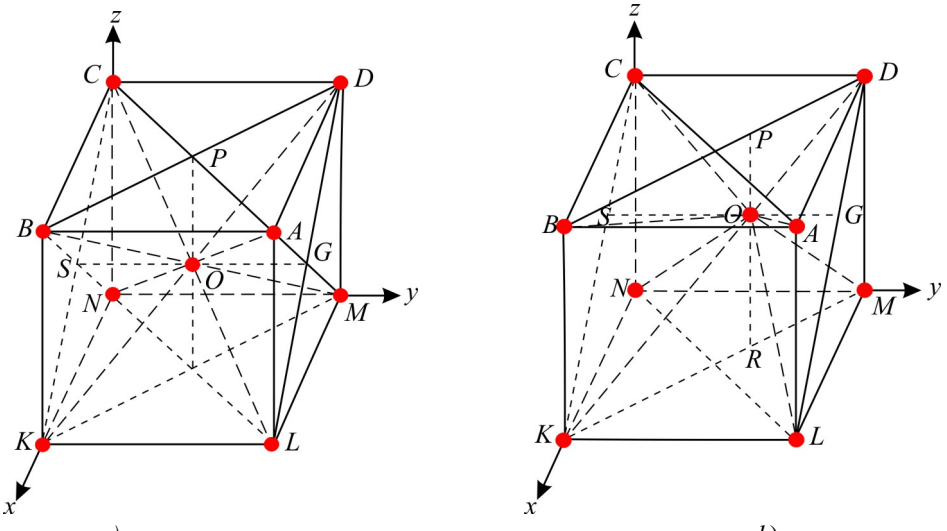

a) *b*)

Fig.2. Schematic of interatomic distances and chemical bonds of the first and second neighbours: a) ideal BCC-lattice of iron; b) real BCC-lattice of iron (first neighbours – $r_1 = OD$, $r_2 = OM$, $r_3 = OL$, $r_4 = OC$, $r_5 = ON$, $r_6 = OK$ u second neighbours - $r_7 = 2{\cdot}OG$, $r_8 = AB$, $r_9 = 2{\cdot}OS$, $r_{10} = 2{\cdot}OP$, $r_{11} = 2{\cdot}OR$).

Estimation of the force constants of iron chemical bonds was made by method [10] with the use of experimental numerical values of elastic moduli [11]. In so doing, in the case of FCC-structure of γ-*Fe* account was taken of 9 nonequivalent distances, and in the case of BCC α-*Fe* - 11 interatomic distances, and the force constants are given in Tables 1 and 2, respectively.

To predict possible peculiarities of behaviour of studied iron modifications in the processes of melting, crystallization, polymorphous transformations, one must have the energy parameters that characterize chemical bonds. In our case these are characteristic frequencies of atomic vibrations along chemical bonds described by nonequivalent hybrid orbitals.

The problem of finding characteristic frequencies was solved by vibrational theory method [12]. In solving it, the initial equations were used for the kinetic and potential vibrational energy as the quadratic function of velocities and coordinates on which basis the equations of vibrational motion took place.

In the case of FCC-structure, calculation of characteristic frequencies reduced to solving 9-th order secular equations, and in the case of BCC-structure -11-th order equations. The results of these calculations are given in Tables 1 and 2.

Table 1

Interatomic distances, force and energy characteristics of γ-Fe chemical bond

Parameters i	r_i, Å	f_i, N/m	$\omega_i \cdot 10^{13}$, s^{-1}	T_i, K
1	2.41	75	5.7	1652
2	2.508	69.25	5.47	1584
3	2.6458	62.23	5.18	1501.8
4	2.7354	58.2	5.012	1452.62
5	3.3092	39.8	4.14	1200.7
6	3.50448	35.56	3.917	1135
7	3.637	32,93	3.77	1092.52
8	3.76952	30.65	3.64	1054
9	3.9648	27.7	3.46	1002

Table 2

Interatomic distances, force and energy characteristics of α-F chemical bond

Parameters i	r_i, Å	f_i, N/m	$\omega_i \cdot 10^{13}$, s^{-1}	T_i, K
1	2.41	54	4.8271	1400.9
2	2.435	52.9	4.8	1385.7
3	2.4598	51.8	4.73	1371.6
4	2.508	49.86	4.638	1346
5	2.532	48.9	4.59	1332.6
6	2.5559	47.857	4.54	1318
7	2.69831	43	4.3	1249.68
8	2.86645	38.08	4.05	1175.66
9	3.03459	34	3.83	1111.9
10	3.99394	19.6	2.9	843.54
11	4.1136	18.53	2.828	820.24

The above approach allowed solving a number of technological problems related to melting and crystallization of materials under study from the standpoint of chemical bond.

Thorough consideration has shown that melting process depends on the structure of crystalline bodies, and the variety of crystal chemical properties causes the ambiguity of melting laws [13 – 14]. When studying the relation between crystal structure and melting we should describe as fully as possible crystal structure, the melt, the methods and models describing transition from the solid to liquid phase. In this connection, here we consider mathematical models enabling us to describe the character of motion Besides, this paper describes a model of rotator wherein at low temperatures there are harmonic vibrations, and with a rise in temperature the amplitude of these vibrations increases until the energy barrier is overcome which corresponds to minimum chemical bond energy of the most distant atoms described by nonequivalent hybrid orbitals (characterized by minimum bond energy).

From this moment on, polymorphous transformations start which are accompanied by changes in the structure and thermodynamic properties. In so doing, the radius of precession orbit which determines the value of rotary moment of atoms of nonequivalent orbital in question, hence the magnetic properties and parameters of domains is directly related to the results of calorimetric measurements. Thus, we get the opportunity to estimate the contribution to thermodynamic functions (in particular, to heat capacity, entropy, etc) due to increase in the inertia moment of oscillating rotator as compared to non-oscillating one, as well as the longitudinal extension of nonequivalent hybrid orbitals related to volume increase. The consistency of the values obtained by calculations of the inverse problem with the use of the results of calorimetric measurements confirms the correctness of molecular models serving the basis for statistical mechanics formulae.

The model of the Lindemann mechanical melting theory and corrections to model of rigid rotator and anharmonic oscillator

The instability of crystal lattices on heating is related to structural changes. Attempts of studying these changes which result in melting have brought about the advent of some theories that can be divided into 2 groups:

- theories which focus on the results of volume increase;
- theories which focus on crystal lattice vibrations.

The former are used in statistical thermodynamic models of volumetric expansion and enable us to relate the entropy of fusion of molecular crystals to the structure of molecules.

The latter come to conclusion that melting includes certain amplification of thermal motion. This idea first got a particular mathematical expression in the Lindemann's theory of vibration instability of crystal lattices leading to melting. Lindemann got the equation [13]:

$$T_{vibr} = c\nu_E^2 V_{\text{к}}^{\frac{2}{3}} M. \qquad (4)$$

It relates characteristic frequency ν_E in "ideal" crystal to vibration melting temperature T_{vibr}, molecular volume V_K and atomic mass M, C – contact. The results of estimating the temperatures of vibration melting of nonequivalent chemical bonds of α- and γ-*Fe* modifications are given in Tables 1, 2.

It was assumed that constant c has equal values for crystals of similar structure and was calculated by the melting temperature of a single substance.

However, the deviations of the Lindemann parameter values were considerable even in the case of simple metals. The initial model prevented from building a single-phase theory of vibration melting.

At the same time, the Lindemann model is very useful for finding "cooperative" dependences between different physical properties of solids related to T_{melt}. One of the reasons is that the energy of crystal positional disordering is closely related to reproducing forces acting at crystal lattice vibrations; any of these values can be used to describe other physical properties of crystal.

It is also noteworthy that loss of stability by certain types of crystal lattice vibrations is quite valid at polymorphous transformations leading to change in crystal structure. As long as melting mechanisms even in the simplest crystals can be different, and the relations $T_{melt} \geq T_{vibr}$ which determine the character of melting vary depending on the specific case, there is a need for "cooperative" realistic model.

Such a model must satisfactorily describe anharmonic effects in order to establish whether some kind of vibration mechanism can bring about melting process, leaving behind at certain pressure various thermodynamic disordering mechanisms.

Another peculiarity of this model lies in transition from quasi-crystalline quasi-liquid state of the system which is characterized by vibrational precession-rotational, rotational and translation motion of microparticles; reflecting within the uniform treatment the relation of these motion types to thermodynamic characteristics of system in question, such as heat capacity, entropy, etc.

Creation of such a model requires a detailed consideration of the prime postulates of the theory from the standpoint of chemical bond. Thus, construction of a realistic model leads to generalization of versatile experimental information on the properties of physics and chemical system, calculations of structural changes, power and energy characteristics of chemical bond, and later, by solving the inverse problems of the system of thermodynamic equations, enables one to calculate process parameters of resulting materials, which in turn leads to development of information-energy approach which allows changing characteristics of the resulting material in the right direction.

In this connection, formula (4) is convenient to find the dependence between physical properties related to temperature of destruction of individual chemical bonds.

Research on the mechanisms of interaction between atoms, molecules and other elementary systems [15] have found that volume change must become apparent, first, in the change of dipole moment of molecules by the value $\Delta P = \alpha F$, where α is their polarizability (including electron component apart from the ion), second, in frequency reduction of intramolecular vibrations of ions in molecules by certain value proportional to local field intensity F being a measure of that part of bonding energy between molecules which corresponds to their dipole interaction. This reduction of frequency v can be calculated, if we know anharmonicity coefficient g in the expression for energy taking into account the contribution of anharmonic oscillations to thermodynamic properties [15]:

$$\Delta U = \frac{1}{2} fx^2 - \frac{1}{8} gx^3, \tag{5}$$

which determines the dependence of molecule potential energy on the change in its length x. Calculation of thermodynamic functions is a complicated task which reduces to calculation of statistical sums [16]. So, in this case various model approximations of Hamiltonians are used. Calculations of thermodynamic functions in the approximation of ideal gas are simplified considerably, but they do not reflect real interactions in materials under study.

Therefore, one has to sophisticate the models under consideration. One of the first such attempts was to calculate the partition function of harmonic single-dimensional oscillator that already took into account the elastic interaction between two particles. This model helped to establish the temperature dependence of frequency and to construct thermodynamic functions. However, it does not reflect the features of interactions in the system related to melting and crystallization processes.

In this model, molecule dissociation is impossible.

In the present paper, model sophistication was attained by taking into account the effect of anharmonicity caused by vibration rotational motion of atoms and with regard to dissociation energy on the formation of chemical bond of polymorphous iron modifications.

Calculation of classical rotational partition function was done in the approximation that nonequivalent orbitals form a solid, and the laws of classical mechanics are obeyed. The energy of such two-atom "molecule" is equal to the sum of energy of precession-rotational motion of atoms of mass m_A and m_B along circular orbits shown in Fig. 3 at a velocity of $\frac{d\varphi}{dt}$ and the rotational energy of molecule s in general at a velocity of $\frac{d\theta}{dt}$.

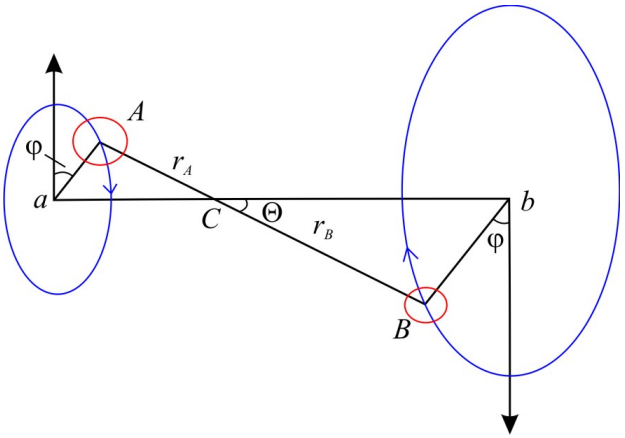

Fig. 3. Model of rigid rotator for the calculation of classical rotational partition function.

The expression for energy in this case will take on the form:

$$E = \frac{1}{2I}\left(P_\theta^2 + \frac{P_\varphi^2}{\sin^2\theta}\right), \tag{6}$$

where P_θ, P_φ are angular moments conjugate to angles θ and φ. I is moment of inertia of "molecule" under study.

With regard to (5) the expression for rotational partition function of a two-atom molecule is given by:

$$Z_{rot} = \frac{8\pi^2 IkT}{h^2}, \tag{7}$$

where k is the Boltzmann constant, and h is the Planck constant. General solution for molecules with three and more atoms is more sophisticated. In so doing, rotational energy is of the form:

$$\varepsilon_{rot} = \frac{P_a^2}{2I_a} + \frac{P_b^2}{2I_b} + \frac{P_c^2}{2I_c}, \tag{8}$$

where I_a, I_b, I_c are main moments of intertia along the *a, b, c* axes, and P_a, P_b, P_c are their respective components of the quantity of motion rotary moment.

Calculation of partition function in this case yields:

$$Z_{rot} = \frac{\sqrt{\pi}}{\sigma h^3}\left(8\pi^2 kT\right)^{\frac{3}{2}}\left(I_a I_b I_c\right)^{\frac{1}{2}}, \tag{9}$$

where σ is the number characterizing molecule symmetry.

It should be noted that when the levels of rotational energy are close and one can use continuous spectrum approximation, in this case quantum-mechanical rotational partition function coincides with classical, and it can be used for the calculations of heat capacity, entropy and some other thermodynamic functions. The above results describe well thermodynamic functions in certain temperature ranges. However, they do not take into account the increase in the moment of inertia of oscillating rotator as compared to rigid (nonoscillating), as well as longitudinal elongations of individual chemical bonds. In this connection, it is necessary to consider due additional corrections. Moreover, they do not describe melting and crystallization processes, since the above models disregard molecule dissociation.

In the present paper, the above drawbacks have been eliminated by taking into account corrections to the model of rigid rotator and harmonic oscillator.

It is not sufficient to consider oscillations of two-atomic molecule as single harmonic oscillations, since in this model dissociation is impossible. Morse [15] proposed the following potential function which fits the real situation better:

$$u(r) = D_c\left\{1-\exp\left[-\beta(r-r_c\right]\right\}^2, \tag{10}$$

where D_c is the energy of molecule dissociation; β is empirical constant; r is the distance between the nuclei of two atoms; r_c is its equilibrium value.

Expanding the exponent in equation (10) and restricting ourselves to the main summand in the expansion of potential energy for low vibration amplitudes, we find force F:

$$F = -2D_c\beta^2\left(r-r_c\right). \tag{11}$$

Equations of motion for two atoms with masses m_1 and m_2 separated by distances r_1 and r_2 from the centre of mass are given by:

$$\left.\begin{aligned} m_1\frac{d^2r_1}{dt^2} &= -2D_c\beta^2(r_1+r_2-r_c)\\ m_2\frac{d^2r_2}{dt^2} &= -2D_c\beta^2(r_1+r_2-r_c)\end{aligned}\right\}. \tag{12}$$

Adding the left and right sides of system (12) and introducing notation

$$r_1+r_2 = r\,u\,\frac{1}{m_1}+\frac{1}{m_2} = \frac{1}{\mu}, \tag{13}$$

we obtain

$$\mu\frac{d^2r}{dt^2} = -2D_c\beta^2(r-r_c). \tag{14}$$

Even if the reduced mass is affected by quasi-elastic force, the stiffness factor being equal to $-2D_c\beta^2$, this mass oscillates at a frequency:

$$v = \frac{1}{2\pi}\left(\frac{2\beta^2 D_c}{\mu}\right)^{\frac{1}{2}}. \tag{15}$$

Using the ratio $v = cw_c$, where c is light velocity, w_c is wave number for molecular vibration with respect to equilibrium position, we find the expression for empirical constant

$$\beta = w_c \left(\frac{2\pi\mu c^2}{D_c} \right)^{\frac{1}{2}}. \tag{16}$$

When the vibration amplitude of two-atomic molecule is increased, the model of simple harmonic oscillator becomes inapplicable for precise calculations and one has to take into account the contribution of anharmonic oscillations to thermodynamic properties. The vibration spectra of two-atom molecules are often empirically represented by the energy levels:

$$\varepsilon_n = hv_c \left(n + \frac{1}{2} \right) - x_c hv_c \left(n + \frac{1}{2} \right)^2 + y_c hv_c \left(n + \frac{1}{2} \right)^3, \tag{17}$$

where n is vibrational quantum number, and parameters x_c, y_c are referred to as anharmonic constants.

The substitution of Morse potential to Schrödinger equation yields the following approximate expression for allowed energy levels:

$$\varepsilon_n = hv_c \left(n + \frac{1}{2} \right) - \frac{(hv_c)}{4D_c} \left(n + \frac{1}{2} \right)^2. \tag{18}$$

Comparing (17) and (18) we get the expression for the anharmonic constant

$$\chi_e = \frac{hv_c}{4D_c} = \frac{hew_c}{4D_c}. \tag{19}$$

Taking into account (18) and introducing notation $hv_c = u$, the partition function for anharmonic oscillator can be written in the form:

$$\begin{aligned} Z_{анг} &= \sum_{n=0}^{\infty} \exp\left[-u\left(n + \frac{1}{2} \right) + ux_c \left(n + \frac{1}{2} \right)^2 \right] = \\ &= \sum_{n=0}^{\infty} \exp\left\{ \left(\frac{1}{4} x_c u - \frac{1}{2} u \right) + \left[-un + x_c un \left(n + \frac{1}{2} \right) \right] \right\}. \end{aligned} \tag{20}$$

By expanding exponential term in x_c and summing we obtain:

$$Z_{анг} = \frac{\exp\left(\frac{1}{4} x_c u - \frac{1}{2} u \right)}{1 - e^{-u}} \left[1 + \frac{2x_e u}{\left(e^u - 1 \right)^2} \right]. \tag{21}$$

Account of increase in the moment of inertia of oscillating rotator as compared to non-oscillating one (δ-summand), as well as of longitudinal elongation of nonequivalent hybrid orbitals (γ-summand) is done by adding to logarithm of the partition function of said summands:

$$\ln Z_\delta = \frac{\delta}{e^u - 1}, \quad \ln Z_\gamma = \frac{8\gamma}{u}, \tag{22}$$

where $\gamma = \frac{h}{8\pi^2 I w_c} = \frac{B_c}{w_c I}$ is the moment of inertia of atoms arranged on equilibrium distances corresponding to nonequivalent orbitals.

Considering that correction to energy and heat capacity is:

$$E_{corr} NkT \frac{d \ln Z_{corr}}{dT}, \quad \text{and} \quad C_{corr} = \left(\frac{dE_{corr}}{dT} \right), \tag{23}$$

we get the opportunity to take into account the influence of said effects on the process of chemical bond formation in materials under study.

The results obtained were used to specify the model of polymorphous transformations of α- and γ-*Fe* modifications from the standpoint of chemical bond, elasticity theory, thermodynamics and statistical physics, microscopic theory of mechanical and thermal properties of crystals.

In the case when system Hamiltonian was chosen in the approximation of a model of simple harmonic oscillator, thus taking into account only vibrational motion of atoms along nonequivalent chemical bonds, calculated values of heat capacity proved to be underrated compared to experimental ones. Hence, such a model did not reflect the entire complexity of interactions in the system. Taking into account, parallel with vibrational motion of atoms along nonequivalent chemical bonds, the precession-rotational motion of nonequivalent chemical bonds about their equilibrium positions permitted to explain the change in properties during polymorphous transformations, to relate magnetic moment value to radius of precession orbit, as well as to describe thermodynamic properties from the standpoint of chemical bonds and to explain the dynamics of system phase transitions from the solid to liquid state and vice versa.

Refinement of parameters of "cooperative" developed model was achieved as follows: analytical expressions were set up for thermodynamic functions in the approximation of developed model with regard to different kinds of motion, and corresponding equation systems were derived with the use of experimental values of thermodynamic functions. Solving this system for parameters (inverse problem) we found model parameters κ_e, w_e, δ and γ, given in Tables 3 and 4 (for α- and γ-*Fe*). The error in this case was found to be within ≤ 4 %.

Table 3

Corrections to models of rigid and harmonic oscillator γ-Fe

I	κ_e	w_e, cm^{-1}	B_e, cm^{-1}	Δ	γ
1.	$4.374 \cdot 10^{-2}$	1900	0.4155	$1.856 \cdot 10^{-2}$	$2.187 \cdot 10^{-4}$
2.	$4.197 \cdot 10^{-2}$	1823	0.3837	$1.657 \cdot 10^{-2}$	$2.1048 \cdot 10^{-4}$
3.	$3.975 \cdot 10^{-2}$	1726.7	0.3448	$1.57 \cdot 10^{-2}$	$1.997 \cdot 10^{-4}$
4.	$3.846 \cdot 10^{-2}$	1671	0.3225	$1.519 \cdot 10^{-2}$	$1.93 \cdot 10^{-4}$
5.	$3.177 \cdot 10^{-2}$	1380	0.2204	$1.256 \cdot 10^{-2}$	$1.597 \cdot 10^{-4}$
6.	$3.005 \cdot 10^{-2}$	1305.67	0.1965	$1.185 \cdot 10^{-2}$	$1.505 \cdot 10^{-4}$
7.	$2.893 \cdot 10^{-2}$	1256.67	0.1825	$1.143 \cdot 10^{-2}$	$1.452 \cdot 10^{-4}$
8.	$2.793 \cdot 10^{-2}$	1213.3	0.1698	$1.102 \cdot 10^{-2}$	$1.4 \cdot 10^{-4}$
9.	$2.655 \cdot 10^{-2}$	1153.3	0.1535	$1.048 \cdot 10^{-2}$	$1.33 \cdot 10^{-4}$

Table 4

Corrections to models of rigid and harmonic oscillator α-Fe

i	κ_e	w_e, cm^{-1}	B_e, cm^{-1}	δ	γ
1	$3.704\cdot10^{-2}$	1609	0.4155	$1.7\cdot10^{-2}$	$2.582\cdot10^{-4}$
2	$3.668\cdot10^{-2}$	1593.3	0.407	$1.683\cdot10^{-2}$	$2.554\cdot10^{-4}$
3	$3.63\cdot10^{-2}$	1576.7	0.3989	$1.666\cdot10^{-2}$	$2.53\cdot10^{-4}$
4	$3.559\cdot10^{-2}$	1546	0.3837	$1.634\cdot10^{-2}$	$2.482\cdot10^{-4}$
5	$3.522\cdot10^{-2}$	1530	0.3765	$1.6187\cdot10^{-2}$	$2.46\cdot10^{-4}$
6	$3.484\cdot10^{-2}$	1513.3	0.3694	$1.6033\cdot10^{-2}$	$2.44\cdot10^{-4}$
7	$3.3\cdot10^{-2}$	1433.3	0.3315	$1.5188\cdot10^{-2}$	$2.31\cdot10^{-4}$
8	$3.108\cdot10^{-2}$	1350	0.2938	$1.43\cdot10^{-2}$	$2.176\cdot10^{-4}$
9	$2.939\cdot10^{-2}$	1276.7	0.262	$1.35\cdot10^{-2}$	$2.052\cdot10^{-4}$
10	$2.225\cdot10^{-2}$	966.67	0.1508	$1.024\cdot10^{-2}$	$1.56\cdot10^{-4}$
11	$2.17\cdot10^{-2}$	942.67	0.1426	$1\cdot10^{-2}$	$1.51\cdot10^{-4}$

Analysis of anharmonic constants χ_e, δ, γ given in Tables 3 and 4 has shown that a relative correction for anharmonicity is responsible for the displacement of characteristic frequencies of nonequivalent hybrid orbitals (NHO). To estimate the value of displacement, characteristic frequencies ν_i, were presented by wave numbers w_i. In so doing, $cw_e = \nu_e$, where c is light velocity. Then according to [17] the displacement of characteristic frequencies (wave numbers Δw_e) of nonequivalent hybrid orbitals was estimated for α- and γ-*Fe*.

Fig. 4 and 5 show the dependences of χ_e, Δw_e, δ_e and γ_e on w_e All these dependences are characterized by the fact that anharmonic contacts and displacements of characteristic frequencies increase with w_e. For different NHO the values of anharmonic corrections differ, which is due to changes in motion form (vibrational, precession-rotational), as well as to deformation effects (extension, bend, shift). The influence of these components on the force and energy characteristics of different NHO makes it possible to establish the dynamics of chemical bond formation, which expands considerably technological opportunities of creating new iron based materials.

Fig. 4 and 5 show the dependences of model parameters on the type of NHO.

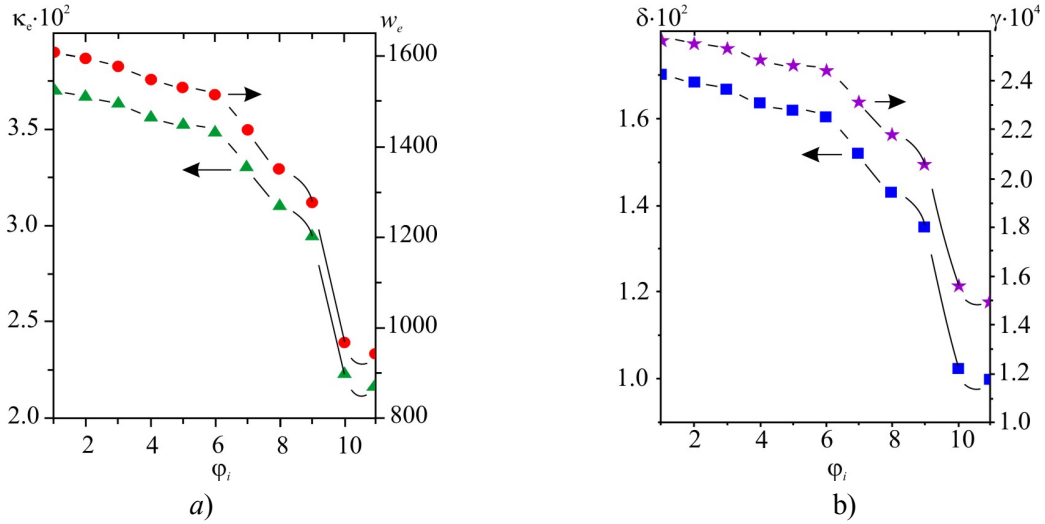

Fig. 4. Dependence of κ_e, w, δ and γ on the NHO type of α-Fe.

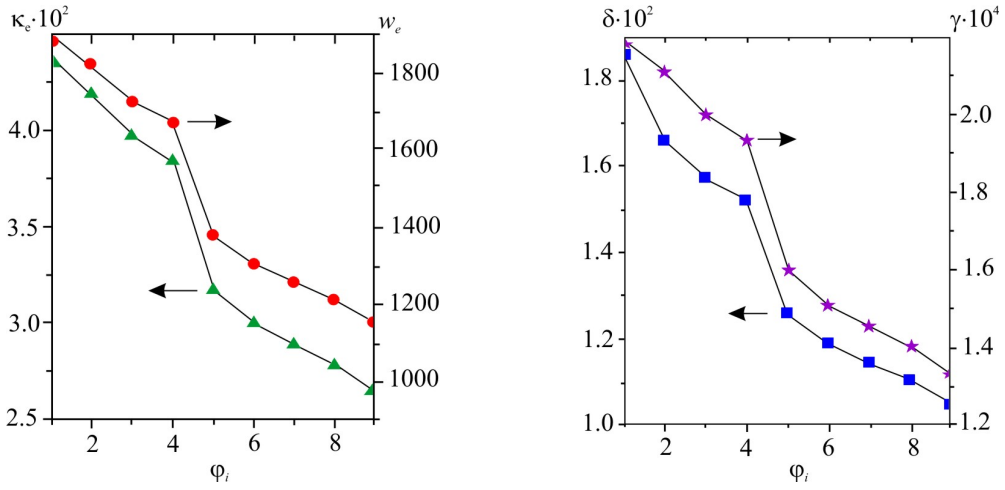

a) b)

Fig. 5. Dependence of κ_e, w, δ and γ on the NHO type of γ-Fe.

The results obtained allow tracing the dynamics of each NHO at polymorphous transformations of α- and *γ-Fe*.

Conclusions

1. An integrated approach to studying new skutterudite-based thermoelectric materials which include iron was proposed with regard to formalism of chemical bond theory, peculiarities of melting theory models, thermodynamics and statistical physics, crystal lattice theory.
2. A molecular model was developed with regard to vibrational motion of atoms along nonequivalent chemical bonds and precession-rotational motion of nonequivalent chemical bonds themselves, and their dissociation energy.
3. Calculations of the force and energy characteristics of chemical bonds of polymorphous iron modifications as the basic components of new thermoelectric materials based on skutterudites were made. "Thin" melting and crystallization structure of this element was revealed.
4. A correlation between polymorphous iron transformations and valence change, as well as processes of chemical bond formation in *n*- and *p*-type thermoelectric materials which include iron was established. The results obtained make it possible to find out the dynamics of chemical bond formation of materials under study.

References

1. D.J.Braun, W. Jeitschko, Preparation and Structural Investigations of Antimonides with the $LaFe_4P_{12}$ Structure, *J. Less-Common Met*. 72, 147 – 156 (1980).
2. D.J.Braun, W. Jeitschko, Ternary Arsenides with $LaFe_4P_{12}$-type Structure, *J. Solid State Chem*. 32, 357 – 363 (1980).
3. D.J.Braun, W. Jeitschko, Thorium-Containing Pnictides with the $LaFe_4P_{12}$ Structure, *J.Less-Common Met*. 76, 33 – 40 (1980).
4. G.S. Nolas, T.M. Tritt, Skutterudites: A Phonon-Glass-Electron Crystal Advanced Thermoelectric Energy Conversion Applications, *Annu. Rev. Mater. Sci*. 29, 89 – 116 (1999).
5. C.Uher, Prospective Novel Thermoelectrics, *Semicond. Semimetals* 69, 139 – 253 (2000).
6. G.Krebs, The Fundamentals of Crystal Chemistry of Inorganic Compounds (Moscow: Mir, 1971), 304p.

7. A.A.Ascheulov, O.N.Manik, T.O.Manik, and V.R.Bilinsky-Slotylo, Molecular Model and Chemical Bond of Tellurium, *Tekhnologiya i Konstruirovanie v Elektronnoi Apparature* **89**(5 – 6), 46 – 50 (2010).
8. A.A.Ascheulov, O.N.Manik, T.O.Manik, and V.R.Bilinsky-Slotylo, Peculiarities of Tellurium Chemical Bond, *Physics and Chemistry of Solid State* **12**(2), 389 – 394 (2011).
9. O.M. Manik, I.V. Gutsul, T.O. Manik, A.I. Savchuk, V.R. Bilinsky-Slotylo, Structure-Energy Peculiarities of *Se*, *Te*, *Sb* and *Fe* Chemical Bond, *J. Thermoelectricity* 3, 29 – 34 (2011).
10. A.A.Ascheulov, I.V. Gutsul, O.N.Manik, T.O.Manik, Optimization peculiarities of *CdSb* Based Material, *Sensor Electronics and Microsystem Technologies* **1**(2), 64 – 70 (2010).
11. N.E.Drits, *Properties of Elements* (Moscow: Metallurgiya, 1985), 672 p.
12. I.V.Gutsul, O.N.Manik, T.O.Manik, and V.R.Bilinsky-Slotylo, Research on the Concentration Dependences of the Power and Energy Characteristics of Crystals of *CdSb-ZnSb* Solid Solutions, *J.Thermoelectricity* 4, 35 – 39 (2010).
13. A.R.Ubbelode, *Molten State of Matter* (Moscow: Metallurgiya, 1982) 376 p.
14. A.A.Ascheulov, O.N.Manik, A.I.Savchuk, and V.R.Bilinsky-Slotylo, Research on the Structure and Chemical Bond of FeSe, *V Ukrainian Scientific Conference ob Physics of Semiconductors (Uzhhorod, October 9 – 15, 2011)*, P. 400.
15. *Problems on Thermodynamics and Statistical Physics, Ed. by P.Landsberg* (Moscow: Mir, 1974), 640 p.
16. Ya.I.Frenkel, *Kinetic Theory of Liquids* (Leningrad: Nauka, 1975), 592 p.
17. M.V.Volkenshtein, M.A.Elyashevich, and B.I.Stepanov, *Vibrations of Molecules* (Moscow-Leningrad: Gostekhteoretizdat, 1949; Moscow: Nauka, 1972).

Submitted 12.05.2016.

A.A. Nikolaeva[1, 2], L.A. Konopko[1, 2], K. Rogatskyi[2], V.G. Shepelevich[3], V.I. Prokoshin[3], S.V. Gusakova[3], P.P. Bodiul[4], R. Gritsko[4]

[1]D.Gitsu Institute of Electronic Engineering and Nanotechnologies
of the Academy of Sciences of Moldova,
Academiei str., 3/3, Kishinev, MD-2028, Republic of Moldova;
[2]International Laboratory of High Magnetic Fields and Low Temperatures,
ul. Gajowicka 95, Wroclaw, 53-421, Poland;
[3]Belarusian State University, 220030 Minsk, 4, Nezavisimosti av., Republic of Belarus;
[4]Technical University of Moldova, 168, Stefan cel Mare blvd., Kishinev, MD-2004,
Republic of Moldova

THERMOELECTRIC PROPERTIES OF FOILS OF SEMIMETAL AND SEMICONDUCTOR $Bi_{1-x}Sb_x$ ALLOYS

The behavior of the Seebeck coefficient α and power factor parameter $\alpha^2\sigma$ in foils of semimetal and semiconductor $Bi_{1-x}Sb_x$ alloys was investigated in the temperature range of 2.1 – 300 K. The $Bi_{1-x}Sb_x$ foils of thicknesses 15 – 30 μm were prepared by high-speed crystallization of a thin melt layer on the inner polished surface of a rotating copper cylinder, at a crystallization rate of ~ $5 \cdot 10^5$ m/s, to provide uniform distribution of the alloys components in the bulk. The concentration and mobility of charge carriers were determined by their Hall effect in the temperature range of 4.2 – 300 K. A comparison of the thermoelectric properties of the foils, single-crystal wires and bulk samples was conducted. It was shown that the power factor has maximum value in the 9 – 15 at. % Sb alloys in the foils, as well as in the wires and bulk samples; however, the peak position is shifted to higher temperatures in both the foils and the wires as compared with the bulk samples of similar composition. It was shown that it is reasonable to expect an increase in thermoelectric figure of merit ZT in foils of $Bi_{1-x}Sb_x$ semiconductor alloys only due to a decrease in the thermal conductivity caused by phonon scattering at grain boundaries which can be provided by variations in the structure and grain size of the foil.

Key words: semiconductor foil, topological insulator, Shubnikov-de Haas effect, power factor, thermoelectric figure of merit.

Introduction

The undying interest in $Bi_{1-x}Sb_x$ alloys is caused exceptionally by the unique physical properties related to reconstruction of *Bi* spectrum on addition of antimony to *Bi* and semimetal-semiconductor transitions ($0 < x < 0.04$), the existence of gapless state at $x \approx 0.04 – 0.07$ and semiconductor phase at $0.07 < x < 0.20$, as well as the use of $Bi_{1-x}Sb_x$ semiconductor alloys in thermoelectricity [1 – 4].

Earlier it was shown that the band structure of bulk (3D) $Bi_{1-x}Sb_x$ samples can vary depending on antimony content (x), temperature (T), pressure and tension, and the Fermi level can control a change in electron properties [5 – 7]. It is known that from a practical point of view the most important parameter which determines the properties of thermoelectric material is its

thermoelectric figure of merit. The thermoelectric figure of merit $ZT = \frac{|\alpha|^2 \sigma T}{\kappa_e + \kappa_p}$ which does not depend on sample size is determined by conductivity σ, the Seebeck coefficient (thermopower) α, electron κ_e and lattice thermal conductivity and absolute temperature *T*.

$Bi_{1-x}Sb_x$ alloys are the best low-temperature thermoelectric and magnetothermoelectric material, specifically for coolers and millivolt electronics [8]. There is a narrow range of choice of materials having thermoelectric, mechanical and other properties necessary for practical applications. Nowadays, increase in thermoelectric figure of merit *Z* is related to new phenomena, such as quantum size effect, the state of "topological insulator". Considerable recent attention focused on $Bi_{1-x}Sb_x$ alloys is caused by predicted thermoelectric figure of merit improvement due to quantum size effect in size-restricted structures [9], which stimulated a wealth of theoretical and experimental works [10 – 12] in this direction. Moreover $Bi_{1-x}Sb_x$ alloys in semiconductor concentration region with inverted spectrum [13] are topological insulators (TI) [14 – 16].

The first observation of surface states with a 2D-Dirac cone for TI was performed in the bulk samples of $Bi_{0.9}Sb_{0.1}$ alloys with the aid of high angle-resolved photoemission spectroscopy (ARPES) [17]. The class of materials identified as topological insulators is promising both in spintronics, quantum computers and thermoelectricity [15, 16, 18, 19]. The majority of works on $Bi_{1-x}Sb_x$ alloys are dedicated to study of films, wires and bulk samples [20 – 23]. In [19, 24], it is shown that high value of *ZT* in TI is achieved when chemical potential is arranged in the area of surface band gap.

The purpose of this paper was to study the thermoelectric properties of $Bi_{1-x}Sb_x$ foils in semimetal ($x < 0.4$) and semiconductor ($0.7 < x < 20$) phases where the properties of surface states must be realized. High crystallization rates in the manufacture of $Bi_{1-x}Sb_x$ foils assure a uniform distribution of *Sb* in the bulk of the foils. Analysis of experimental results was conducted to compare the thermoelectric figure of merit in the foils to that in the wires and the bulk samples of similar composition.

Samples and experimental procedure

The foils of $Bi_{1-x}Sb_x$ ($0 < x < 0.15$) alloys were obtained by high-speed crystallization of liquid-alloy droplet of proper composition on the internal polished surface of rotating copper cylinder (Fig. 1) [25, 26].

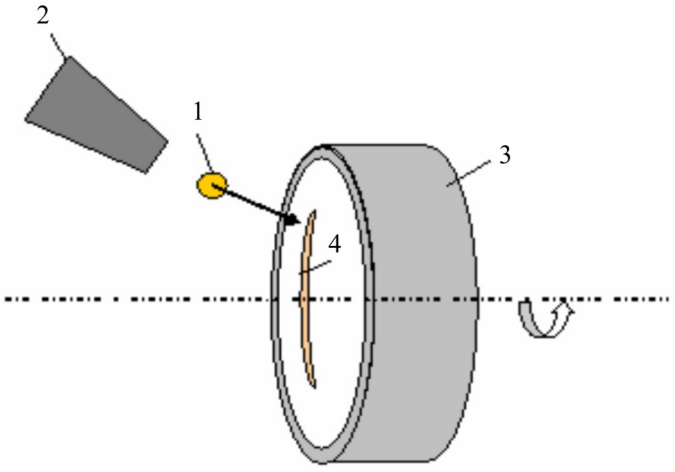

Fig. 1. Schematic of installation for manufacturing foils of $Bi_{1-x}Sb_x$ alloys.
1 – liquid-alloy droplet, 2 – ampoule with the melt, 3 – rotary crystallizer, 4 – foil.

Melt temperature was controlled by a thermocouple arranged in the furnace in the immediate vicinity of the melt and was assigned within 550 – 570 K. For homogenization of the melt the time of its holding in the furnace was 60 seconds.

It is known that at low and medium melt cooling rates of the above materials a dendritic segregation takes place which causes inhomogeneous splitting of components degrading the thermoelectric parameters of alloys [27]. Therefore, linear crystallizer velocity in the manufacture of $Bi_{1-x}Sb_x$ foils was 15 m/s. The thickness of studied foils was 15 – 50 μm. According to calculation, the liquid phase cooling rate was not less than 5·105 m/s. The microstructure of foils was studied with the use of scanning electron microscope LEO 1455 VP which has attachments for carrying out electron probe microanalysis. The texture of foils was studied by means of "inverse" pole figures, and pole density of diffraction lines was calculated by the Harris method [28]. X-ray diffraction studies were performed on DRON-3 diffractometer in copper radiation.

The foil surface A contacting to crystallizer is of specular form. However, there are micron-size caverns on it. On the opposite foil surface there are dimples and asperities. The cross-section of *Bi*-9 at. % *Bi* foil is represented in Fig. 2*a*. The distribution of bismuth and antimony concentration along the line shown in Fig. 2*b* testifies to homogeneous component distribution.

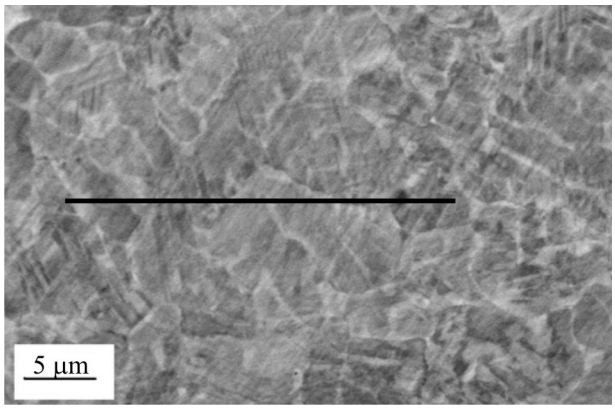

a)

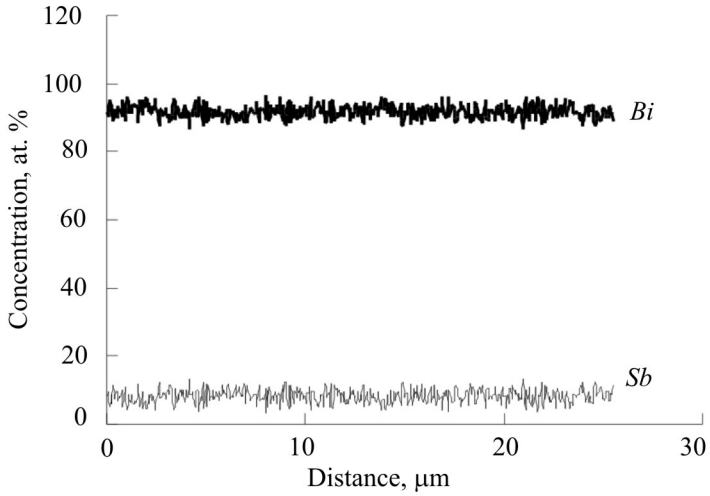

b)

Fig. 2. Microstructure of cross-section of fast-curing foil of Bi-9 at. % Sb alloy (a) and distribution of bismuth and antimony concentration along line (b).

In the fast-curing foil of *Bi*-9 at. % *Sb* the average grain size is 9 μm. Formation of microcrystalline structure is caused by considerable overcooling of liquid phase due to its high

cooling which leads to nucleation rate increase. In the fast-curing foil of the alloy there are twins of length 10 μm and thickness 0.4 μm.

The values of pole densities of foil diffraction lines of *Bi*-9 at. % *Sb* alloy for layers adjacent with surfaces *A* and *B* are characterized by diffraction lines, which points to formation of texture, i.e. grains are arranged with said planes parallel to foil surface, and symmetry axis C_3 coincides with normal to foil surface. Shift of crystallization front from surface *A* to *B* results in texture weakening.

Formation of texture is caused by orientation of covalent bonds in bismuth. Each bismuth atom has covalent bonds with the nearest neighbouring atoms. In so doing, two bonds of each atom are in planes, and the third covalent bond connects bismuth atoms in the neighbouring planes. At crystal-liquid interface which coincides with the above planes high density of active centres is formed as broken covalent bonds. They are accompanied by atoms from liquid forming an atomic step joined by other atoms. Owing to this, crystallization centres where interface coincides with considered planes and is perpendicular to heat flux grow at maximum rate and form the observed structure.

A four-contact method was used for comprehensive investigation of galvanomagnetic effects, Shubnikov-de Haas oscillations (SdH) in longitudinal ($H \parallel I$) and transverse ($H \perp I$) magnetic fields up to 14 T in the temperature range of $1.3 < T < 300$ K of $Bi_{1-x}Sb_x$ foils (Fig. 3).

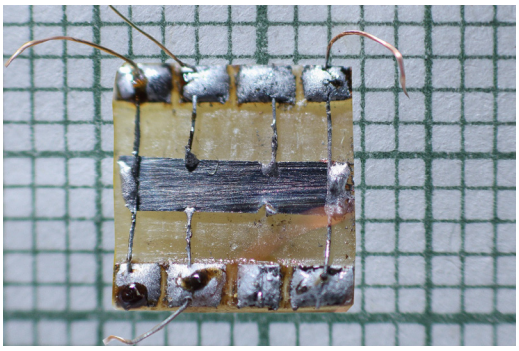

Fig. 3. Sample of $Bi_{1-x}Sb_x$ foil on the substrate of foil-clad paper-based laminate with soldered potential and Hall contacts.

SdH oscillations were observed only in *Bi*-3 at. % *Sb* foils on a derivative of magnetoresistance $\partial R/\partial H(H)$, when magnetic field is perpendicular to foil plane, i.e. parallel to trigonal axis C_3.

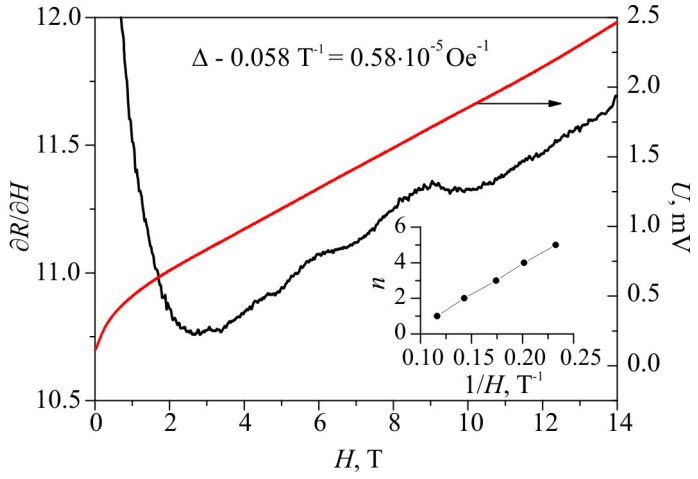

Fig. 4. Field dependences of signal of transverse magnetoresistance U(H)(mV), $H \perp I$ and derivative $\partial R/\partial H(H)$. The insert shows dependence of quantum number n of SdH oscillations on the reverse field 1/ H.

Fig. 4 represents dependences of magnetoresistance ($H \perp I$) and SdH oscillations of *Bi*-3 at. % *Sb* foil, confirming monocrystallicity and trigonal orientation in the direction perpendicular to foil plane.

The period of SdH oscillations $\Delta(1/H) = 0.58 \cdot 10^{-5}$ Oe^{-1} corresponds to the value obtained on the bulk samples of *Bi*-3 at. % *Sb* in the magnetic field direction along the C_3 axis [29] confirming preferable orientation of trigonal axis perpendicular to foil plane. The Hall effect and the temperature dependences of magnetoresistance in the temperature range of 2 – 300 K were measured on PPMS installation (Physical Property Measurement System).

The temperature dependences of resistance $R(T)$, thermopower $\alpha(T)$, the Hall effect $R_x(T)$ of $Bi_{1-x}Sb_x$ foils were studied in semimetal and semiconductor states.

Measurements in high magnetic fields at low temperatures were performed on PPMS installation in the International Laboratory of High Magnetic Fields and Low Temperatures (Poland, Wroclaw).

Results and discussion

The Hall effect was studied in semimetal *Bi*-3 at. % *Sb* foils in the temperature range of 2.1 – 300 K in magnetic fields up to 14 T on PPMS installation. The induction axis of a magnetic field was perpendicular to foil surface, i.e. parallel to C_3 axis.

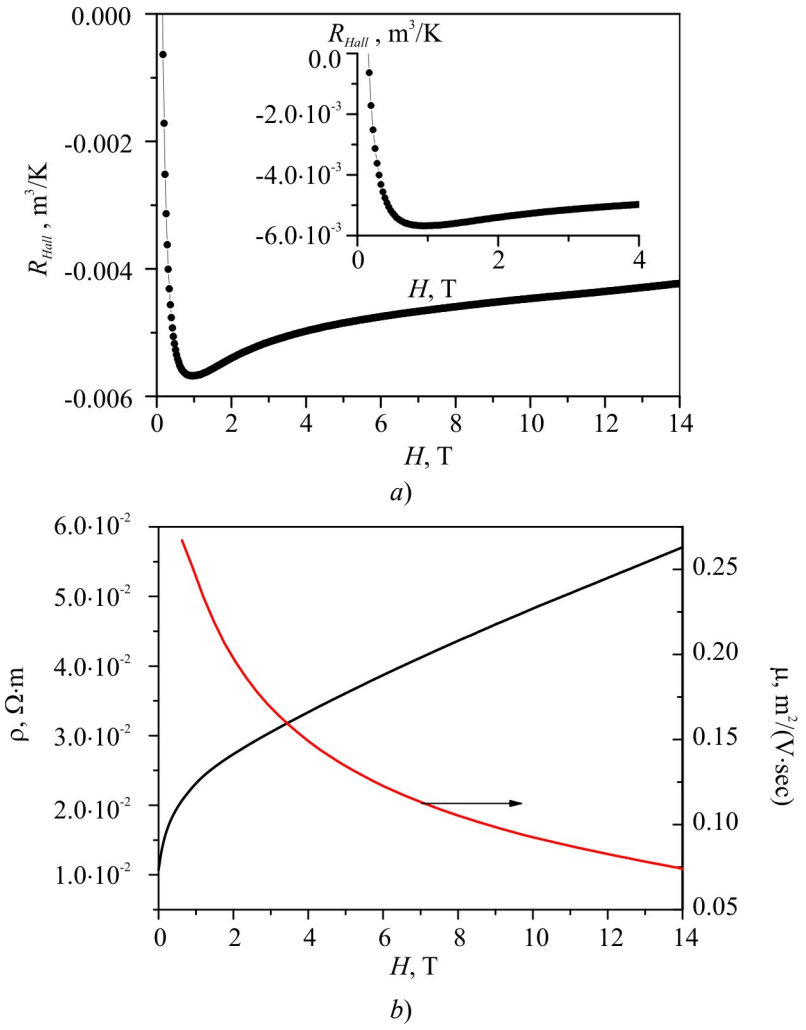

Fig. 5. Dependences of the Hall effect $R_{Hall}(H)$ (a) and resistivity $\rho(H)$ and charge carrier mobilities (b) on the magnetic field of Bi-3 at. % Sb foil sample, with d = 12.2 μm. On the insert: a) initial section of curve $R_{Hall}(H)$, T = 2.1 K.

Fig. 5 *a*, *b* shows dependences of the Hall effect and magnetoresistance for one pair of measuring contacts at 2 K of *Bi*-3 at. % *Sb* foil, 12 μm thick.

The sign of the Hall effect, just as that of thermopower, is negative, which corresponds to conductivity of electron current carriers in the entire temperature range. The dependences $R_{Hall}(H)$ and $\rho(H)$ shown in Fig. 5 *a*, b were used to estimate the concentration and the Hall mobility of charge carriers at 2 K.

The Hall coefficient was determined from the expression:

$$R_x = \frac{U_x}{I} \cdot \frac{d}{H}, \tag{1}$$

where U_x is the measured signal of the Hall effect, I is current through the sample, d is thickness. Carrier concentration n was determined from the expression:

$$R_H = \frac{A}{nec}, \tag{2}$$

where $A = 1.93$ at scattering on impurity ions, and in strong magnetic fields $A = 1$.

The Hall mobility was estimated from the formula:

$$\mu = R\sigma, \tag{3}$$

where σ is conductivity in a zero magnetic field.

$$\sigma = \frac{1}{U} \cdot \frac{l}{S}, \tag{4}$$

where l is the distance between potential probes.

As a result of calculation, the electron concentration $n = 3.1 \cdot 10^{15}$ cm^{-3} and the Hall concentration at 2 K is $\mu_n = 14^{20}$ cm^2/V·sec, decreasing with a rise in temperature by a factor of ≈ 6. In a magnetic field up to 14 T there was exponential mobility decrease by a factor of ≈ 4.

It should be noted that charge carrier mobility in semimetal single-crystal wires *Bi*-2 at. % *Sb* calculated at 3 K from Shubnikov-de Haas oscillations was 80000 ÷ 100000 cm^2/V·sec [30], which is much in excess of the values obtained on *Bi*-3 at. % *Sb* foil. A similar effect of charge carrier mobility decrease as compared to the bulk samples was observed in the foil of all compositions under study. A more detailed calculation of partial mobilities of electrons *L* and holes *T* will be given elsewhere.

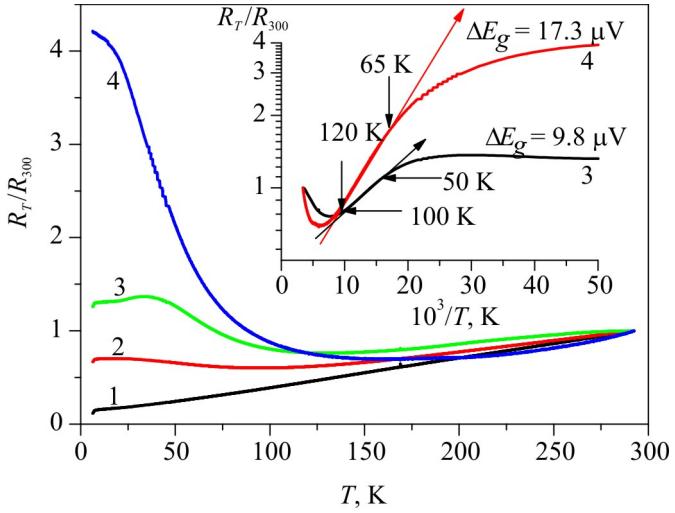

Fig. 6. Temperature dependences of relative resistance RT/R300(T) of $Bi_{1-x}Sb_x$ foils of various compositions. On the insert: dependences lgR(103/T).

Fig. 6 gives temperature dependences of resistance $R(T)$ of $Bi_{1-x}Sb_x$ foils of different compositions ($0 < x < 16$ at. % *Sb*). A can be seen from the figure, there is a distinct transition from the metal dependence of $R(T)$ for pure *Bi* to semiconductor dependence at $x = 0.09 \div 0.16$ *Sb*.

Curves 4, 5 have a linear section on dependences $\lg R(103/T)$ (insert in Fig. 6) which was used to determine the activation energy (energy gap width) for compositions *Bi*-9 at % *Sb*, *Bi*-16 at % *Sb*, that made 9.8 μV and 17.3 μV, respectively, which correlates fairly well with the data obtained on the bulk samples $Bi_{1-x}Sb_x$ of corresponding composition.

For comparison, Fig. 6 shows the temperature dependence of resistance $R(T)$ which we obtained on the bulk sample *Bi*-9 at % *Sb*. Unlike the dependence $R(T)$ obtained on the foil, the area of linear dependence in the bulk sample expands considerably to intrinsic range, which allows a more precise determination of the gap that made 8.5 μV.

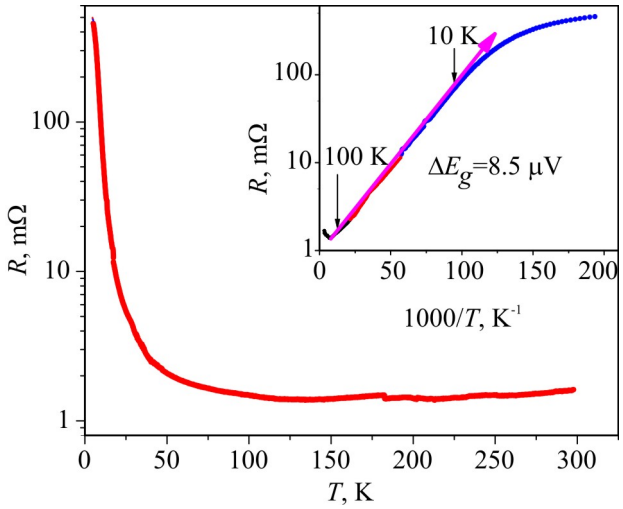

Fig. 7. Temperature dependence of resistance R(T) of the bulk sample Bi-9 at. % Sb. On the insert: dependence lgR(1000/T).

With a decrease in temperature from 300 to 3 K, the resistance of the bulk sample *Bi*-9 at. % *Sb* increased more than 2 orders of magnitude, whereas in the foil ($d = 27$ μm) of the same composition the resistance increased by a factor of 1.5.

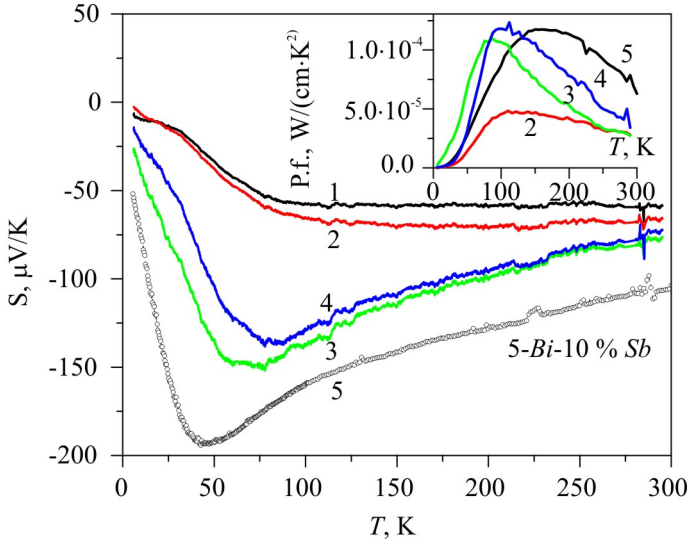

Fig. 8. Temperature dependences of thermopower of $Bi_{1-x}Sb_x$ foils. 1 – Bi, d = 15 μm, 2 – Bi-3 at. % Sb, d = 12 μm, 3 – Bi-9 at. % Sb, d = 27 μm, 4 – Bi-16 at. % Sb, d = 23 μm, 5 – Bi-10 at. % Sb wire, d = 1.8 μm. On the insert: temperature dependences of power factor P.f.(T).

Fig. 8 shows the temperature dependences of thermopower $\alpha(T)$ of $Bi_{1-x}Sb_x$ foils in the temperature range of 4.2 – 300 K. Just as in the bulk samples, maximum α values are achieved in the alloys 9 – 16 at. % *Sb* in the temperature range of 50 – 100 K, however, maximum absolute α values which make – 190 μV/K, are somewhat lower that in the bulk samples and single-crystal wires of similar composition (Fig. 8, curve 5).

With the use of experimental data for $\rho(T)$ and $\alpha(T)$ (Fig. 6, 8), the power factor P.f. = $|\alpha|^2\sigma$ was calculated for foils of all compositions under study (insert in Fig. 8). Maximum P.f. values are achieved in *Bi*-9 at. % *Sb* and *Bi*-16 at. % *Sb* foils in the temperature range of 90 – 150 K and make P.f. = $1\cdot10^{-4}$ W/cm·K^2 and $1.2\cdot10^{-4}$ W/cm·K^2. In *Bi*-3 at. % *Sb* foils maximum value is $5\cdot10^{-5}$ W/cm·K^2. For comparison, Fig. 8 shows the values obtained in *Bi*-10 at % *Sb* wires [31]. P.f. values in single-crystal wires *Bi*-10 at. % *Sb*, $d = 1.8$ μm are close to the values obtained in 9 ÷ 16 at. % *Sb* foil, however, the area of maximum values is considerably wider and shifted to high-temperature region (120 – 200 K). If we assume the values of thermal conductivity χ in foils to be the same as in the bulk samples of similar composition [32], for *Bi*-16 at. % *Sb* foil (with maximum power factor value), $\chi = 2.3\cdot10^{-2}$W/cm·K (at $T = 130 – 150$ K), we obtain $ZT = 0.6$, and for *Bi*-10 at. % *Sb* wires $ZT = 0.85$. Both values exceed ZT for the bulk samples of similar composition, which according to [32] is $ZT = 0.4$ at 80 K.

Analysis of P.f. dependences and estimation of ZT in foils, wires and bulk samples of $Bi_{1-x}Sb_x$ allows a conclusion that an improvement of thermoelectric figure of merit $ZT = \alpha^2\sigma/\chi$ in foils should be expected due to a decrease in thermal conductivity χ caused by phonon scattering at grain boundaries, which will result in ZT growth at $T > 100$ K.

Conclusions

The thermopower and resistance of semimetal and semiconductor foils based on $Bi_{1-x}Sb_x$ alloys of thickness 12 ÷ 30 μm, obtained by high-speed crystallization method in the temperature range of 2 K < T < 300 K were studied.

It was shown that charge carrier mobilities both at 4.2 K and 200 K are lower than in the bulk samples and single-crystal wires of similar composition.

It was established that power factor value of foils of semiconductor alloys $Bi_{1-x}Sb_x$ almost coincides with P.f. value in the wires and bulk samples, however, the area of maximum value is shifted toward higher-temperature region, and ZT values of semiconductor foil and $Bi_{1-x}Sb_x$ ($x > 0.09$) wires exceed ZT values in the bulk samples.

Estimates show that it is reasonable to expect increase in thermoelectric figure of merit in foils of $Bi_{1-x}Sb_x$ semiconductor alloys due to decrease in thermal conductivity caused by phonon scattering at grain boundaries in the range of $T > 100$ K.

This work was performed with support of Institutional project 15.817.02.09A.

References

1. W.M.Yim, A. Amith, Alloys for Magneto-Thermoelectric and Thermomagnetic Cooling. Solid-State Electronics 15(10), 1141 – 1165 (1972).
2. G.A.Ivanov, V.A.Kulikova, V.L.Naletov, A.F.Panarin, and A.R.Regel, Thermoelectric Figure of Merit of Pure and Doped Bismuth-Antimony Alloys in a Magnetic Field, Semiconductors 6(7), 1296 – 1299 (1972).

3. L.I.Anatychuk, Thermoelements and Thermoelectric Devices: Reference Book (Kyiv: Naukova Dumka, 1979), 768 p.
4. N.A.Rodionov, G.A.Ivanov, and N.A.Redko, Thermoelectric Figure of Merit of *p*-type $Bi_{1-x}Sb_x$ ($0.12 < x < 0.14$) Alloys at Low Temperatures, Physics of the Solid State 24(6), 1881 – 1884 (1982).
5. S.Golin, Band Model for Bismuth-Antimony Alloys, Phys. Rev. 176 (3), 830 (1968).
6. H.T.Chu and Yi-Han Kao, Shubnikov-de Haas Effect in Dilute Bismuth-Antimony Alloys. II. Quantum Oscillations in High Magnetic Fields, Phys.Rev.B 1(6), 2377 − 2384 (1970).
7. 7. B.Lenoir, A.Dauscher, M.Cassat, Yu.Ravich, and H. Sherrer, Effect of Antimony Content on the Thermoelectric Figure of Merit of $Bi_{1-x}Sb_x$ Alloys, J. Phys. Chem. Sol. 59, 129 (1998).
8. P.Jandl and U.Birkholz, Thermogalvanomagnetic Properties of *Sn*-doped $Bi_{95}Sb_5$ and its Application for Solid State Cooling, J. Appl. Phys. 76(11), 7351-7366 (1994).
9. L.D.Hicks and M.S.Dresselhaus, Thermoelectric Figure of Merit of a One-Dimensional Conductor, Phys. Rev. B 47, 16631 (1993).
10. Y.-M. Lin, S.Cronin, O.Rabin, J.Y.Ying, and M.Dresselhaus, Transport properties of $Bi_{1-x}Sb_x$ Alloy Nanowires Synthesized by Pressure Injection, Appl. Phys. Lett. 79, 677 – 679 (2001).
11. Y.-M. Lin, O.Rabin, S.Cronin, J.Y.Ying, and M. Dresselhaus, Semimetal-Semiconductor Transition in $Bi_{1-x}Sb_x$ Alloy Nanowires and Their Thermoelectric Properties, Appl. Phys. Lett. 81, 2403 – 2405 (2002).
12. O.Rabin, Y.-M. Lin, and. M. Dresselhaus, .Anomalously High Thermoelectric Figure of Merit in $Bi_{1-x}Sb_x$ Nanowires by Carrier Pocket Alignment, Appl. Phys. Lett. 79(1), 81 – 83 (2001).
13. N.B.Brandt, R.Muller, and Ya.G.Ponomarev, Study of the Law of Carriers Dispersion in Bismuth Doped with Acceptor-Type Impurities, JETF 71, 6(12), 2268 – 2277 (1976).
14. L.Fu, C.L. Kane, Superconducting Proximity Effect and Majorana Fermions at the Surface of a Topological Insulator, Phys. Rev. Lett. 100 (9), 96407 (2008).
15. X.L.Qi, R.Li, J.Zang, and S.C.Zhang, Inducing a Magnetic Monopole with Topological Surface States, Science, 323(5918), 1184 – 1187 (2009).
16. Dong-Xia Qu, Sarah K. Roberts, and George F. Chapline, Observation of Huge Surface Hole Mobility in the Topological Insulator Bi0.91Sb0.09 (111), Phys. Rev. Lett. 111, 176801 (2013).
17. D.Hsieh, D.Qian, L.Wray, Y.Xia, Y. S. Hor, R.J.Cava, and M.Z.Hasan, Nature 452 (7190), 970 − 974 (2008).
18. J.E.Moore, "The birth of topological insulators," Nature 464(7286), 194 – 198 (2010).
19. Shuang Tang and Mildred S. Dresselhaus, Electronic Phases, Band Gaps, and Band Overlaps of Bismuth Antimony Nanowires, Phys. Rev. B 89, 045424 (2014).
20. E.I. Rogacheva, A.A. Yakovleva, V.I. Pinegin, and M.S. Dresselhaus, Concentration Anomalies of Properties in *Bi-Sb* Semimetallic Solid Solutions, J. Physics and Chemistry of Solids 69(2 – 3), 580 – 584 (2008).
21. D.Partin, J.Heremans, D.Morelli, C.Thrush, C.Olk, and T.Perry, Growth and Characterization of Epitaxial Bismuth Films, Phys. Rev. B 38 (6), 3818 (1988).
22. Shuang Tang and Mildred Dresselhaus, Constructing Anisotropic Single-Dirac-Cones in $Bi_{1-x}Sb_x$ Thin Films, Nano Lett. 12(4) 2021 – 2026 (2012).
23. Albina A. Nikolaeva, Leonid A.Konopko, Tito E.Huber, Pavel P.Bodiul, and Ivan A.Popov, Prospects of Nanostructures $Bi_{1-x}Sb_x$ for Thermoelectricity, J. Solid State Chemistry 193, 71 – 75 (2012).
24. 24. Ryuji Takahashi and Shuichi Murakami, Thermoelectric Transport in Topological Insulators, Semicond. Sci. Technol. 27, 124005 (2012).

25. A.V.Demidchik, V.G.Shepelevich, Thermal Stability of *Bi*-*Sb* (8 – 12 at % *Sb*) Foils Prepared by Rapid Solidification, Inorganic Materials 40(4), 391 – 394 (2004).
26. V.A.Yarmolovich, S.V.Gusakova, V.I.Prokoshin, and V.G.Shepelevich, Structure Formation of *Bi*-9 at. % *Sb* System Alloys with High-Speed Crystallization, Priborostroyenie – 2013: Proc. of 6-th International Science and Technical Conference (Minsk, November 20 – 22, 2013), P. 401 – 403.
27. I.S.Miroshnichenko, Quenching from the Liquid State (Moscow: Metallurgiya, 1982).
28. A.A.Rusakov, X-Radiography of Metals (Moscow: Atomizdat, 1977).
29. K.F.Cuff, M.R.Ellett, R.B.Horst, and L.R.Williams, Shubnikov-de Haas Investigations of the $Bi_{1-x}Sb_x$ ($0 < x < 0.3$) System, Proc. of The International Conference on the Physics of Semiconductors (Kyoto, Japan, 1966), J. of the Physical Society of Japan 21, Supplement, 666 – 671 (1966).
30. A.Nikolaeva, L.Konopko, T.Huber, J.-P.Ansermet, P.Bodiul, and I.Popov, Magneto-Thermoelectric Properties and Quantum Oscillations in $Bi_{1-x}Sb_x$ Nanowires in Semimetal, Gapless and Semiconductor region, MRS Spring Meeting & Exhibit, April 6 – 10, 2015, San Francisco, California. Symposium S-Semiconductor Nanowires and Devices for Advanced Applications, Abstract S3.22.
31. P.P.Bodiul, E.F.Moloshnik, I.A.Popov, O.V.Botnar, and E.K.Istrate, Thermoelectric Properties of $Bi_{1-x}Sb_x$ ($0 \le x \le 0.12$) Wires as a Function of Diameter, Composition and Temperature, J.Thermoelectricity 1, 10 (2010).
32. N.A.Redko, Electron and Phonon Transport Phenomena in Semimetal and Semiconductor Bismuth-Antimony Alloys, Thesis for a Degree of Doctor of Physical and Mathematical Sciences (Saint-Petersburg, 1998).

Submitted 03.05.2016.

V.V. Antonyuk, I.M. Skrypskyi, M.M. Krechun

Institute of Thermoelectricity of the NAS and MES of Ukraine,
1, Nauky Str., Chernivtsi, 58029, Ukraine

EFFECT OF SURFACE PREPARATION ON MECHANICAL PROPERTIES OF CONTACTS OF ANTI-DIFFUSION STRUCTURES FOR TEM BASED ON BISMUTH TELLURIDE

Methods for cleaning contact surface of thermoelectric material (TEM) based on bismuth telluride by means of chemical and electrochemical etching and their combined use were analyzed. Comparative analysis of the effect of etchants on adhesion strength of interconnect layers was made. It was established that alternative chemical and electrochemical etching enables one to reach high values of adhesion strength of contact structures to thermoelectric material surface.
Key words: bismuth telluride, thermoelectric material.

Introduction

One of important steps in the manufacture of thermoelectric converters is creation of reliable anti-diffusion and connecting structures. Preliminary preparation of thermoelectric material surface is a prerequisite for obtaining high values of coating adhesion strength [1]. In turn, adhesion strength of interconnect layers depends on contact surface condition, in particular, the presence of a damaged layer, its thickness, compound, structure and properties [2]. In the process of cutting samples of solid solutions obtained by directional crystallization, deformation results in crystallite fragmentation (possibly due to formation of basic cracks), atomic plane bending and formation of polycrystalline areas on the cut surface. The depth of a damaged layer of samples of Bi_2Te_3-Sb_2Te_3, Bi_2Te_3-Bi_2Se_3 solid solutions is different and makes 20 – 30 and 10 – 20 μm, respectively. In extruded samples the thicknesses of these layers for both compositions are close to each other and make 3 – 5 grains, i.e. 10 – 15 μm [3]. The depth and composition of damaged layer on the surface of TEM legs changes contact resistance of transient structures. Metallization of thermoelectric legs allows reducing the value of transient contact resistance at metal-semiconductor interface and improving considerably the thermoelectric figure of merit of thermoelements. For obtaining reliable metal coatings on semiconductors of decisive importance is semiconductor surface condition which affects the interaction of atoms deposited with the surface which is coated.

Various methods are known [4, 5] of thermoelectric material surface treatment prior to deposition of contact layers: mechanical grinding and polishing, chemical and electrochemical etching and their combined alternative application.

Chemical etching lies in TEM surface treatment with mixtures of strong acids, aqueous solutions of salts of hexavalent chromium in the presence of nitric acids or with etchants which include halogens. Their use makes impossible precise thickness control of a layer being stripped.

Electrochemical etching is easy to use and enables one to control stripping speed. However, as practice shows and according to authors [6], electrochemical treatment alone is not enough to get a reliable adhesion of contact layers to TEM surface.

The purpose of the work is to study the effect of thermoelectric material surface preparation on adhesion strength of contact structures.

Experimental

Investigations of the depth of a damaged layer on the surface of bismuth telluride legs and its gradual stripping with the use of various methods and etchants were performed. The results of etching TEM surface were studied by means of scanning optical microscope NT-206.

Chemical etching. For both types of TEM a bichromate etchant $K_2Cr_2O_7$:HNO_3:H_2O (4:10:20) was investigated with different etching duration. As-etched discs were cleared in a solution of potassium hydroxide and tartaric acid, washed with dilute chlorous acid and distilled water in ultrasonic cleaning installation.

Electrochemical etching. For *n*- and *p*-type TEM etchants of different composition were used. Etchant for *n*-type was composed of aqueous solution of potassium hydroxide and sodium citrate. Etchant for *p*-type was composed of an aqueous solution of sodium hydroxide and tartaric acid. In all experiments anti-diffusion coating of nickel-tin galvanic alloy was deposited from standard electrolyte 10 – 12 μm thick. Adhesion strength for *n*-type TEM was 205 ± 58 kg/cm^2, for *p*-type TEM – 141 ± 67 kg/cm^2.

For electrochemical etching of TEM of both types an aqueous solution of sodium carbonate was used. Adhesion strength for *n*-type TEM was 236 ± 57 kg/cm^2, for *p*-type TEM – 153 ± 62 kg/cm2.

Combined chemical and electrochemical etching. One part of *p*-type TEM discs preliminarily treated by bichromate etchant was further subject to electrochemical etching in the etchant for *p*-type, the other part – in carbonate etchant. The dependence of adhesion strength of transient structures at TEM – anti-diffusion layer interface is given in Fig. 1.

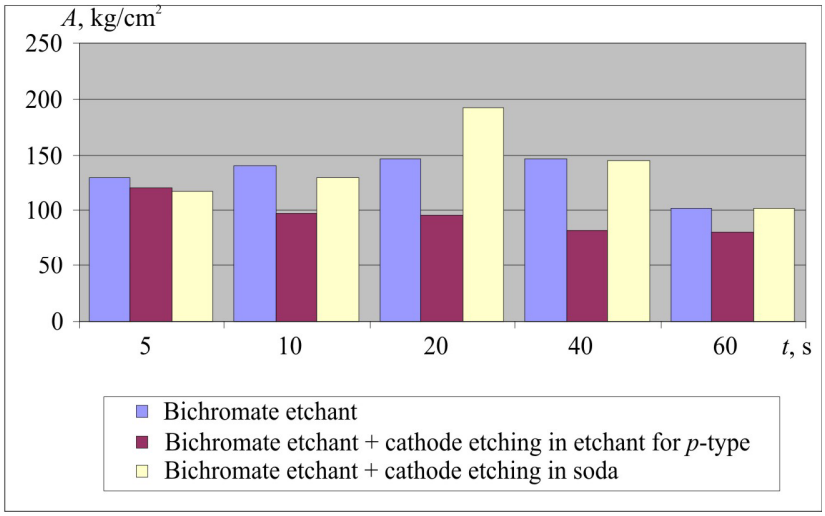

Fig. 1. Dependence of adhesion strength of transient contacts at TEM-anti-diffusion layer interface on the duration of treatment in bichromate etchant.

Due to structural differences of material, adhesion strength of contact layers to *n*-type TEM is always greater, so our main attention was focused on *p*-type samples.

Discussion of the results

As is seen from Fig. 1, preliminary treatment of *p*-type discs with a bichromate etchant produces an essential and unambigous effect on the adhesion strength values. Thus, further electrochemical etching of TEM surface in the etchant for *p*-type is all cases reduces the value of adhesion strength as compared to electrochemical etching alone. At the same time, with the use of carbonate etchant there is considerable growth (192 kg/cm^2 against 153 kg/cm^2 without chemical

etching) with a twenty-second preliminary chemical etching in bichromate etchant.

This indicates that the method of double treatment of *p*-type TEM surface facilitates better cleaning of samples surface from the damaged layer and contributes to better adhesion to contact material.

It should be noted that at determining adhesion strength of nickel coating to the surface of TEM samples by pull-off test, separation was always observed in material inside the sample, as can be seen from Fig. 2.

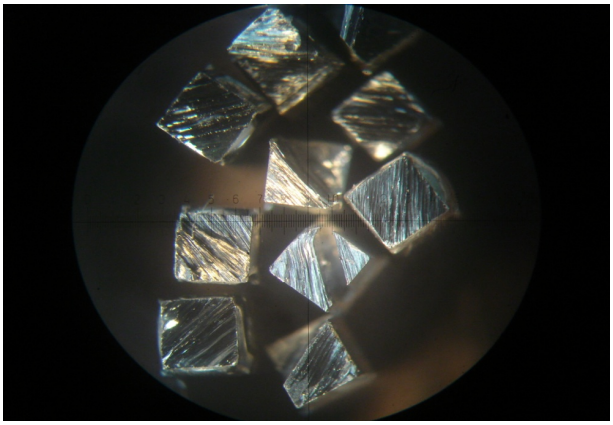

Fig. 2. Galvanic coating separation from thermoelectric material. This indicates that adhesion strength at thermoelectric material-contact structure interface is higher than cohesion strength of material itself.

Conclusions

Reliable connection of legs in thermoelectric devices requires additional preparation of contact surfaces of legs prior to deposition of interconnect layers.

Combination of chemical and electrochemical etching as a method of preliminary preparation of surface allows considerable improvement of adhesion strength between thermoelectric material surface and contact layer and assures precise control of the thickness of layer being stripped.

References

1. L.I.Anatychuk, Current status and some prospects of thermoelectricity // J. Thermoelectricity 2, pp. 7 – 20 (2007).
2. A.V.Simkin, A.V.Biryukov, N.I.Repnikov, and O.N.Ivanov, Effect of Contact Surface Condition on the Adhesion Strength of Interconnect Layers of Thermoelements Based on Extruded Bismuth Telluride, J.Thermoelectricity 2, pp.73 – 78 (2012).
3. T.D.Alieva, N.M.Akhundova and D.Sh.Abdinov, Electronic and Physicochemical Effects in Connecting Contacts of Thermoelements of Thermoelectric Coolers, Applied Physics 3 (1999).
4. D. Ilzycer, A. Sher, and M. Shiloh, Third International Conference on Thermoelectric Energy Conversion (1980), pp. 200 – 202.
5. H.P. Feng, B. Yu, S. Chen, K. Collins, C. He, Z.F. Ren, and G Chen, Electrochim. Acta 56, 3079 (2011).
6. S. Kashi, M.K. Keshavarz, D. Vasilevskiy, R.A. Masut, and S. Turenne, Effect of Surface Preparation on Mechanical Properties of *Ni* Contacts on Polycrystalline $(Bi_{1-x}Sb_x)2(Te_{1-y}Se_y)3$ Alloys, J. Electronic Materials 41(6), 1227 – 1231 (2012).

Submitted 07.04.2016.

L.I. Anatychuk

L.I. Anatychuk[1, 2], A.V. Prybyla [1]

[1]Institute of Thermoelectricity of the NAS
and MES Ukraine,
1 Nauky str., Chernivtsi, 58029, Ukraine;
[2]Yu.Fedkovych Chernivtsi National University
2, Kotsyubinsky str., Chernivtsi, 58012 Ukraine

A.V. Prybyla

COMPARATIVE ANALYSIS OF THERMOELECTRIC AND COMPRESSION HEAT PUMPS FOR INDIVIDUAL AIR-CONDITIONERS

This paper presents the results of comparative analysis of thermoelectric and compression heat pumps for their use in individual air conditioners. Dependences of air-conditioners energy conversion coefficient and weight on the value of heat fluxes created for various temperature differences are described and the most rational areas of their use are determined.

Key words: thermoelectric heat pump, compression heat pump, human air conditioner.

Introduction

General characterization of the problem. In the literature, mention is made of the possibility of human body air-conditioning by various methods [1 – 8]. Of particular interest are methods based on the use of compression and thermoelectric heat pumps. This is due to their advantages, namely high energy conversion efficiency and possibility of operation both in cooling and heating modes. Paper [9] gives a classification of individual air conditioners and proposes new promising variants of using thermoelectric and compression heat pumps.

The purpose of this paper is to determine the opportunities for further quality improvement of individual air conditioners based on thermoelectric and compression heat pumps by their comparative analysis.

Energy characteristics of thermoelectric heat pumps

Physical model of thermoelectric heat pump

In the majority of cases to determine the efficiency of thermoelectric heat pumps (THP), use is made of the properties of thermoelectric modules in cooling and heating modes. The values of their coefficient of performance ε and heating coefficient μ are found from commonly known equations [10 – 12]:

$$\varepsilon = \frac{Q_c}{W_{TE}} = \frac{\alpha I T_c - 0.5 I^2 R - \lambda (T_h - T_c)}{\alpha I (T_h - T_c) + I^2 R}, \tag{1}$$

$$\mu = \frac{Q_h}{W_{TE}} = \frac{\alpha I T_h + 0.5 I^2 R - \lambda (T_h - T_c)}{\alpha I (T_h - T_c) + I^2 R}. \tag{2}$$

where Q_c is cooling capacity, W_{TE} is power supply to thermoelectric module, Q_h is heating efficiency,

T_h is the hot side temperature of thermoelectric module, T_c is the cold side temperature of thermoelectric module, α is differential Seebeck coefficient of material, I is current strength, R is electric resistance of thermoelectric module, λ is average specific thermal conductivity coefficient of thermoelectric module legs.

Typical dependence of coefficient of performance ε on supply current for various temperature differences between module sides ($\Delta T = T_h - T_c$) is given in Fig. 1 (experimental characteristics of thermoelectric modules ALTEC 127 $2.0 \times 2.0 \times 2.5$ based on *Bi-Te* [13] at $T_h = 30$ °C were used).

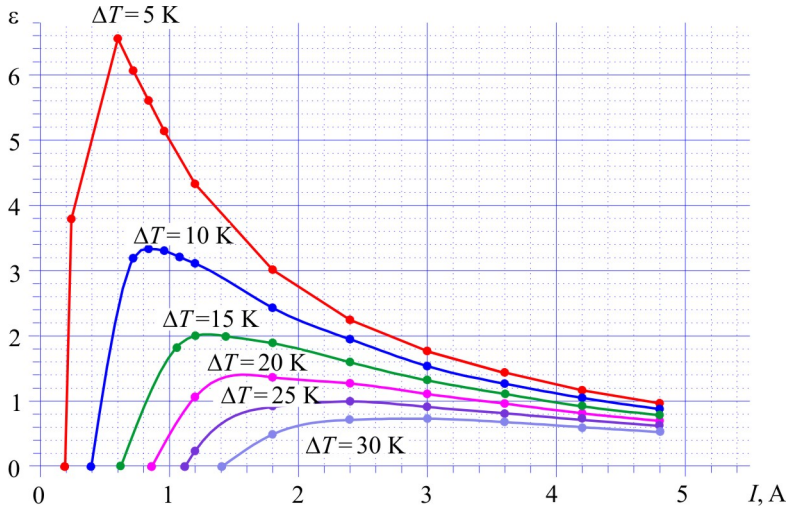

Fig. 1.Dependence of coefficient of performance of thermoelectric cooling modules ALTEC 127 2.0 × 2.0 × 2.on supply current for various temperature differences between the hot and cold module sides.

The plots demonstrate sufficiently high values of coefficient of performance ε with relatively low temperature differences ΔT inherent in air-conditioners. Heating coefficient of thermoelectric converters μ ($\mu = \varepsilon + 1$) is even higher.

However, in real conditions the efficiency of heat pumps is somewhat lower than that of modules themselves. This is due to additional losses of temperature difference in heat exchangers and contact heat resistances between heat exchangers and thermoelectric modules. Moreover, when determining real values of the energy characteristics of THP one should also take into account additional losses of electric energy on transfer of heat carriers through heat exchangers.

A physical model of thermoelectric heat pump with regard to the above is presented in Fig. 2.

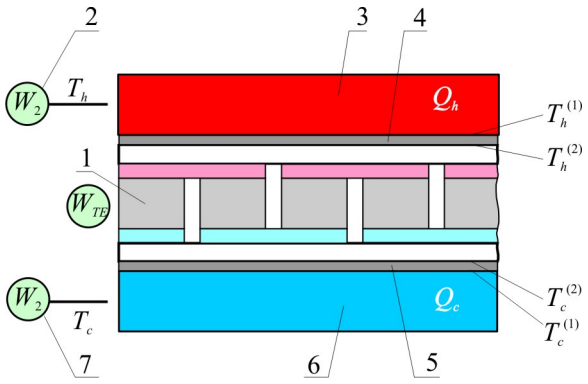

Fig. 2. Physical model of thermoelectric heat pump.

It comprises thermoelectric modules 1, the hot 3 and cold 6 heat exchangers, thermal contact resistances between them 4, 5 and liquid pumps 2, 7 which assure motion of heat carriers through heat exchangers (W_1, W_2).

Consider characteristics of heat pumps according to model described where temperature differences along heat exchangers are considered to be minor and can be ignored.

A system of equations describing coefficient of performance and heating coefficients depending on parameters of physical model elements is determined from heat balance equations in the heat pump:

$$\begin{cases} Q_c = \chi_1 (T_c^{(1)} - T_c) \\ Q_c = \chi_2 (T_c^{(2)} - T_c^{(1)}) \end{cases}, \tag{3}$$

$$\begin{cases} Q_h = \chi_3 (T_h^{(2)} - T_h^{(1)}) \\ Q_h = \chi_4 (T_h^{(1)} - T_h) \end{cases}, \tag{4}$$

$$Q_h = Q_c + W_{TE} \tag{5}$$

here χ_1 is thermal resistance of the cold heat exchanger 6, χ_2 is thermal contact resistance 4, χ_3 is thermal contact resistance 5, χ_4 is thermal resistance of the hot heat exchanger 3, Q_c is cooling capacity of thermal pump, Q_h is its heating efficiency.

With regard to (3 – 5), as well as power spent on assurance of heat exchange system, the expression for a real coefficient of performance of thermoelectric heat pump will be rewritten as follows:

$$\varepsilon_r = \frac{Q_c}{W_{TE} + W_1 + W_2} = \frac{\alpha I (T_c + Q_c N_1) - 0.5 I^2 R - \lambda (T_h - T_c - (Q_h N_2 + Q_c N_1))}{W_{TE} + W_1 + W_2}, \tag{6}$$

where $N_1 = \dfrac{(\chi_1 + \chi_2)}{\chi_1 \chi_2}$, $N_2 = \dfrac{(\chi_3 + \chi_4)}{\chi_3 \chi_4}$.

Heating coefficient in this case will be given by:

$$\mu_r = \frac{Q_h}{W_{TE} + W_1 + W_2} = \frac{\alpha I (T_h + Q_h N_2) + 0.5 I^2 R - \lambda (T_h - T_c - (Q_h N_2 + Q_c N_1))}{W_{TE} + W_1 + W_2}. \tag{7}$$

Calculation of the energy characteristics of thermoelectric heat pump

Based on the physical model presented in Fig. 2, computer optimization of thermoelectric heat pump was made with regard to energy losses on the operation of heat exchange system. In the simulation, structural parameters of thermoelectric heat pump used in space qualified devices were used [14, 15]. This choice is due to the fact that the level of coefficient of performance and heating coefficients achieved with its use outperforms known world analogs. Moreover, thermoelectric heat pump described in [14, 15] is comprised of identical units assuring its possible modification for getting the required level of heat fluxes without sacrificing its efficiency.

Computer simulation procedure

The paper employs computer methods of object-oriented simulation and numerical methods of search for optimal values of target functions, namely coefficient of performance and heating coefficient of thermoelectric heat pump. These are nonlinear functions which depend on the

combination of parameters which in turn are expressed implicitly, with the aid of a plurality of empirical equalities. So, it is impossible to use the methods of search for first-order and second-order extremes (due to impossibility of determination of derivatives). In the search for optimal value of coefficient of performance use was made of gradient-free zero-order method, namely modified Hooke and Jeeves method [16].

In each iteration of the main program cycle a system of nonlinear equations (3 – 5) is solved and cooling capacity is determined. In the program, coefficients of the approximating polynomials are calculated whereby empirical relations between physical parameters of optimization problem are found. A detailed description of simulation procedure is presented in [17].

Computer simulation results

Thus, the input parameters of the model are: the number of thermoelectric modules – 80; their dimensions – 50 × 50 × 5 mm; parameters of thermoelectric converters are assigned by empirical relationships between coefficient of performance, temperature difference and supply current for modules ALTEC 127 2.0 × 2.0 × 2.5 based on *Bi-Te* [13] (Fig. 1); thermal contact resistance between heat exchangers and thermoelectric modules – $\chi_{2,3}$ = 0.035 K/W. Heat exchange system consists of 90 aluminum liquid heat exchangers of dimensions 55 × 55 × 10 mm with 6 parallel connected channels of inner diameter 4 mm and liquid pumps.

To determine maximum coefficient of performance of thermoelectric heat pump, its optimization was made depending on the power spent on assurance of heat exchange system. Fig. 3 shows a dependence of coefficient of performance of thermoelectric heat pump on supply power of liquid pumps for various temperature differences on its sides. It is seen that this dependence has an optimum. It is related to the fact that power increase of liquid pumps leads to improvement of ε_r (by reducing losses of temperature difference on heat exchangers) only to a certain limit, following which ε_r is reduced (since supply power of liquid pumps is in the denominator of relationship (6)). Hence, from Fig. 3 it is seen that coefficient of performance of thermoelectric heat pump acquires its maximum value at W_n = 8 W.

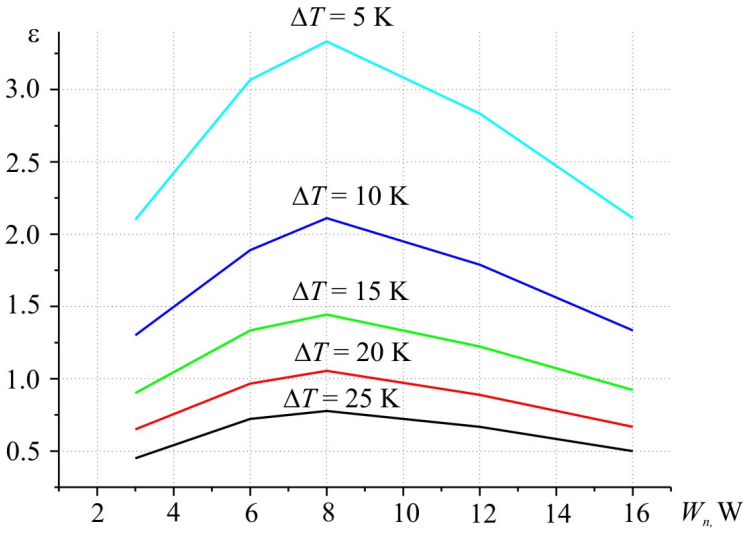

Fig. 3. Dependence of coefficient of performance of thermoelectric heat pump on the supply power of liquid pumps.

Fig. 4 shows the results of simulation of thermoelectric heat pump in the form of dependences of coefficient of performance of thermoelectric heat pump on supply current for various temperature differences between the sides of thermoelectric heat pump (Fig. 4).

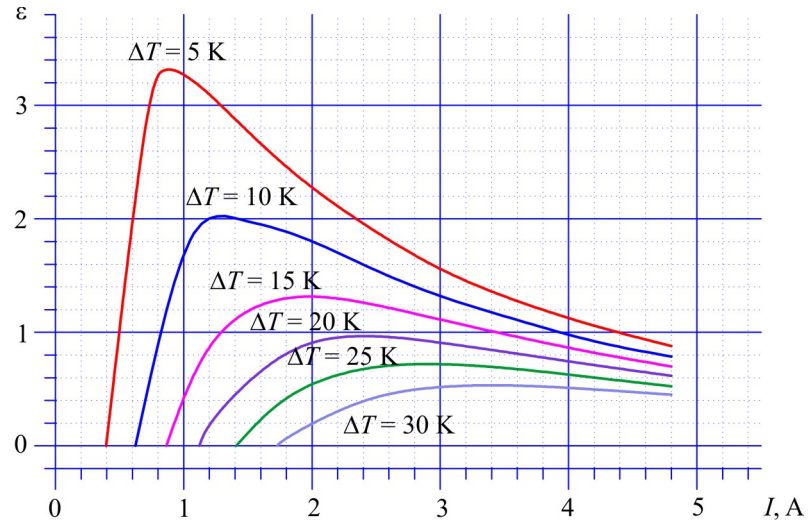

Fig. 4. Dependence of coefficient of performance of thermoelectric heat pump on supply current for various temperature differences between its hot and cold sides.

Thus, the value of coefficient of performance of thermoelectric heat pump with regard to real temperature differences on its sides and energy losses on the operation of heat exchange system reaches 3.3 at $\Delta T = 5$ K, which correlates with the experimental data for thermoelectric heat pump.

Comparison of thermoelectric and compression individual air-conditioners

The values of heat release from human body are from 100 W in quiescent state to 800 W under strong exercise [18]. In this connection, human air-conditioner must assure removal of such thermal power. This motivates requirements to the range of thermal power of individual air-conditioners.

Analysis of the literature on compression heat pumps was done with a view to determine their energy and weight-size parameters in the range of temperatures and heat fluxes that correspond to operating conditions of individual air-conditioners.

Table 1

Characteristics of low- temperature compressors

Model	Power consumption, W	Cooling capacity (W) at boiling point, °C / coefficient of performance						Weight, kg
		-30	-25	-20	-15	-10	-5	
C-K 100H5	92	58/0.6	92/1	130/1.4	169/1.8	212/2.3	267/2.9	7.4
C-K 120H2	123	116/0.9	157/1.2	203/1.6	262/2.1	337/2.7	430/3.5	7.7
C-K 140H5	147	109/0.7	145/1	186/1.2	271/1.8	300/2	483/3.2	7.9
C-K 160H5	147	107/0.7	152/1	265/1.8	271/1.8	336/2.2	433/2.9	8.2
C-K 175H5	184	128/0.7	167/0.9	225/1.2	284/1.5	358/1.9	457/2.5	8.5
C-K 200H5-1	184	151/0.8	201/1.2	263/1.3	331/1.8	412/2.2	533/2.9	8.6

Tables 1 and 2 [19 – 24] present characteristics of compression heat pumps for various operating conditions and heat flux levels:

Table. 2.

Characteristics of medium- and high- temperature compressors

Model	Boiling point, °C	Condensation temperature, °C	Power consumption, W	Cooling capacity, W	Coefficient of performance	Weight, kg
AE 41ZF11 H	-15	36.7	279	413	1.5	17
	-10	38.5	298	476	1.6	
	-5	41.8	322	565	1.7	
	0	43.6	349	667	1.9	
	5	47.2	382	762	2	
	10	48.6	423	872	2	
	15	50.6	472	989	2.1	
TRK 5480 Y	-15	45	616	1028	1.7	11.2
	-10	45	626	1235	2	
	-5	45	639	1506	2.3	
	0	45	653	1840	2.8	
	5	45	670	2239	3.3	
	10	45	689	2702	3.9	
	15	45	709	3229	4.5	
TRK 5450 Y	-15	45	388	643	1.6	11.2
	-10	45	401	760	1.9	
	-5	45	414	920	2.2	
	0	45	426	1124	2.6	
	5	45	437	1370	3.1	
	10	45	448	1660	3.7	
	15	45	458	1992	4.3	
AE5465	-15	35	500	605	1.2	12.6
	-10	35	545	835	1.5	
	-5	35	578	1110	1.9	
	0	35	599	1431	2.4	
	5	35	608	1798	2.9	
	10	35	604	2211	3.6	
	15	35	589	2669	4.5	

For illustrative reasons let us graphically construct a comparative characteristic of the coefficient of performance of compression (found from Tables 1, 2) and thermoelectric (shown in Fig. 4) heat pumps versus heat capacity level (Fig. 5). As can be seen from Fig. 5, coefficient of performance of compression heat pumps has a strong dependence on cooling capacity, reaching high values at high powers. Coefficient of performance of thermoelectric heat pumps (THP, red dashed line in the plot) does not depend on cooling capacity and is determined only by the value of temperature difference on thermoelectric converters. Thus, thermoelectric heat pumps offer

undeniable advantage over compression heat pumps in the range of low cooling capacities (up to 500 W) that correspond to operating conditions of individual air-conditioners.

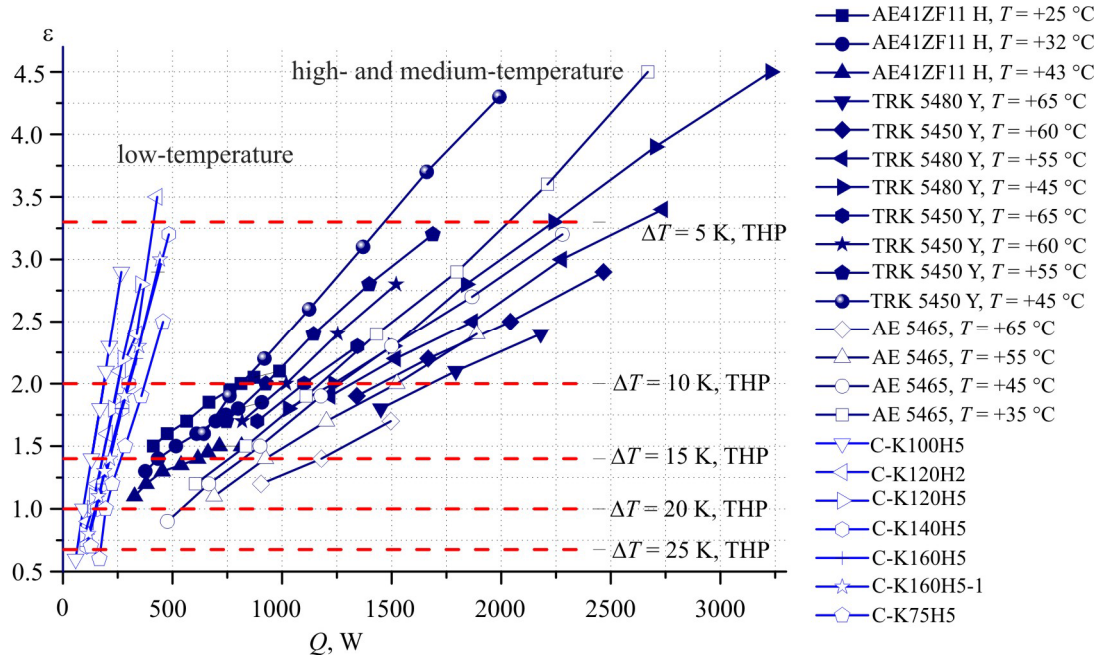

Fig. 5. Dependence of coefficient of performance of compression (blue lines) and thermoelectric (red dashed lines) heat pumps on their cooling capacity.

An important parameter for individual air-conditioners is their weight. Fig. 6 shows a dependence of the weight of thermoelectric and compression heat pumps on heating capacity. Unlike the energy characteristics, the weight of thermoelectric converters (THP, red dashed line) depends on cooling capacity, for to increase heat fluxes pumped by them it is necessary to use more thermoelectric modules with proper heat exchangers. Comparison shows the weight advantages of thermoelectric heat pumps over compression pumps in the range of heat flux powers up to 500 W.

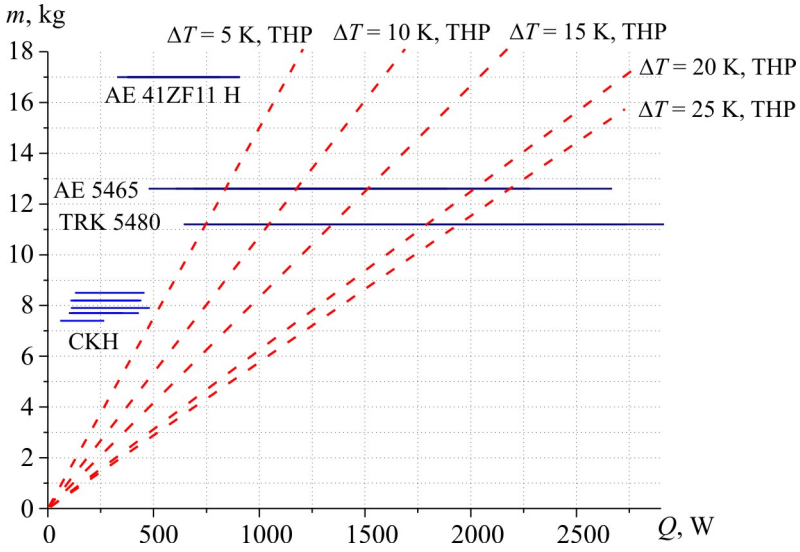

Fig. 6. Dependence of weight of compression (blue lines) and thermoelectric (red dashed lines) heat pumps on their cooling capacity.

Thus, comparative analysis of the energy and weight-size characteristics (Fig. 5 and 6) of thermoelectric and compression heat pumps proves the advantages of THP in the range of cooling capacities which give the best fit to the operating conditions of individual air-conditioners.

Conclusions

1. Coefficient of performance of thermoelectric heat pump for individual air conditioners was calculated which achieves 3.3 at $\Delta T = 5$ K.
2. Optimal electric supply power of THP heat exchange system was determined which makes 8 W for the above structural parameters of heat pump.
3. Comparison between compression and thermoelectric heat pumps was made, and it was established that thermoelectric heat pump has higher values of coefficient of performance in the range of cooling capacities up to 500 W which give the best fit to the operating conditions of individual air conditioners.
4. Comparison of the weight of thermoelectric and compression heat pumps in the range of cooling capacities up to 500 W proves the advantages of thermoelectric heat pumps, which makes reasonable their use in human air conditioners.

References

1. Pat. 66389 Ukraine, InCl 2011.01, Overheat Protective Garment / L.V.Moroz; Publ. 26.12.11, Bul № 24.
2. Pat. US 3950789, Dry Ice Cooling Jacket / Stephan A. Konz, Jerry R. Duncan.- Pub. Date: Apr. 20, 1976.
3. Pat. CN 203633537 U, Fan Type Cooling Human Body Air Conditioning Clothes / Tian Weiguo.- Pub. Date: June, 11, 2014.
4. Pat. US 20060191270 A1, Air Conditioning System for a Garment / Ray Warren.- Pub. Date: Aug, 31, 2006.
5. Pat. US 20020073481 A1, Cooling Garment / Christopher Creagan, Charles Bolian, Irwin Singer.- Pub. Date: June, 20, 2002.
6. K.-Ch.Noutel, Systems of Working Clothes for Extremely Cold Working Conditions, *Mining Information-Analytical Bulletin* 2 (2002).
7. Pat. US3524965 A, Electric Heating Element for Apparel / Stanley Arron.- Pub. Date: Aug. 18, 1970.
8. Pat. US 2010/0107657 A1, Appparel with Heating and Cooling Capabilities / Kranthi K. Vistakula.- Pub. Date: May. 6, 2010.
9. A.V.Prybyla, Physical Models of Personal Air-Conditioners (part one), *J.Thermoelectricity* 1, 16 –39 (2016).
10. A.I.Burshtein, Basic Physics for Calculation of Semiconductor Thermoelectric Devices (Moscow: Gosizdatfizmatlit, 1962), 135 p.
11. L.I.Anatychuk, *Thermoelectricity, Volume II, Thermoelectric Power Converters* (Kyiv-Chernivtsi: Institute of Thermoelectricity, 2005), 348 p.
12. L.P.Bulat, E.V.Buzin, Thermoelectric Cooling Devices: Instructional Guidelines for Students of Specialty 070200 “Low-Temperature Technology and Physics” (Saint-Petersburg State University of Low-Temperature and Food Technologies, 2001), 41 p.
13. http://www.ite.inst.cv.ua.

14. L.I.Anatychuk, A.V.Prybyla, Optimization of Thermal Connections in Liquid-Liquid Thermoelectric Heat Pumps for Water Purification Devices of Space Application, *J.Thermoelectricity* 4, 43 – 47 (2015).
15. L.I.Anatychuk, A.V.Prybyla, Optimization of Power Supply System of Thermoelectric Liquid-Liquid Supply Pump, *J.Thermoelectricity* 6, 59 – 64 (2015).
16. V.M.Verzhbitsky, Numerical Methods (Linear Algebra and Nonlinear Equations): Manual for Higher Educational Institutions (Moscow: "Oniks 21 Century" Publ.House, 2005), 432 p.
17. L.I.Anatychuk, R.V.Kuz, and A.V.Prybyla, The Effect of Heat Exchange System on the Efficiency of Thermoelectric Air Conditioner, *J.Thermoelectricity* 1, 75 – 81 (2013).
18. N.K.Vitte, *Human Heat Exchange and its Health-Related Value* (Kyiv: Gosmedizdat, 1956), 148p.
19. http://www.holodilshchik.ru/index_holodilshchik_issue_4_2005_Compressors_hermetic_Atlant.htm.
20. http://www.aholod.ru/upload/docs/tabl-compr.pdf.
21. http://www.eurobi.ru/zapchasti/kompressory/rotary/tecumseh.html.
22. http://www.rembittex.ru/holod/remholod.pdf.
23. http://holodprom.com.ua/sites/default/files/Catalog.pdf.
24. L.I.Anatychuk, A.V.Prybyla, Experimental Studies of Thermoelectric Heat Pump, J.Thermoelectricity 5 (2015).
25. http://www.garantzelremont.ru/images/remont-holodilnikov.pdf.

Submitted 11.05.2016.

L.I. Anatychuk

L.I. Anatychuk[1, 2], R.R. Kobylianskyi[1, 2]

[1]Institute of Thermoelectricity, 1, Nauky str.,
Chernivtsi, 58029, Ukraine;
[2]Yu.Fedkovych Chernivtsi National University
2, Kotsyubinsky str., Chernivtsi, 58012 Ukraine

R.R. Kobylianskyi

COOLING OF HUMAN BRAIN BY MEANS OF THERMOELECTRICITY

In this paper, object-oriented computer simulation is used to study the possibilities of human brain cooling. As a thermal physical model of the head we selected a hemisphere with 4 concentric layers which take into account the thermophysical properties of head structure. Simulation of thermal status in normal conditions yielded the results that correspond to real temperature distribution. Three methods of human brain cooling are considered, namely reduction of head surface temperature, cooling of arterial blood and reduction of blood supply. It is established that cooling of head surface leads to temperature reduction only in the near-surface layers of human brain. Reduction of blood supply leads to a slight increase of brain temperature. Cooling of brain and head in general is efficient with temperature reduction of arterial blood coming to head.

Key words: brain hypoxia, human head cooling, computer simulation.

Introduction

One of current problems in medical practice is oxygen starvation (hypoxia) of human brain [1, 2]. It is observed at cerebrovascular accidents, shock states, acute cardiovascular insufficiency, atrioventricular heart block, head injuries, carbon monoxide poisoning and asphyxia of different origin. Besides, brain hypoxia can be a complication of cardiac surgery and vascular procedures, at hypoxic brain edemas, intoxication and central nervous system injuries [3].

It is known that cooling of brain reduces its oxygen demand, increases resistance to hypoxia, thus increasing the allowed time of oxygen starvation. Thus, for instance, cooling of brain by 5 °C increases its lifetime by several times [4 – 6]. That is why this research is of vital importance.

Brain temperature is the outcome of several main factors: heat generation in the head, heat exchange between the head and the environment, blood temperature and blood circulation intensity. Cooling of head surface seems to be the simplest, accessible and convenient method of effect on human brain temperature. So, this is the object of research in a number of papers [7 – 10].

An efficient tool for studying thermal processes in human head is possibly correct and precise computer simulation of temperature and heat flux distributions. Paper [7] presents a simplified 2D model of human head in the form of a hemisphere with concentric layers taking into account the thermophysical properties of brain, skull and skin.

Paper [8], unlike the previous work, employs a 3D model of head. However, computer simulation of human head cooling is done here only for the case when blood perfusion is disregarded.

Paper [9] presents a 3D-model of head composed of four layers: the white and grey matter, skull and skin. It is established that there will be a slight reduction of brain surface temperature, but, similarly to [8], the model does not take into account blood perfusion, and arterial blood temperature is permanent $T_{blood} = +37$ °C.

In [10], computer simulation of brain cooling was done only for the case when blood temperature is equal to + 37 °C, which restricts the informative value of the results obtained.

Thus, the results testify to the necessity of a more perfect computer simulation of human brain cooling, which is *the purpose of this paper*.

Physical Model of Human Head

Physical model of human head is a hemisphere of radius R equal to the average radius of an adult human head (Fig. 1). This hemisphere has near-surface layers 1 – 3 whose thicknesses are equal to the average thicknesses of scalp h_1, subcutis layer h_2 and cranial bones h_3, respectively. Inside the hemisphere there is brain 4 of radius R_4. The corresponding layers 1 – 4 are considered as volumetric sources of heat. In each of them uniformly in the volume of the layer a metabolic heat q_{METi} (i = 1…4) is generated, and heat exchange with the circulating blood takes place which is assigned by blood perfusion coefficient ω_{bi}. The temperatures at the boundaries of corresponding layers are T_1, T_2, T_3, T_4. The thermophysical properties of these biological layers are given in Table [11 – 12].

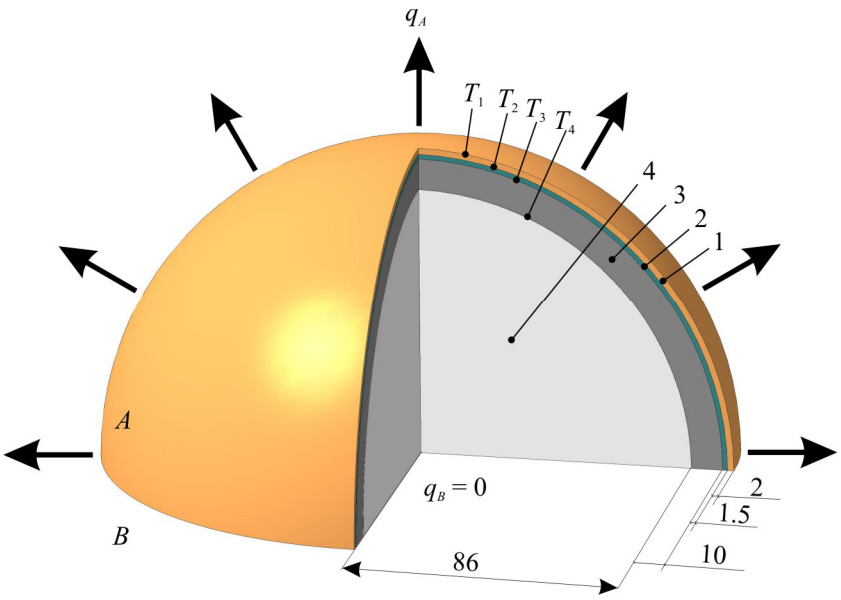

Fig. 1. Physical model of human head.

Table

Thermophysical properties of human head biological layers [11 – 12]

Anatomical organization of human head	Thermal conductivity (k) (W/m·K)	Density (ρ) (kg/m^3)	Specific heat (C_p) (J/kg·K)	Blood perfusion (W_b) (l·s^{-1} m^{-3})	Metabolism (q_{met}) (W/m^3)
Scalp	0.47	1000	3680	1.5	363
Subcutis	0.16	850	2300	0.2	130
Scull	1.16	1500	1591	0.15	130
Brain	0.49	1080	3850	8.5	10437
Blood	0.5	1069	3650	–	–

The A surface of the hemisphere is in the state of heat exchange with the environment or at temperature + 2 ºC. Thermal flux dissipated from human head surface to the environment is q_A. The B surface of the hemisphere is adiabatically isolated ($q_B = 0$).

Mathematical description of physical model

An equation of heat exchange in biological tissue is given below [7 – 12]:

$$\rho_i \cdot C_i \cdot \frac{\partial T}{\partial t} = \nabla(\kappa_i \cdot \nabla T) + \rho_b \cdot C_b \cdot \omega_{b_i} \cdot (T_b - T) + q_{met_i}, \quad (1)$$

where $i = 1…4$ are corresponding layers of human head physical model,
ρ_i is the density of corresponding biological tissue layer,
C_i is specific heat of corresponding biological tissue layer,
ρ_b is blood density,
C_b is specific heat of blood,
ω_{bi} is blood perfusion rate in corresponding biological tissue layer,
T_b is human blood temperature,
q_{meti} is the amount of metabolic heat of corresponding layer,
T is absolute temperature,
κ_i is thermal conductivity of biological tissue layer,
t is time.

The left-hand side of equation (1) is the rate of change in thermal energy comprised in the unit volume of biological tissue. Three summands on the right-hand side of this equation are the rate of change in thermal energy due to thermal conductivity, blood perfusion and metabolic heat, respectively.

The equation of heat exchange in biological tissue (1) should be solved with the following boundary conditions (2) – (3):

$$q_A = q_{rad} + q_{conv} = \varepsilon \cdot \sigma \cdot (T^4 - T_0^4) + h_{conv} \cdot (T - T_0), \quad (2)$$

$$q_B = 0, \quad (3)$$

where q_A is heat flux dissipated from human head surface to the environment, q_B is heat flux from B surface of the hemisphere, q_{rad} is heat flux due to radiation, q_{conv} is heat flux due to convection, ε is emissivity factor, σ is the Boltzmann constant, T is abs olute temperature, T_0 is ambient temperature, h_{conv} is coefficient of convective heat exchange.

Computer simulation results

In order to solve the equation of heat exchange in biological tissue (1) with the boundary conditions (2) – (3), a 3D computer model of human head was created in Comsol Multiphysics software package (Fig. 2) [13]. Computer model allows simulation of thermophysical processes in human body biological tissue with account of blood circulation and metabolism in conformity with the physical model. Calculation of temperature and heat flux density distributions inside human head was done by finite element method (Fig. 3) [14].

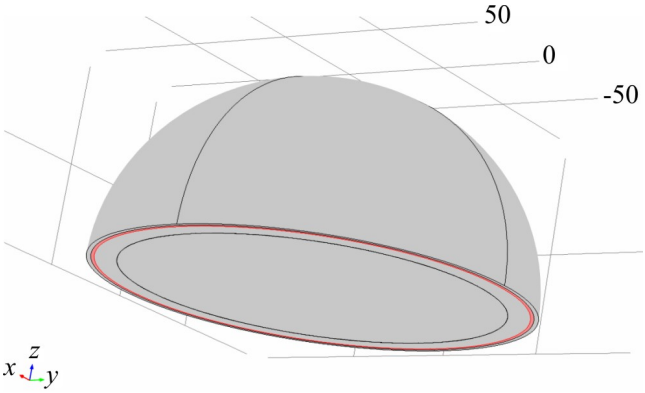

Fig. 2. 3D computer model of human head in Comsol Multiphysics computer program.

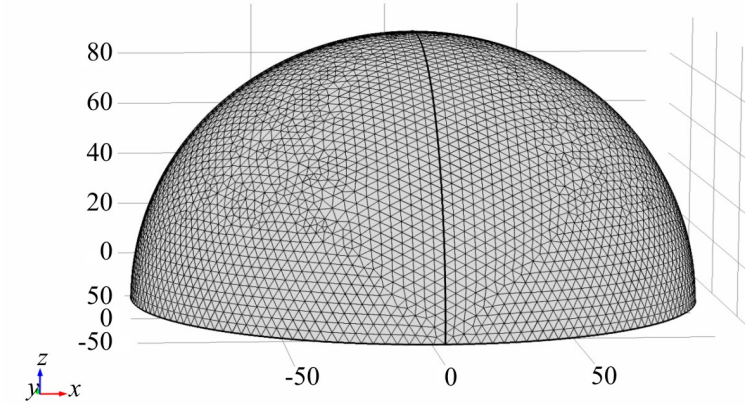

Puc. 3. Finite element method mesh in Comsol Multiphysics computer program.

At first, computer simulation was done for a typical quiescent human state at ambient temperature + 20 ºC. The pattern of temperature distribution in the section of human head is given in Fig. 4. In this case the temperature in the brain centre is + 37 ºC which corresponds to real values [15] and is proof that the model simulates correctly the real processes in human head.

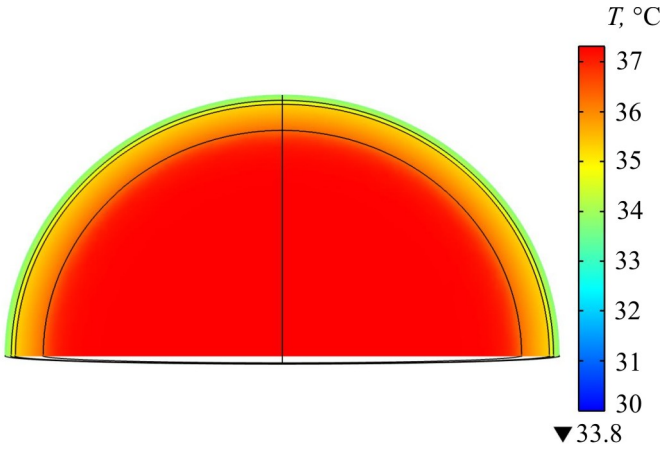

Fig. 4. The pattern of temperature distribution in the section of human head at convective heat exchange with the air at temperature + 20 ºC.

Also, with a convective heat exchange between the head and the air at temperature + 20 ºC the

temperature distributions along the radius of hemisphere of human head were determined with permanent blood supply to brain and arterial blood temperature variation from 30 ºC to 37 ºC at 1 ºC intervals (Fig. 5) which corresponds to temperature distribution given in Fig. 4.

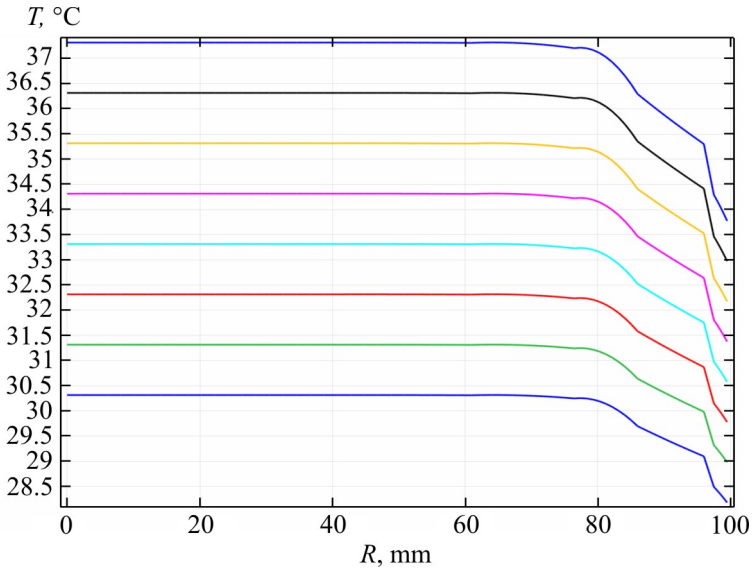

Fig. 5. Temperature distributions along the radius of human head hemisphere at convective heat exchange between the head and the air at temperature + 20 ºC, permanent blood supply to brain and arterial blood temperature variation from 30 ºC to 37 ºC at 1 ºC intervals.

We will now consider the case when the temperature of head surface is + 2 ºC which according to medical requirements is minimum permissible temperature [2, 3]. The pattern of temperature distribution in human head section in this case is given in Fig. 6, and temperature distribution along the radius of human head hemisphere at head surface temperature + 2 ºC – in Fig. 7.

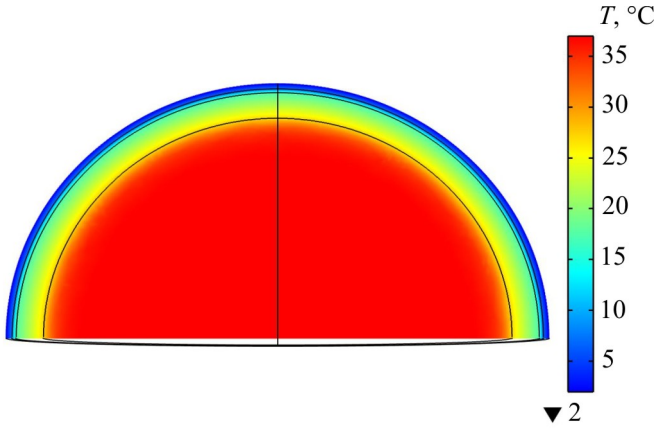

Fig. 6. The pattern of temperature distribution in human head at head surface temperature + 2 ºC.

The influence of head surface cooling on brain temperature is found from comparison of the results given in Fig. 5 and Fig. 7. This comparison shows a real temperature variation on head skin cover from + 34 ºC to + 18 ºC. Essential temperature variation occurs in the external scull parts. In so doing, temperature variation at the boundary between the scull and the brain is about 10 ºC. Temperature changes also take place in the brain near-surface layer 6 – 10 mm thick, namely up to 10 ºC. In the deeper layers temperature variation is minor, and in the central brain part it remains practically unchanged. Such minor changes in human brain temperature on cooling head surface

result from low thermal conductivity of skull (k = 1.16 W/m·K) and brain biological tissue (k = 0.49 W/m·K), as well as considerable effect of arterial blood temperature. Owing to a determining effect of these factors even simpler models described in [7 – 10] yield coinciding results, namely the temperature of central brain part is little dependent on cooling of human head surface. Such results found empirical support while investigating human head surface cooling in [16]. Therefore, the use of head surface cooling can be of practical interest only in the cases when it is necessary to reduce the temperature of brain near-surface layer 6 – 10 mm thick.

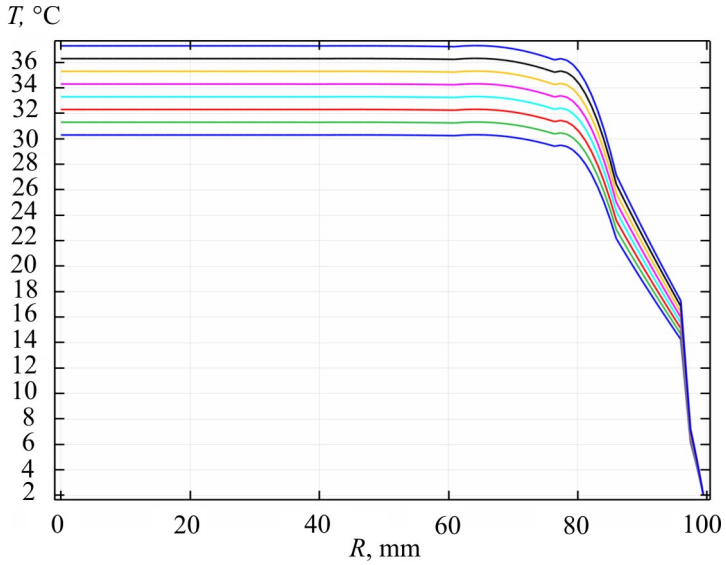

Fig. 7. Temperature distributions along the radius of human head hemisphere at head surface temperature + 2 ºC, permanent blood supply to brain and arterial blood temperature variation from 30 ºC to 37 ºC at 1 ºC intervals.

In [8] it was assumed that human brain cooling can take place with artificial reduction of arterial blood flow. Computer simulation used here allows verification of this assumption. The pattern of temperature distribution with a twofold reduction of arterial blood flow is given in Fig. 8. Temperature distributions along the radius of human head hemisphere at constant temperature of arterial blood + 37 ºC, variation of blood supply to brain from 20 % to 100 % of its normal value every 10 % for the case of convective heat exchange between the head and the air at temperature + 20 ºC and for the case of head surface temperature + 2 ºC are given in Fig. 9 and 10, respectively.

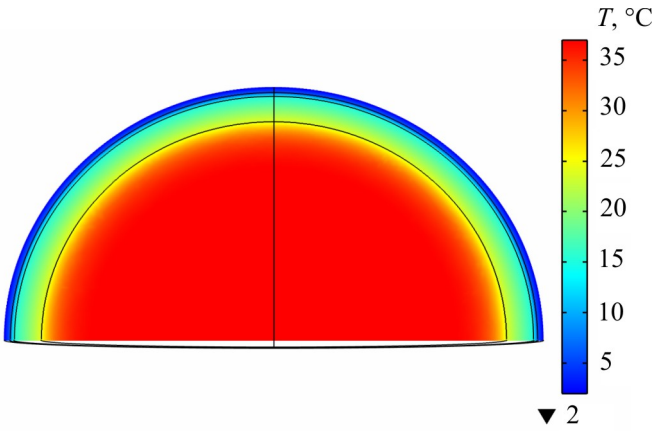

Fig. 8. The pattern of temperature distribution in human head section at head surface temperature + 2 ºC and twofold reduction of arterial blood flow.

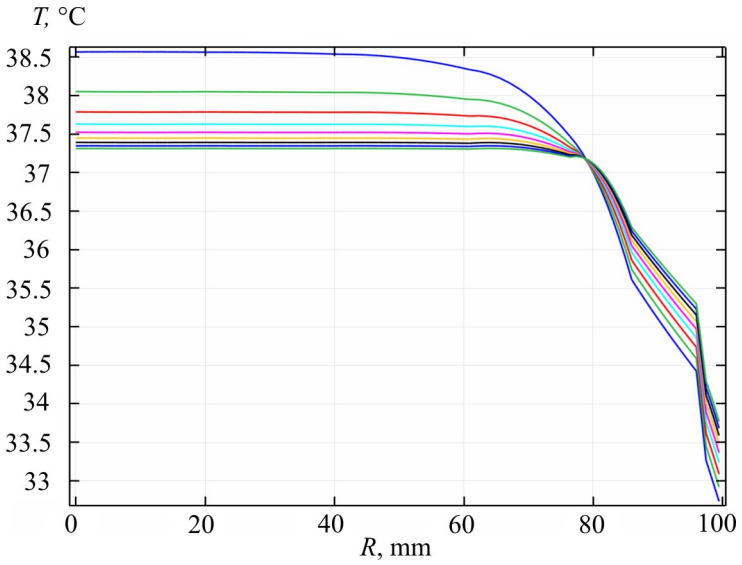

Fig. 9. Temperature distributions along the radius of human head hemisphere at convective heat exchange between the head and the air at temperature + 20 ºC, permanent arterial blood temperature + 37 ºC and variation of blood supply to brain (blood perfusioni) from 20, 30… 100 % of its normal value.

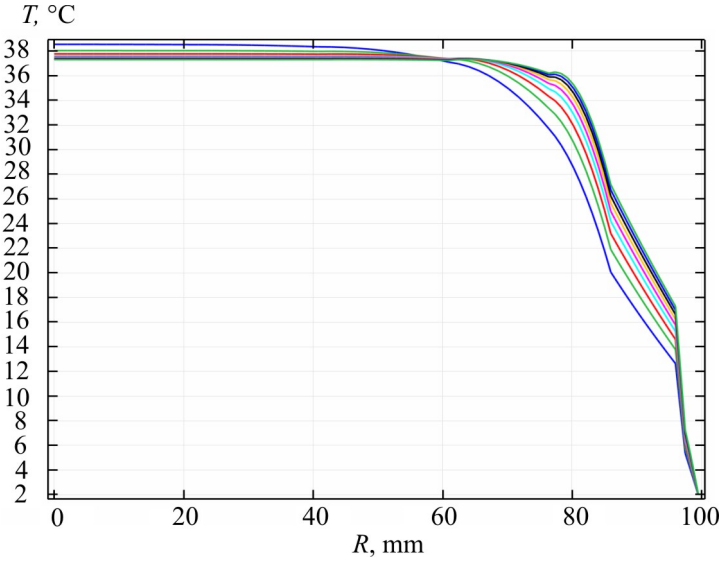

Fig. 10. Temperature distributions along the radius of human head hemisphere at head surface temperature + 2 ºC, permanent arterial blood temperature + 37 ºC and variation of blood supply to brain (blood perfusion) from 20, 30… 100 % of its normal value.

This suggests, at first sight, a paradoxical result that a reduction of arterial blood flow does not cause human brain temperature reduction even on cooling head surface to + 2 ºC. On the contrary, in this case there is an additional heat-up of human brain. In fact, such results are understandable, since the density of brain heat release is much in excess of specific heat release of the human body. In this case, a body with circulating blood serves a peculiar heat-exchanger for heat removal from the head. So, a reduction of arterial blood flow leads to a reduction of heat removal from the head and, hence, the rise in human brain temperature. From Fig. 9 – 10 it is seen that with a twofold reduction of blood supply to brain from its normal value the temperature of brain core is increased by 0.4 ºC, and with a fivefold reduction – by 1.3 ºC.

The simulation results suggest a relation between the temperature of incoming blood and the

temperature of human brain. It was established that with a normal blood supply the temperature of central brain part is higher that the temperature of arterial blood by 0.3 ºC. Thus, at the temperature of arterial blood + 32 °C the temperature of human brain central part is reduced to + 32.3 °C.

Thus, from the results of computer simulation it follows that an efficient method of human brain cooling is to reduce the temperature of arterial blood coming to head. Such reduced temperatures can be achieved through reduction of human body temperature due to increase of its heat release to the environment. For this purpose one should use heat-exchange blanket that can be cooled by thermoelectric liquid thermostat. Estimates show that cooling capacity of such thermoelectric device is within 20 ÷ 100 W.

Conclusions

1. Computer simulation was used to determine temperature distributions in the head in normal conditions of convective heat exchange (+ 20 °C). The results obtained correspond to real temperature values + 37 °C in the brain centre and + 36.5 °C on its surface, which proves the correctness of simulation.
2. Cooling of head surface to temperature + 2 °C does not result in temperature reduction of brain central part. Cooling of head surface can be of practical interest only when it is necessary to reduce the temperature of brain near-surface layer 6 – 10 mm thick to + 27 ÷ + 36 °C.
3. It was established that reduced blood supply to brain does not reduce its temperature even on cooling of head surface to minimum permissible temperature + 2 ºC. On the contrary – reduction of blood supply by a factor of 5 raises brain temperature to + 38.6 °C.
4. Efficient reduction of human brain temperature is achieved at the reduction of temperature of arterial blood coming to the head. At supplied blood temperature + 37 ºC ÷ + 30 ºC the temperature of brain central part changes proportionally from + 37.3 ºC to + 30.3 ºC. It was established that with a normal blood supply the temperature of brain central part is higher than arterial blood temperature by 0.3 ºC.

References

1. Liu Jing, Cooling Strategies and Transport Theories for Brain Hypothermia Resuscitation, *Frontiers of Energy Power Engineering in China* **1**(1), 32 – 57 (2007).
2. A.M.Belous, V.I.Grischenko, *Cryobiology* (Kyiv: Naukova Dumka, 1994), 431 p.
3. E.I.Gusev, V.E.Grechko, and G.S.Burd, *Nervous Diseases* (Moscow, 1988), 640 p.
4. T.M.Darbinyan, A.N.Zirakadze, S.M.Zolnikov, P.Ya.Kintraya, B.A.Komarov, S.N.Kopshev, N.P.Kupin, and K.D.Chachava, *Artificial Hypothermia* (Moscow: Soviet Encyclopedia, 1989).
5. R.R.Kobylianskyi, I.A.Moskalyk, On the Prospects of Using Thermoelectricity for Human Head Cryotherapy, *J.Thermoelectricity* 4, 85 – 94 (2015).
6. R.R.Kobylianskyi, I.A.Moskalyk, On Temperature Distribution in Human Head at Given Thermal Fluxes on its Surface, *J.Thermoelectricity* 6, 57 – 65 (2015).
7. Xiaojiang Xu, Peter Tikuisis, and Gordon Giesbrecht, A Mathematical Model for Human Brain Cooling during Cold-Water Near-Drowning, *J. Appl Physiol.* **86**, 265 – 272 (1999).
8. Brian H. Dennis, Robert C. Eberhart, George S. Dulikravich, Steve W. Radonsб Finite Element Simulation of Cooling of Realistic 3D Human Head and Neck, *J.Biomechanical Engineering* January (2004).
9. Matthew A. Neimark, Angelos-Aristeidis Konstas, Jae H. Choi, Andrew F. Laine, and John Pile-

Spellman, Brain Cooling Maintenance with Cooling Cap Following Induction with Intracarotid Cold Saline Infusion: A Quantitative Model, *J.Theoretical Biology* **253**(2), 333 – 44 (2008).

10. Michael Christiansen, Nikolai Rakhilin, Anna Tarakanova, and Kevin Wong, *Modeling Brain Cooling Treatment Approved for Hypoxic-Ischemic Encephalopathy in Infants to Treat Stroke and Cardiac Arrest in Adult Patients*, Cornell University. Fall 2010.
11. D.Fiala, K.J.Lomas, and M.A.Stohrer, Computer Model of Human Thermoregulation for a Wide Range of Environmental Conditions: the Passive System, *J. Appl. Physiol*. **87**(5):1957 – 1972 (1985).
12. S.C.Jiang, N.Ma, H.J.Li, and X.X.Zhang, Effects of Thermal Properties and Geometrical Dimensions on Skin Burn Injuries, *Burns* **28**, 713 – 117 (2002).
13. *COMSOL Multiphysics User's Guide*, COMSOLAB, 2010, 804 p.
14. A.D.Legostayev, *Finite Element Method, Synopsis* (Kyiv: KNUBA, 2004), 112 p.
15. V.M.Pokrovsky, G.F.Koro'tko, *Human Physiology* (Moscow: Medicine, 2003), 656 p.
16. B.A.Harris, P.J.D.Andrews, I.Marshal, T.M.Robinson, and G.D.Murray, Forced Convective Head Cooling Device Reduces Human Cross-Sectional Brain Temperature Measured by Magnetic Resonance: a Non-Randomized Healthy Volunteer Pilot Study, *British J.Anaesthesia* **100** (3), 365 – 72 (2008).

Submitted 17.03.2016.

M.V. Maksimuk

M.V. Maksimuk

Institute of Thermoelectricity of the NAS and MES of Ukraine,
1, Nauky Str., Chernivtsi, 58029, Ukraine

COMPUTER DESIGN OF THERMOELECTRIC AUTOMOBILE STARTING PRE-HEATER OPERATED WITH PETROL FUEL

The results of computer design of a 150 – 130 W thermoelectric automobile heater operated with petrol fuel for start heating of automobile engine under low ambient temperatures are presented.
Key words: internal combustion engine, starting pre-heater, thermoelectric generator, physical model, computer design.

Introduction

In the carburetor internal combustion engine the air-petrol mixture is ignited by a spark. However, for a reliable start-up of "cold" engine one must first of all create the conditions for burning mixture formation with the wide ignition limits. Under low ambient temperatures the low speed of carburetor engine crankshaft during start-up causes a degradation of parameters of the end of the compression stroke (pressure and temperature), which have a considerable impact on the conditions of mixture preparation for ignition in cylinders. Pressure reduction of saturated petrol vapours in combination with low velocities of air-petrol mixture in the engine aspirating stroke and cold walls impair the conditions for petrol evaporation and formation of burning mixture with the necessary ignition limits. Moreover, a reduction of engine crankshaft speed will have a negative effect on the operation of ignition system, owing to which the reliability of spark formation will be reduced. So, prior to start-up the engine must be heated.

So far, the most efficient method for pre-heating of carburetor engines and their reliable start-up is autonomous start heating. Moreover, the use of such equipment provides for a reduction of toxic discharge with automobile exhaust gases by a factor of 5, increase in engine service life by 50 – 60 thousand km and saving of 90 – 150 l of fuel during only one winter season [1].

However, one of the main constraining factors for a wide practical application of starting pre-heaters is the need for power supply to fuel pump, a fan for air delivery to combustion chamber, a circulating pump for pumping of liquid heat carrier, which in the majority of cases leads to a "deep" discharge of automobile storage battery.

As shown in [2], said problem is solved by means of thermoelectric generator which employs the heat of the heater and provides for autonomous power supply to its components.

In [3], analysis of technical specifications of starting pre-heaters for various kinds of transport means is made, and electrical parameters of thermal generators necessary for the autonomous operation of such heaters are determined. Thus, total electric power of thermal generator for starting pre-heaters of transport means with engine displacement to 4 l must be 70 – 90 W; for transport means with engine displacement 4 – 10 l and over 10 l – 130 – 150 W, 230 – 250 W, respectively. Besides, such electric powers of thermal generator will allow storage battery recharging and power supply to other automobile equipment.

In [4], the design, operating principle and computer simulation results of a 70 – 90 W thermoelectric automobile starting pre-heater operated with diesel fuel are presented. The purpose of this work is to design a 130 – 150 W thermoelectric automobile starting pre-heater operated with petrol fuel for start heating of engine under conditions of low ambient temperatures.

Design selection of thermoelectric starting pre-heater

As a source of heat, use was made of a petrol burner (Fig. 1) with a pulse-type metering fuel pump (Fig. 2) of liquid starting pre-heater "Thermo Top C" (Webasto).

Fig. 1. Appearance of petrol burner of liquid starting pre-heater "Thermo Top C" (Webasto) [5]. Maximum thermal power 5 kW.

Fig. 2. Appearance of metering fuel pump of liquid starting pre-heater "Thermo Top C" (Webasto) [5]. Maximum fuel consumption 510 g/h.

With regard to burner design, the most rational shape of the hot heat exchanger in terms of efficient heat exchange with the source of heat is a cylinder pipe accommodating a burner in its internal space, and its external surface having the form of planes where thermoelectric modules are arranged.

The thermoelectric converter is composed of thermoelectric modules based on bismuth telluride of the type "ALTEC-1061" which on arrival of the necessary amount of heat to the hot side and on achievement of optimal operating temperatures assure generation of the assigned electric power.

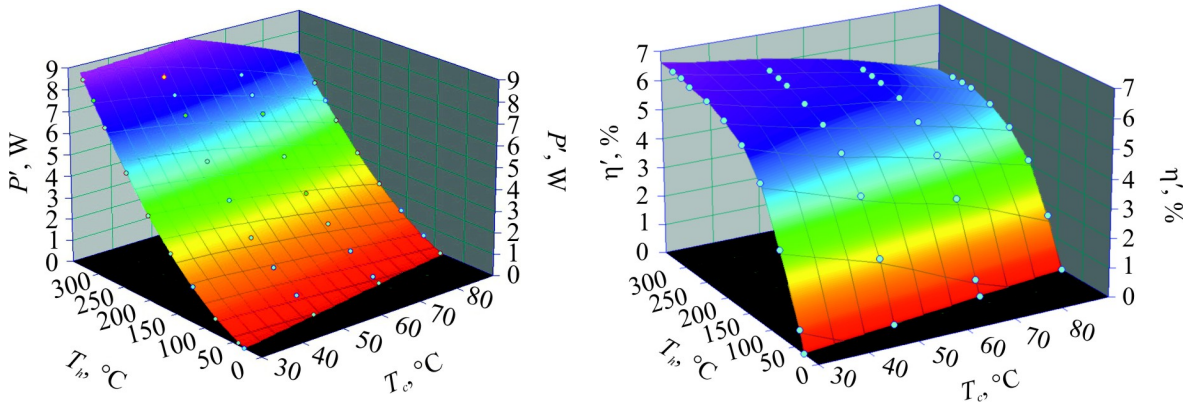

a) *b)*

Fig. 3. Dependence of electric power P (a) and efficiency η (b) on the hot side Th and cold side Tc temperature of thermoelectric module "ALTEC-1061" [6].

Fig. 3 shows a three-dimensional graphical image of the dependence of electric power P' and efficiency η' on the hot side T_h and cold side T_c temperature of thermoelectric module "ALTEC-1061".

From the analysis of the data presented in Fig. 3 it follows that to provide the output electric

power of the heater 130 – 150 W, it is necessary to have 20 modules "ALTEC-1061". From these considerations, the most efficient design of the hot heat exchanger is a regular decahedron, with 2 thermoelectric modules arranged on each side thereof. In so doing, the hot side temperature of the modules must be 280 – 310 °C, the cold side – 30 – 70 °C.

Taking into account that the efficiency of thermoelectric generators using single-stage modules based on bismuth telluride is 3 – 3.5 % [7], to assure the output electric power of the heater 130 – 150 W, it is necessary to spend ~ 4.3 – 4.7 kW of heat which corresponds to fuel consumption 350 – 375 g/h.

As a circulating pump, the liquid pump (Fig. 4) of starting pre-heater "Thermo Pro 90 ST" (Webasto) was used.

Fig. 4. Appearance of liquid pump 12V U4847 of starting pre-heater "Thermo Pro 90 ST" (Webasto) [5].

This type of the pump is specially designed for pumping of heat carrier in transport means with engine displacement 4 – 10 l. Nominal supply voltage of the pump is 12 V, maximum heat carrier consumption is 1.6 m^3/h.

Physical model of thermoelectric starting pre-heater and its description

In [5] it is shown that for the calculation of the basic energy and design parameters of the heater it is convenient to use a physical model (Fig. 5) where the process of heat transfer from the source of heat to thermopile takes place as a result of gas flow passing through the hot heat exchanger at velocity v and temperature T_G.

In so doing, the amount of heat Q released due to petrol combustion is used for heating of gases that formed as a result of complete fuel combustion:

$$g_n G_n = C_p \cdot (T_G - T_o), \quad (1)$$

where g_n and G_n are consumption and calorific power of petrol fuel, C_p is total heat capacity of gases (CO_2, H_2O, N_2 and air) that formed as a result of fuel combustion, T_0 is ambient temperature.

Heat Q_1 coming from the heated gases to the hot heat exchanger is transferred due to convection:

$$Q_1 = \alpha \cdot (T_G - T_r) \cdot S_R, \quad (2)$$

where α is convective coefficient of heat transfer from the gas to the heat-absorbing surface of the hot heat exchanger;

T_r is temperature of the heat-absorbing surface of the hot heat exchanger;

S_R is the area of the heat-absorbing surface of the hot heat exchanger;

Heat Q_2 is transferred due to thermal conductivity from the heat-absorbing surface of the hot heat exchanger to the hot side of thermopile:

$$Q_2 = \frac{S_r \cdot \lambda_r}{\delta_r} \cdot (T_r - T_h) \tag{3}$$

S_r is the area of the heat-releasing surface of the hot heat exchanger;
λ_r is thermal conductivity of heat exchanger material;
δ_r is the thickness of heat exchanger base;
T_h is the hot side temperature of thermopile.

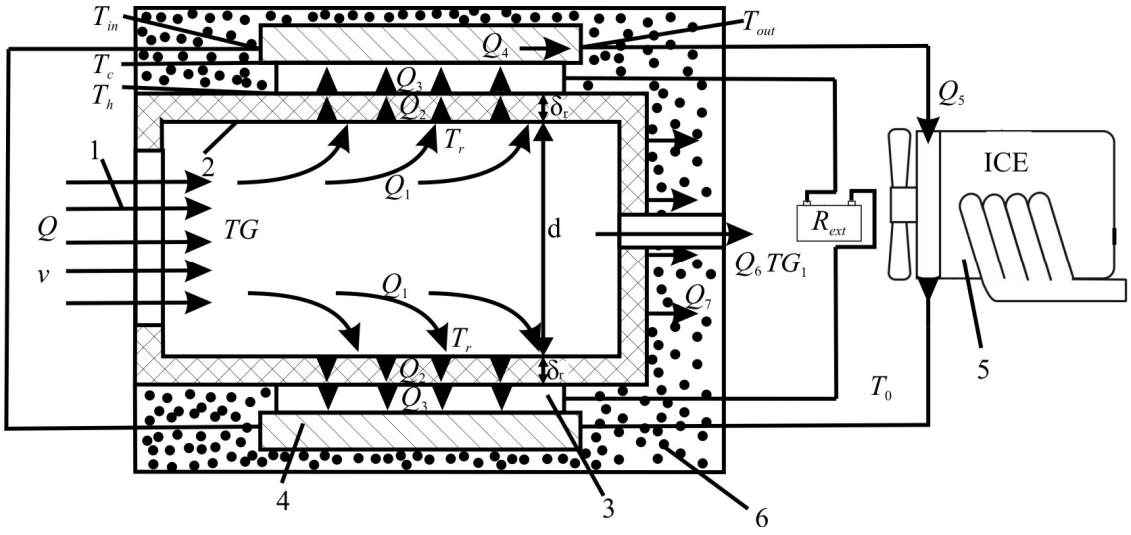

Fig. 5. Physical model of thermoelectric automobile heater:
1 – gas flow; 2 – hot heat exchanger; 3 – thermopile;
4 – cold heat exchanger; 5 – automobile engine; 6 – thermal insulation.

Useful heat Q_3 coming to thermoelectric modules was calculated from the power P' of one module with determined hot side T_h and cold side T_c temperatures of thermopile, its efficiency η' and the number of modules n:

$$Q_3(T_h, T_c) = n \cdot \frac{P'(T_h, T_c)}{\eta'(T_h, T_c)}. \tag{4}$$

Heat Q_4 is removed from the cold side of thermopile by heat carrier flow circulating in the cold liquid heat exchanger 4:

$$Q_4 = g_T \cdot c_{pT} \cdot (T_{in} - T_{out}), \tag{5}$$

where g_T is heat carrier consumption c_{pT} is heat carrier heat capacity T_{in}, T_{out} are heat carrier temperatures at inlet to and outlet of thermopile cooling system, respectively.

The heat removed by liquid heat carrier from the modules Q_5 is spent on start heating of engine:

$$Q_5 = c_{eng} \cdot m_{eng} \cdot (T_{out} - T_0), \tag{6}$$

where c_{eng}, m_{eng} are heat capacity and mass of automobile engine, respectively; T_0 is ambient temperature.

Basic heat losses:

1) Q_6 – with reaction products (water H_2O, carbon dioxide CO_2 and nitrogen N_2):

$$Q_6 = C_c \cdot m_c \cdot (T_{G1} - T_0), \tag{7}$$

where C_c is average heat capacity of reaction products, m_c is mass of reaction products, T_{G1} is temperature of reaction products.

2) Q_7 – on thermal insulation:

$$Q_7 = \frac{\lambda S_{ph}}{L}(T_{termopile} - T_0), \tag{8}$$

where λ is thermal conductivity of insulating material; S_{ph} is the area of the hot heat exchanger surface which is not occupied by thermopile; L is the thickness of thermal insulation layer.

Thus, heat balance equation for the selected model of thermoelectric automobile heater can be written as:

$$\begin{cases} Q = Q_1 + Q_6, \\ Q_1 = Q_2 + Q_7, \\ Q_2 = Q_3, \\ Q_3 - P = Q_4, \end{cases} \tag{9}$$

where P is output electric power of the heater

Solving the system of heat balance equations (9) enables one to determine the basic energy and design parameters of thermoelectric automobile heater.

Computer design aimed at determining:

– gas temperature T_G in the hot heat exchanger and the effective area of the heat-absorbing surface of the hot heat exchanger S_R to assure on the hot side of the thermopile the temperature T_h = 330 – 280 °C;

– thermal power Q_5 removed by heat carrier to estimate the warm-up rate of automobile engine.

Calculation results

Calculation procedure of gas temperature T_G is described in detail in [5].

As a result of appropriate calculations, ratio (10) was obtained to determine air delivery velocity v to the hot heat exchanger as a function of temperature T_G:

$$v = 5 \cdot \left[\frac{\frac{G_n}{T_G - T_0} - 19.27}{17.4} + 1 \right] \cdot \frac{3.47 \cdot g_n}{\rho_{T0} \cdot S_R}, \tag{10}$$

where 19.27 and 17.4 are coefficients that determine the content of carbon dioxide, water, nitrogen and air that formed as a result of complete combustion of petrol fuel, 3.47 is coefficient that determines the amount of oxygen necessary for complete combustion of petrol, ρ_{T_0} is the density of air at given ambient temperature.

The Mathcad application software package was used to determine the inverse dependence of hot gas temperature T_G on air velocity v (Fig. 4) at G_n = 44 MJ/kg, T_0 = 0 °C, g_n = 375 g/h, ρ_{T_0} = 1.29 kg/m^3 and combustion chamber diameter d = 90 mm.

From the analysis of data given in Fig. 6 it follows that for further calculations of the hot exchanger design it is not reasonable to use T_G < 300 ° and T_G > 500 °C: in the former case it is impossible to achieve the necessary hot side temperatures of module, in the latter case the rise in temperature leads to increase in the heat exchanger dimensions due to possible overheating of thermopile.

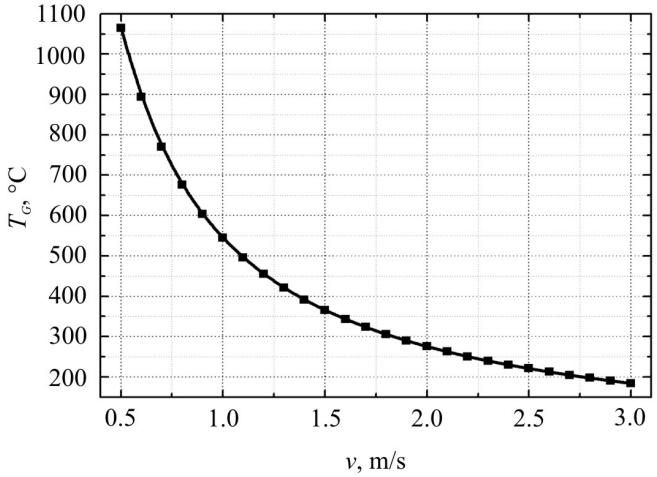

Fig. 6. Dependence of gas temperature T_G on air delivery velocity to the hot heat exchanger.

So, to determine the dependence of the module hot side temperature T_h on the area of the heat-absorbing surface, we used hot gas temperature $T_G = 500 – 300$ °C which corresponds to air velocities 1.2 – 1.8 m/s. Simulation was done by finite element method with the use of "Comsol Multiphysics" application software package [8].

In the process of computer design the following values were used as the input data:

– hot gas temperature T_G = (300; 400; 500) °C;

– gas velocity in the heat exchanger v = (1.2; 1.4; 1.8) m/s;

– the area of the heat-absorbing surface S_R = (0.03; 0.06; 0.09; 0.12) m^2;

– thermal conductivity of the hot heat exchanger material λ_r = 140 W/m·K;

– thermal resistance of thermoelectric module κ_m = 0.7 m·K/W.

In so doing, it was assumed that heat sinks are at the outlet of combustion products from the heat exchanger and at places of modules location, and thermal adiabatic insulation conditions are imposed on the rest of the boundaries.

Fig. 7 shows computer designed dependences of the module hot side temperature T_h on the area of the heat-absorbing surface S_R at hot gas temperature T_G within 500 – 300 °C.

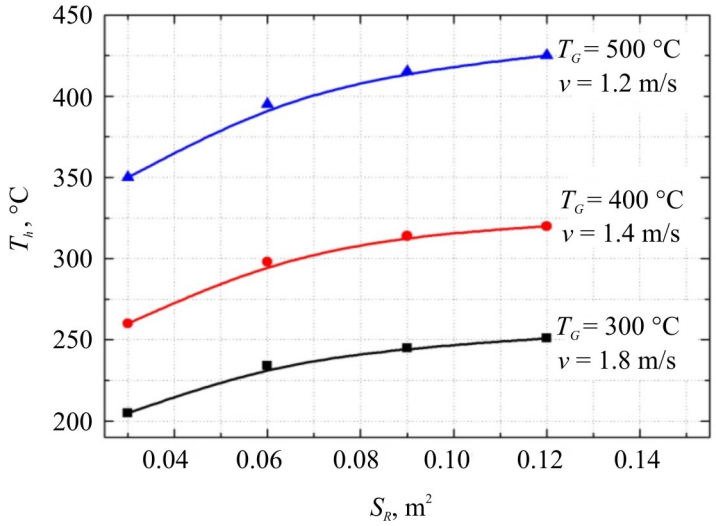

Fig. 7. Dependence of the module hot side temperature T_h on the area of the heat-absorbing surface S_R of heat exchanger.

From the data presented in Fig. 7 it is seen that the hot side temperature of module 330 °C is achieved at gas temperature T_G = 400 °C and the area of the heat-absorbing surface of the hot heat exchanger S_R = 0.12 m^2.

Fig.8 shows temperature distribution in the "hot heat exchanger-thermoelectric modules", Fig. 9 – the finite element method mesh.

As it follows from the analysis of temperature distribution, as the gases flow to heat sink, T_G is reduced, which results in the reduction of temperature T_h by ~100 °C. However, as long as in a real design the source of heat is directly in the heat exchanger, it can be considered that the hot side temperature of modules is identical.

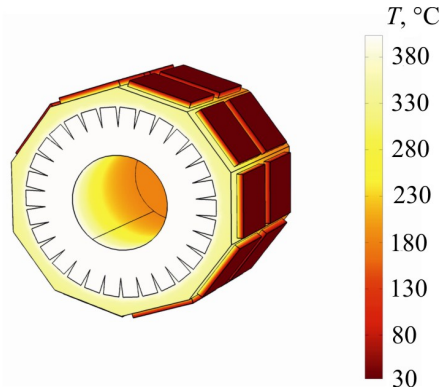

Fig .8. Temperature distribution in the "hot heat exchanger – thermoelectric modules" system. T_G = 400 °C. S_R = 0.12 m^2.

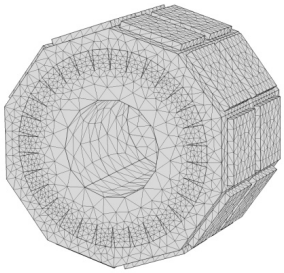

Fig. 9. Finite element method mesh.

Similar calculations to determine T_G at S_R = 0.12 m^2 and g_n = 350 g/h show that to assure the hot side thermopile temperature 280 °C, the temperature of hot gases in the heat exchanger must be 370 °C. In this case air delivery velocity must be 1.3 m/s.

For quick heating of automobile engine and the efficient operation of thermoelectric converter, it is necessary, on the one hand, to assure maximum transfer of thermal power from the modules to the cold heat carrier, on the other hand, to create such conditions whereby the difference in heat carrier temperature at the inlet to and outlet of heat exchangers would be minimal.

With this aim, the effective channel area of the cold heat exchangers and optimal consumption of liquid heat carrier were determined. The cold heat exchanger simulation was done by finite element method with the use of "Comsol Multiphysics" application software package.

In the process of computer design the following values were used as the input data:

– cold heat carrier temperature at inlet to cold heat exchanger T_{in} = 30 °C;

– total thermal power removed from the modules in operating mode Q_4 = 2.3 kW;

– heat carrier consumption (heat carrier – antifreeze) g_T = (0.7; 1; 1.3; 1.6) m^3/h;

– channel area of the cold heat exchanger S_c = (10 – 70) cm^2;

– thermal conductivity of cold heat exchanger material λ_{r1} = 105 W/m·K;

– heat carrier (antifreeze) heat capacity c_{pT} = 3151 J/kg·K;

– heat carrier thermal conductivity λ_T = 0.34 W/m·K.

In the design, heat sink was assigned at points of heat carrier outlet from the heat exchanger, and adiabatic thermal insulation conditions were imposed at the rest of the boundaries.

Fig. 10 shows a dependence of thermal power Q_5 removed from thermoelectric modules to

automobile engine on the total area of channels S_c of the cold heat exchangers with different heat carrier consumption.

From the analysis of data represented in Fig. 10 it follows that for complete transfer of thermal power from the modules to the engine the area of channels in the cold heat exchangers must be at least 40 cm^2. With such channel area Q_5 is practically independent of heat carrier consumption, which in turn allows reducing the losses of the output electric power of the heater on power supply to circulation pump. Moreover, as is seen from Fig. 11, at S_K = 40 cm^2 heat carrier consumption has no essential effect on the difference in heat carrier temperature at the inlet to and outlet of cold heat exchangers (ΔT = 1 – 2 °C). So, the choice of optimal g_T will be determined only by engine displacement and automobile cooling circuit.

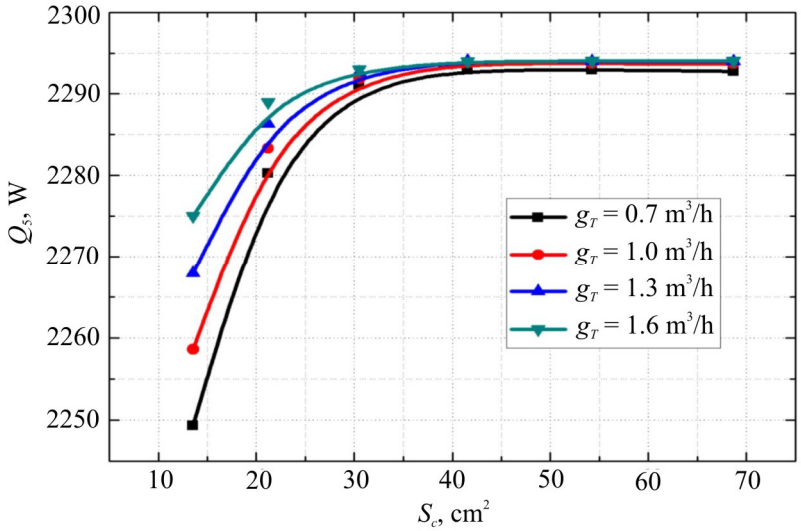

Puc. 10. Dependence of thermal power Q_5 on the channel area S_c of the cold heat exchangers.

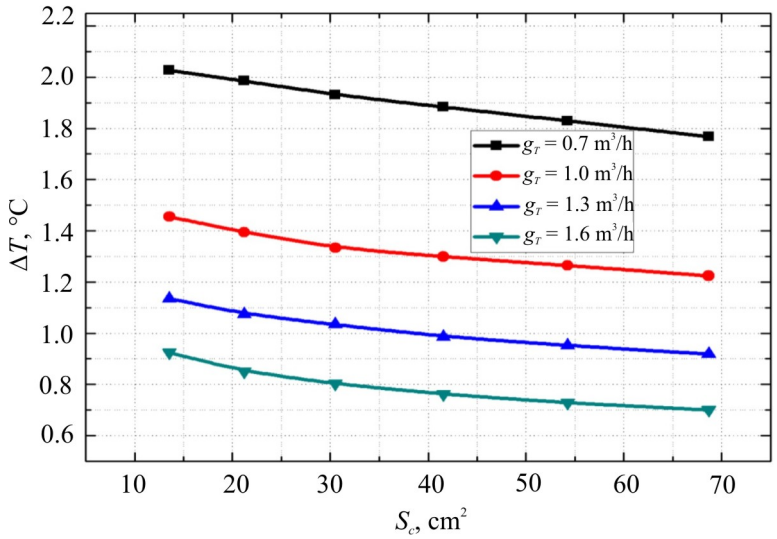

Fig. 11. Dependence of heat carrier temperature difference ΔT between the inlet to and outlet of the cold heat exchangers on the channel area S_c.

Fig. 12 shows an example of temperature distribution in the mesh points (Fig. 13) of finite element method for the cold heat exchanger.

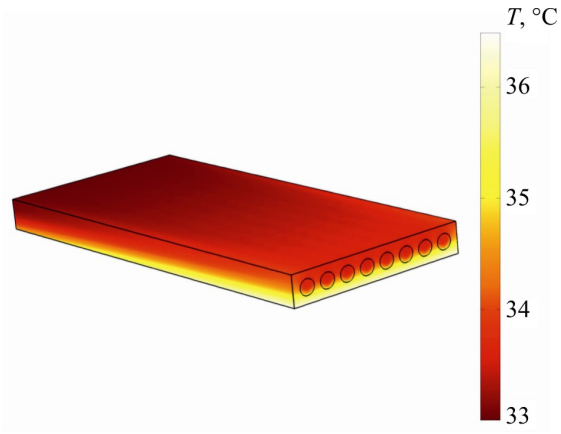

Fig. 12. Temperature distribution in the cold heat exchanger. $S_c = 40cm^2$. $g_T = 1.6\ m^3/h$.

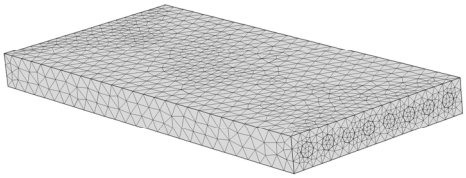

Fig. 13. Finite element method mesh.

According to (6), the amount of thermal energy that must be spent on heating internal combustion engine of displacement ~ 4 l, heat capacity 0.462 kJ/(kg K) (engine material – steel) and weight 260 kg from 0 °C to 30 °C will make ~ 3.5 MJ. Taking into account that total thermal power removed from the thermopile by heat carrier with temperature 30 – 70 °C is ~ 2.29 kW (Fig. 14), start heating of such engine will require ~ 30 min.

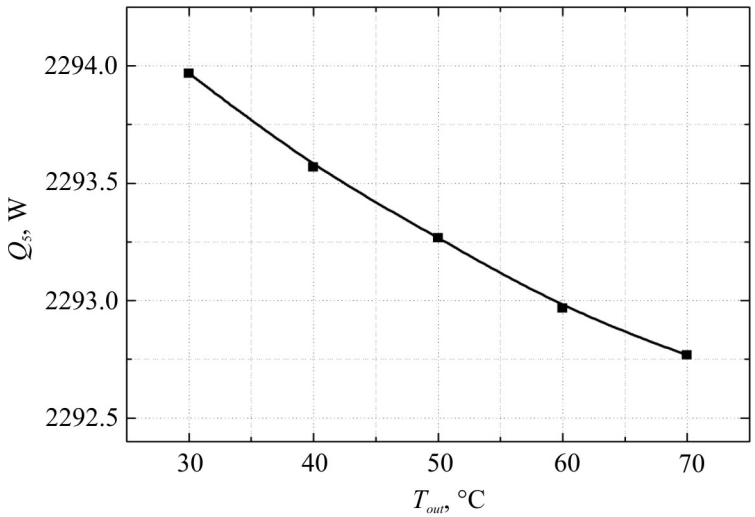

Fig. 14. Dependence of thermal power Q_5 *removed by heat carrier on heat carrier temperature* T_{out} *at the outlet of the cold heat exchangers.*

Similarly, start heating of the engine of displacement ~ 10 l and weight 750 kg will require ~ 80 min.

Under real conditions the time of engine heating will be somewhat longer which is related to heat losses due to engine heat exchange with the environment, losses of heat transfer along cooling circuit, as well as due to the availability of hydraulic resistances in the "heater-engine" system.

Conclusions

1. It is established that the output electric power of the heater 130 – 150 W is attained through use of 20 modules "ALTEC-1061" with the hot and cold side temperatures 280 – 330 °C and 30 – 70 °C, respectively. With the heater efficiency within 3 – 3.5 %, to attain such electric

power, it is necessary to spend ~ 4.3 – 4.7 kW of heat, which corresponds to fuel consumption 350 – 375 g/hour.

2. It is shown that the necessary temperature level on the hot side of thermopile is attained at gas temperature in the hot heat exchanger in the range of 370 – 400 °C, the velocity of air delivery to combustion chamber 1.3 – 1.4 m/s and the area of the heat-absorbing surface of the hot heat exchanger 0.12 m^2.
3. It is established that total thermal power transferred from the thermopile of the heater to heat carrier of the engine is ~2.9 kW. At heat carrier temperature 30 – 70 °C the start heating of engines of displacement 4 – 10 l from 0 °C to 30 ^oC will require ~ 30 – 80 min.

The author would like to express his gratitude to academician L.I. Anatychuk for the subject of the research and to junior research fellow R.M. Mochernyuk for the helpful advice on computer simulation.

References

1. V.S.Naiman, *All about Starting Pre-Heaters* (Moscow: ACT, 2007), p. 213.
2. V.Ya.Mykhailovsky, M.V.Maksymuk, Automobile Operating Conditions at Low Temperatures. The Necessity of Applying Heaters and the Rationality of Using Thermal Generators for their Work, *J.Thermoelectricity* 3, 20 – 31 (2015).
3. V.Ya.Mykhailovsky, M.V.Maksymuk, Rational Powers of Thermal Generators for Starting Pre-Heaters of Vehicles, *J.Thermoelectricity* 4, 69 – 77 (2015).
4. V.Ya.Mykhailovsky, V.V.Maksimuk, Computer Design of Thermoelectric Automobile Starting Pre-Heater Operated with Diesel Fuel, J.Thermoelectricity 1, 50 – 63 (2016).
5. http://www.webasto.com/ua.
6. http://www.inst.cv.ua.
7. L.I.Anatychuk, V.Ya.Mykhailovsky, Gas-Fuelled Two-Sectional Thermoelectric Generator, *J.Thermoelectricity* 1, 76 – 86 (2008).
8. www.comsol.com.

Submitted 28.03.2016.

V.O. Dudal, R.V. Kuz

Institute of Thermoelectricity of the NAS
and MES of Ukraine,
1, Nauky Str., Chernivtsi, 58029, Ukraine

V.O. Dudal

R.V. Kuz

TEMPERATURE DISTRIBUTIONS IN SOIL AND POSSIBILITIES OF UNDERGROUND THERMOELECTRIC GENERATORS

Computer model is created for the determination of temperature distribution in soil with a dynamic effect on the Earth surface of the diurnal solar radiation thermal power. Temperature distributions in soil for different geographic latitudes and soil types are obtained. Maximum specific electric power of underground thermoelectric generator using temperature difference in soil is determined.
Key words: temperature distribution in soil, underground thermoelectric generator.

Introduction

General characterization of the problem. The present-day problem of humankind is a search for new energy sources. Currently known energy sources are divided into renewable, namely solar energy, wind energy, hydroenergy of rivers, power from the heat in the Earth, and exhaustible energy sources, namely fossil mineral fuel and nuclear energy. The relevance of development of renewable power engineering is caused by restricted lifetime of exhaustible energy sources and their negative environmental impact [1].

Analysis of references [2 – 7] has shown that one of promising low-power electric energy sources are underground thermoelectric generators using as the source of heat thermal processes occurring in soils and on their surface.

The main indicator of soil thermal state is its temperature which is determined by solar energy input and the thermal properties of soil itself. The key thermal processes, as noted in [3], take place in the near-surface soil layer.

Soil temperature is a dynamic value which changes at different depths of soil profile in different periods of time. It is characterized by daily periodicity [8, 9] which is pronounced at shallow depth. With depth, the amplitude of temperature variation is reduced and the diurnal dynamics at the depth of 50 cm decays almost completely. The curve of the diurnal temperature variation is a wavelike line. On some days correct diurnal temperature variation is violated by non-periodic changes caused by frontal passages, mix of clouds and sun, precipitation. The diurnal temperature variation of soil is best expressed in warm season and fine weather.

With regard to the foregoing, it can be stated that a thorough analysis of the regularities of thermal processes occurring in soils will make possible an in-depth evaluation of the efficiency of underground thermoelectric generators.

The purpose of this paper is to obtain temperature distributions in various types of soil for different geographic latitudes and to determine maximum possible specific electric power of underground thermoelectric generator.

Problem formulation and its solution

To obtain temperature distribution in soil, a physical model of soil area shown in Fig. 1 was considered.

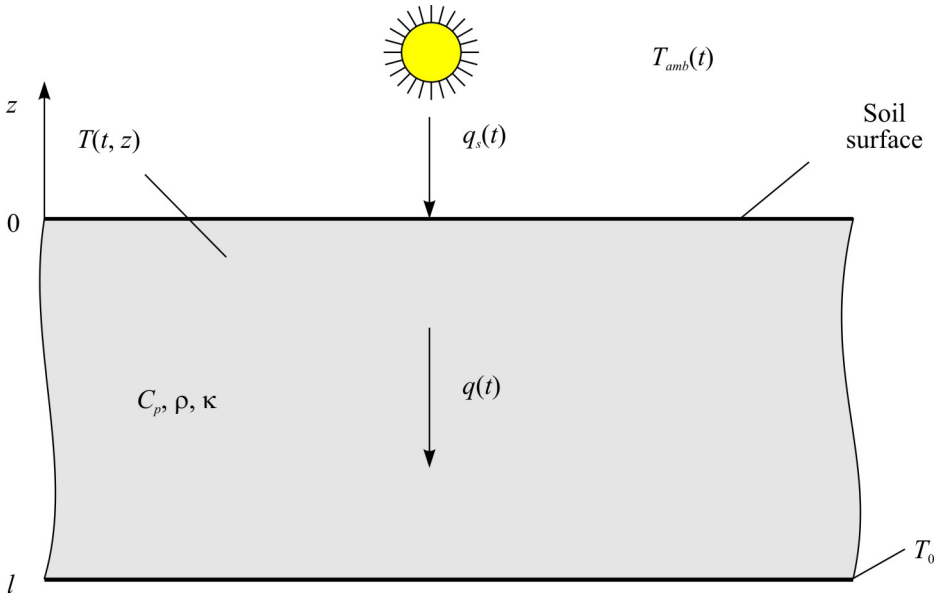

Fig. 1. Physical model of soil area.

The model considers thermal processes in soil with a dynamic effect on its surface of solar radiation thermal power $q_s(t)$ (W/m^2) within 24 hours. The properties of soil are characterized by the values of its heat capacity C_p, density ρ and thermal conductivity κ.

The model takes into account the diurnal variation of ambient temperature $T_{amb}(t)$, heat exchange between soil area with the environment due to heat transfer, convection and radiation. At certain depth l the temperature of soil T_0 is considered constant.

The sought-for values are temperature distribution in soil $T(t,z)$ and heat flux density $q(t)$ versus depth z and the time of day t.

Temperature distribution in soil stratum is described by the nonstationary Fourier's law:

$$\rho C_p \frac{dT}{dt} + \nabla\left(-\kappa \nabla T\right) = 0 . \tag{1}$$

Convective heat exchange on the soil surface is described by equation

$$-\vec{n} \cdot \vec{q} = q_0 , \tag{2}$$

where $\vec{n}$ is normal to the soil surface, $\vec{q}$ is thermal flux through the soil surface, q_0 is thermal flux from the soil surface due to convection:

$$q_0 = h\left(T_{amb} - T\right), \tag{3}$$

where h is coefficient of convection.

Radiation from the soil surface is described by the Stephan-Boltzmann law

$$q_r = \sigma\varepsilon\left(T_{amb}^4 - T^4\right), \tag{4}$$

where σ is the Stephan-Boltzmann constant, ε is surface emissivity factor.

The boundary conditions for Eq. (1) – (4) are:

– at $z = 0$ thermal flux on the soil surface $q = (1 - k_s) q_s(t)$, where k_s is soil reflection factor (albedo), $q_s(t)$ is solar radiation thermal power [10];

– at $z = l$ $T = T_0$.

Computer model for solving Eq. (1) – (4) was created in Comsol Multiphysics environment [10]. Calculation of temperature distribution in soil was done by finite element method the essence of which is that the object under study is broken up into a large number of elements, and in each of them the value of function is sought for which satisfies given second-order differential equations with the respective boundary conditions. The accuracy of solving the formulated problem depends on the level of breaking up and is assured by using a large number of finite elements.

Ambient temperature $T_{amb}(t)$ was assigned as the function of time according to averaged data of climatological observations within recent 10 years [11] for geographical points of various latitudes. For the investigation the following cities were selected: Murmansk (Russia) – 68^0 north latitude, 33^0 east longitude; Saint-Petersburg (Russia) – 60^0 north latitude, 30^0 east longitude; Chernivtsi (Ukraine) – 48^0 north latitude, 26^0 east longitude; Madrid (Spain) – 40^0 north latitude, 3^0 west longitude; Cairo (Egypt) – 30^0 north latitude, 31^0 east longitude; Yaounde (Cameroon) – 3^0 north latitude, 11^0 east longitude.

In the model, the temperature of soil at the depth of 2 m is considered to be constant and equal to + 7^0C [8]. Calculations were performed for one day – the summer solstice (June 21).

In the paper, several types of soil are analyzed. Their thermophysical characteristics are given in Table.

Table

Thermophysical characteristics of soils

Main soil component	Thermal conductivity, W/(m·K)	Heat capacity, J/(kg·K)	Density, kg/m^3	Reflection factor (albedo), %	Radiation factor, %
Clay	0.45	775	1500	23	0.8
Sand	0.52	770	1200	30 – 35	0.9
Black soil	0.63	960	1650	14	0.87

Analysis of the results and their discussion

Computer simulation was used to obtain temperature distributions in soils with a dynamic effect on their surface of solar radiation thermal power at different depths from the surface to the depth of 2 m every 10 cm.

Fig. 2 shows an example of temperature distribution in sand soil for the geographical position of Chernivtsi. Similar dependences were obtained for other geographical points and soil types. Analyzing temperature distributions shown in Fig. 2, it can be seen that the soil surface temperature has the greatest amplitude of variation. With depth, these variations decay and at the depth of 50 cm they are almost absent.

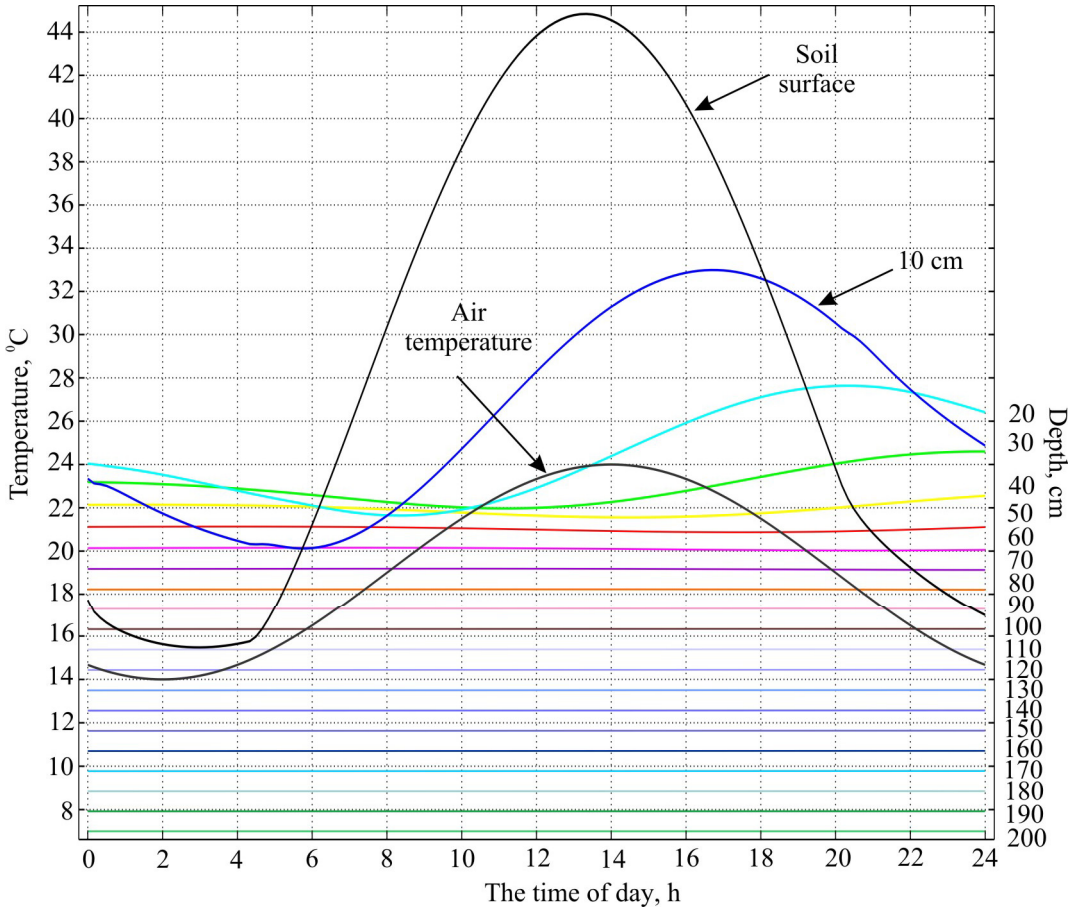

Fig. 2. Temperature distribution in sand soil for the geographical position of Chernivtsi.

Fig. 3 shows temperature distribution curves on the surfaces of sand soil, clay and black soil within 24 hours. The highest temperature is observed about 13:00 p.m. on the surface of black soil, which is attributable to its better thermophysical characteristics as compared to other considered soil types. Considering this, further analysis was made for black soil.

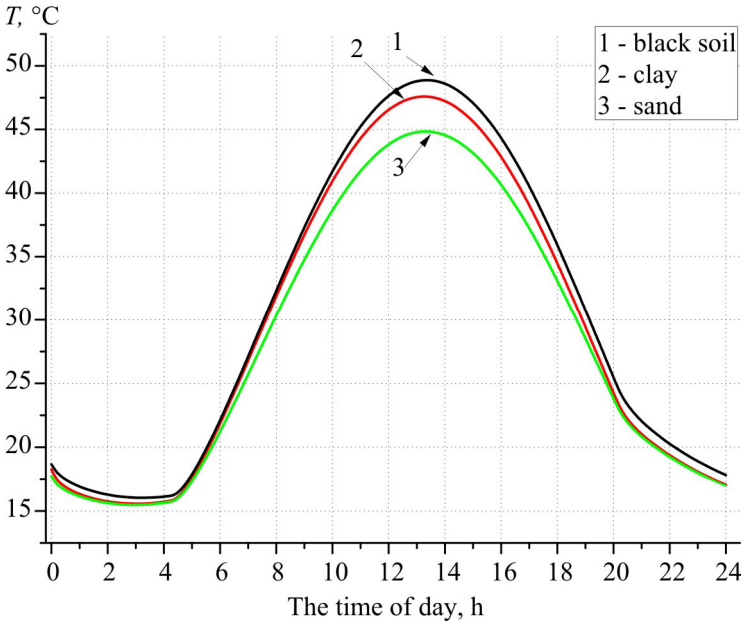

Fig. 3. Temperature distribution on the soil surface within 24 hours for different soil types.

Based on the obtained temperature distributions at different depths, temperature drops between the soil surface and the depths of 30, 40 and 50 cm were calculated (Fig. 4). As is seen from Fig. 4, temperature drops at the depths of $30-50$ cm are not essentially different. Thus, design of underground thermoelectric generator can be optimized to assure maximum economic efficiency with minimum energy losses.

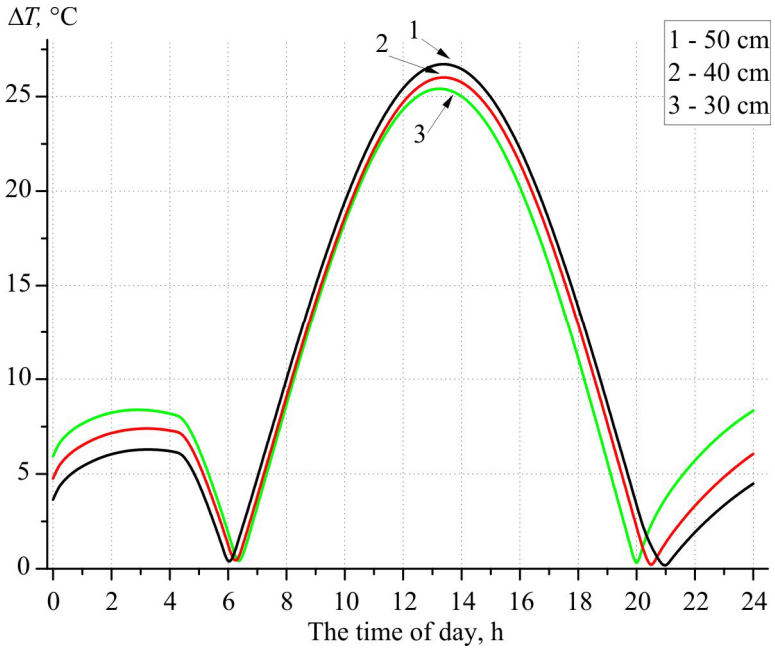

Fig. 4. Temperature drops between the soil surface and the depths of 30, 40 and 50 cm.

Specific thermal flux passing through the soil surface to the depth of 50 cm can be determined by means of expression:

$$q = \kappa \cdot \frac{(T_2 - T_1)}{L}, \tag{5}$$

where κ, L are thermal conductivity and black soil layer thickness, respectively; T_1, T_2, are temperatures of the soil surface and at the depth of 50 cm, respectively.

To calculate the efficiency of underground thermoelectric generator, one can use the expression

$$\eta = \frac{1}{4} \cdot \frac{(T_2 - T_1)}{T_2} \cdot Z \cdot \frac{(T_2 + T_1)}{2}, \tag{6}$$

where Z is the figure of merit of thermoelectric material which for calculations was $3 \cdot 10^{-3}$ K^{-1}. According to [12], the divergence between the efficiency in formula (6) and the exact values usually does not exceed 10 %.

Thus, from the formula

$$W = \eta \cdot q, \tag{7}$$

one can determine specific electric power (W) that can be obtained from underground thermoelectric generator.

Fig. 5 shows the diurnal variation of maximum possible specific electric power that can be obtained from underground thermoelectric generator under the above conditions.

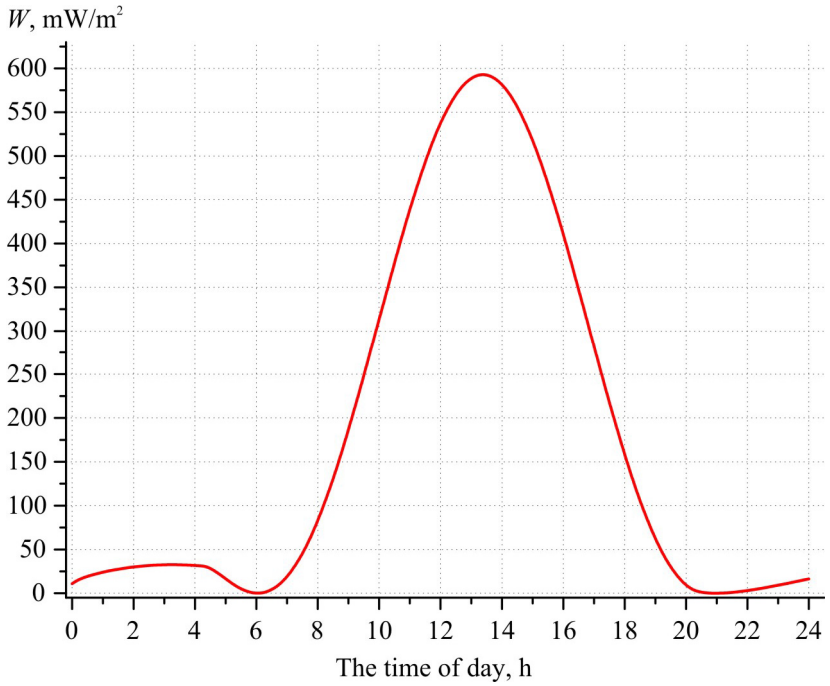

Fig. 5. Diurnal variation of maximum possible electric power of underground thermoelectric generator.

Analyzing Fig. 5, it can be said that within 24 hours the value of average specific electric power is about 300 mW/m^2. Integrating the curve of specific electric power yields total specific energy that can be obtained during a day. Fig. 6 gives the results of calculation of electric energy that can be produced by underground thermoelectric generator within 24 hours in various types of soils for different latitudes.

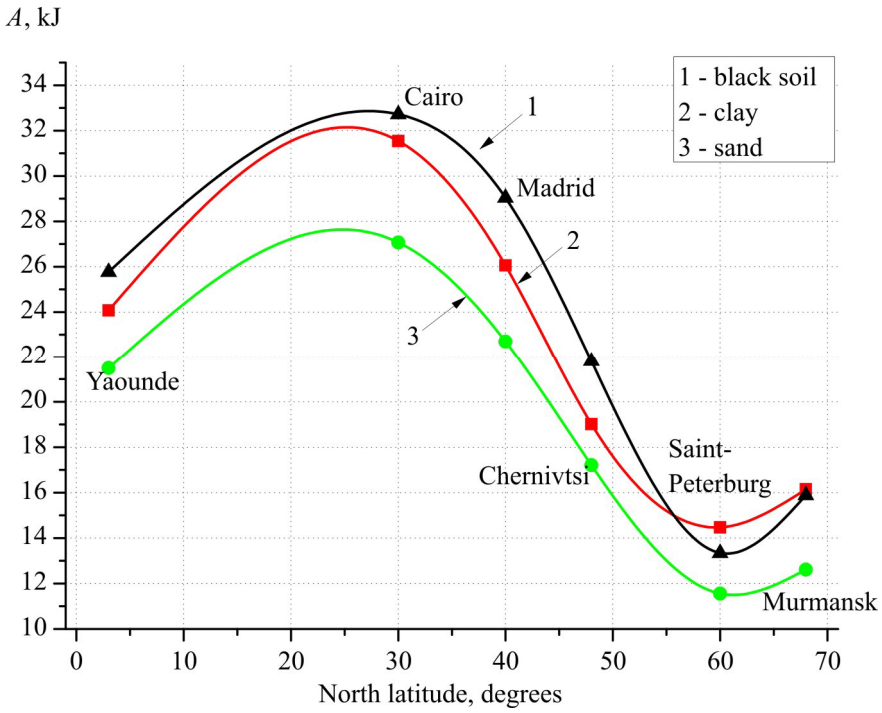

Fig. 6. Diurnal variation of maximum possible electric power of underground thermoelectric generator.

The authors would like to express their sincere gratitude to academician L.I. Anatychuk for the formulation of relevant problem and the assistance in its solution.

Conclusions

1. Computer model was created for the determination of temperature distribution in soil with a dynamic effect on the Earth surface of the diurnal solar radiation thermal power.
2. It was established that with depth the diurnal variations of soil temperature decay and at the depth of 50 cm they make less than 1 %.
3. The values of surface temperature for different types of soil were calculated. It was established that the discrepancy in the values of surface temperature of various types of soils under study does not exceed 7 %.
4. Maximum possible values of specific electric energy were calculated that can be obtained within 24 hours from underground thermoelectric generator in various types of soil for different geographic latitudes. The largest value was 32.8 kJ/m^2 at latitude 30^o N.

References

1. https://uk.wikipedia.org/wiki/Renewable Power Engineering.
2. L.I.Anatychuk, P.D.Mykytyuk, Thermal Generators Using Thermal Flows in Soils, *J.Thermoelectricity* 3, 86 – 95 (2003).
3. P.D.Mykytyuk, Devices for Thermoelectric Conversion of Thermal Energy of Soil, *Thesis for PhD in Physics and Mathematics:* 01.04.01, 2004 p.
4. P.D.Mykytyuk, N.S.Petrenko, Thermoelectric Power Supply Using the Heat of Soil, *J.Thermoelectricity* 2, 73 – 80 (2003).
5. P.D.Mykytyuk, V.O.Dudal, Testing Area for Studies of Renewable Thermoelectric Generators in Soil, *Scientific Herald of Chernivtsi University: Proceedings. Physics. Electronics*, Vol. 4, Issue 1 (Chernivtsi: Chernivtsi National University, 2015), p. 54 – 59.
6. V.O.Dudal, Peculiarities of Using Soil Thermoelectric Generators and Thermoelectric Converters for Them, *Scientific Herald of Chernivtsi University: Proceedings. Physics. Electronics,* Vol 3, Issue 2 (Chernivtsi: Chernivtsi National University, 2014), p. 75 – 81.
7. P.D.Mykytyuk, Thermal Generators with Renewable Sources of Thermal Energy, *Avtonomnaya Energetika* 26, 61 – 68 (2009).
8. V.A.Kovda, B.G.Rozanova, *Soil Science, Part 1, Soil and Pedogenesis* (Moscow: Vysshaya Shkola, 1988), 400 p.
9. V.A.Kovda, B.G.Rozanova, *Soil Science, Part 2, Types of Soils, their Geography and Use* (Moscow: Vysshaya Shkola, 1988), 368 p.
10. *Comsol Multiphysics User's Guide* (COMSOLAB, 2010), 804 p.
11. https://rp5.ua.
12. L.I.Anatychuk, *Thermoelements and Thermoelectric Devices. Reference Book* (Kyiv:Naukova Dumka, 1979), 767 p.

Submitted 18.04.2016.

V.V. Lysko

V.V. Lysko

Institute of Thermoelectricity of the NAS and MES of Ukraine,
1, Nauky Str., Chernivtsi, 58029, Ukraine

THE TEMPERATURE DEPENDENCES OF ERRORS IN MEASURING THERMAL CONDUCTIVITY BY THE ABSOLUTE METHOD

The results of studying the errors in measuring thermal conductivity by the absolute method in the range from room temperature to 900 C are presented. The main sources of errors in measuring thermal conductivity are investigated for different temperatures whereby measurement is performed. It is established that the greatest contribution to measurement error is made by radiation from the surface of samples and the reference heater. The efficiency of using the existing methods for reduction of such errors in different temperature ranges is considered. It is established that at temperatures up to 550 °C the best variant is to use radiation screens of special design, and at temperatures from 550 to 900 °C it is more efficient to use gradient thermal screens filled with heat insulating powders.

Key words: measurement, absolute method, thermal conductivity, errors.

Introduction

General characterization of the problem. Creation of thermoelectric materials, efficient in different temperature ranges, is one of important problems of thermoelectricity [1 – 3]. Its solution requires high-precision methods and equipment for measuring the temperature dependences of thermoelectric properties of materials.

Analysis of the literature. With regard to possible values of errors, measuring thermal conductivity is the most complicated process. In [4 – 7] it is shown that the most efficient method to assure acceptable accuracy of thermal conductivity measurement is the absolute method (Fig. 1). However, when using this method, particular attention must be paid to creation of conditions for an ideal physical model, namely adiabaticity and uniformity of heat flux through the sample.

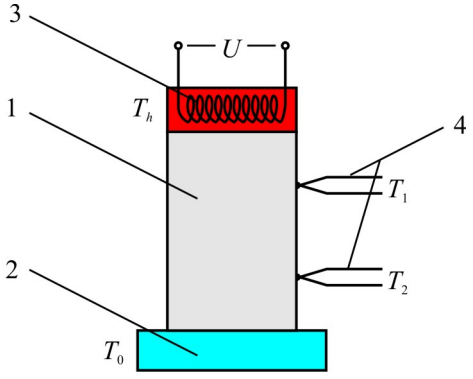

Fig. 1. Schematic of the absolute method 1 – sample under study; 2 – thermostat; 3 – reference heater; 4 – thermocouples.

In [6, 7], a real physical model of the absolute method is constructed that takes into account all

main sources of errors of the absolute method – radiation from the surfaces of the sample and the reference heater, heat removal along the conductors of thermocouples, current and potential electrodes of the heater, the non-point character of measuring thermocouples, low quality thermal contacts between the sample and the heater and thermostat, etc. Using the methods of object-oriented computer simulation, temperature distributions in the sample and structural members of measuring installation were obtained and possible measurement errors were studied. They may be divided into two main groups. The first group is related to losses of heat from the sample and the reference heater along the pressure mechanism and conductors – thermocouples, current and potential electrodes of the heater. For their minimization it is proposed to use the so-called thermal switches. These are units made of thermally conductive insulators, such as beryllium oxide, whose thermal conductivity is close to copper thermal conductivity. They have embedded electrodes which are brought into thermal contact with ceramics. The latter, in turn, is in thermal contact with the radiation screen. In this case the temperature difference on the electrodes is considerable, heat flux through the electrodes is minimized and the values of errors are minimized accordingly. Computer simulation has shown that total error due to these losses will be ~ 0.5 %. Besides, an important factor causing the errors is the influence of current and thermal contacts of the sample. With the use of pressure contacts, the heater touches the sample at least in three places, which can distort the uniformity of thermal and electric fluxes. The latter will influence the distribution of temperature and electric potential in the sample. Optimization calculations and computer simulation showed that leveling of heat flux density requires metallization of sample ends. The optimal set of metal coatings was determined: *Ni* ~ 10 μm, *Cu* ~ 100 μm, *Ni* ~ 10 μm. Also, computer simulations of thermal field distortions at points of sample contact to measuring probes were performed. It was established that even with contact diameters 0.1 – 0.5 mm the probes average the temperature, yielding rather precise value, as with a point contact. The error in this case does not exceed 0.05 %.

Another group of errors is caused by thermal radiation from the surfaces of the sample and the reference heater. These errors, according to investigations, are the greatest and can reach 75 %. For the minimization of these errors it is recommended to use special radiation screens with rings and a shining reflector on the surface of the thermostat. The error in measuring thermal conductivity in this case at temperatures to 500 °C is not more than 2.4 %. The efficiency of using such screens at higher temperatures, when heat fluxes due to radiation increase drastically, is not investigated.

In [8], to eliminate the losses of heat due to radiation at high temperatures, it is proposed to use powder heat insulating materials for filling the space between the sample and the thermostat, and in [9, 10] – to use in addition a protective heater whose temperature must be maintained equal to that of the reference heater.

The purpose of this paper is to study the efficiency of using various techniques to reduce the errors in measuring thermal conductivity by the absolute method in a wide temperature range and to decide on the optimal ones for the measuring equipment designed for some or other operating temperature range.

Using radiation screens at temperatures to 900 °C

A physical model of measuring cell for the case of using special radiation screens with rings is given in Fig. 2. The model comprises a cylinder sample of length l and diameter d, a reference heater, a thermostat and a screen with a heater. The temperature of the thermostat is T_0, of the reference and screen heaters – T_h; the thermal conductivity of sample material is κ_1, of the reference heater – κ_2, of

the screen – κ_3, of the screen heater – κ_4; the absorption factor of the sample is ε_1, of the reference heater – ε_2, of the screen – ε_3, of the screen heater – ε_4, of the thermostat – ε_5.

The model takes into account: heat exchange due to radiation between the surfaces of the sample, the screen, the heaters and the thermostat; heat transfer along the sample and the screen; heat exchange due to radiation between the screen and the thermostat, heat fluxes along the conductors of the thermocouples, the electrodes of the heaters, etc.

To find temperature distribution in measuring equipment, it is necessary to solve a system of thermal conductivity equations for each of its components

$$\nabla(-\kappa_i \nabla T) = Q_i, \tag{1}$$

where Q_i is the power of internal heat sources.

This problem was solved with the use of COMSOL Multiphysics applied program package.

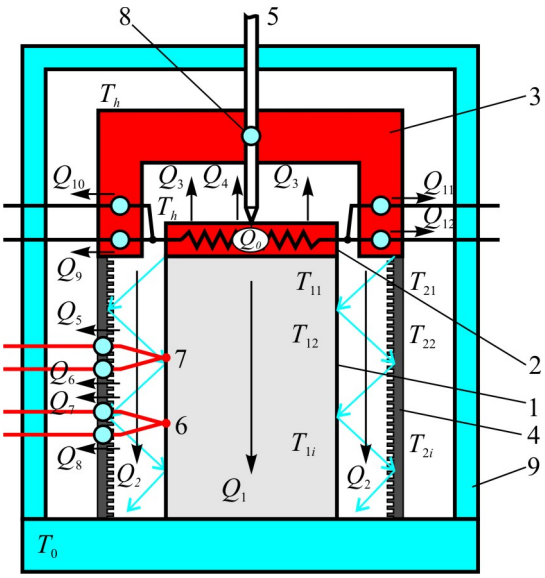

Fig. 2. Physical model of a device for measuring thermal conductivity by the absolute method with the use of special radiation screen. 1 – sample under study; 2 – reference heater; 3 – screen heater; 4 – radiation screen; 5 – pressure mechanism; 6, 7 – thermocouples; 8 – thermal switches; 9 – thermostat.

The boundary conditions that take into account heat exchange due to radiation between the elements of measuring system

$$q = \varepsilon_i (G - \sigma T^4), \tag{2}$$

where σ is the Stephan-Boltzmann constant, G is heat flux due to radiation

$$G = G_m + F_{amb} \sigma T_{amb}^4, \tag{3}$$

G_m is heat flux from other device components, F_{amb} is ambient view factor equal to part of ambient view that is not subject to other surfaces, T_{amb} is temperature at a distant point in directions included into F_{amb}. Coefficient G_m which depends on mutual arrangement of surfaces is calculated by introducing into computer model of additional variable J assigned by equation

$$J = (1-\varepsilon)\left\{G_m(J) + F_{amb}\sigma T_{amb}^4\right\} + \varepsilon\sigma T^4. \tag{4}$$

Results of optimization of a device for measuring thermal conductivity in the range from room temperature to 500 °C are discussed in detail in [9]. With expansion of the operating temperature range of measurement the role of radiation will grow. Fig. 3 shows the values of errors in measuring thermal conductivity δκ for different thermal conductivity values of sample under study. It is seen that even with the use of radiation rings on the screen and a reflector on thermostat, the errors at higher than 600 °C temperatures increase considerably and reach 25 – 30 %.

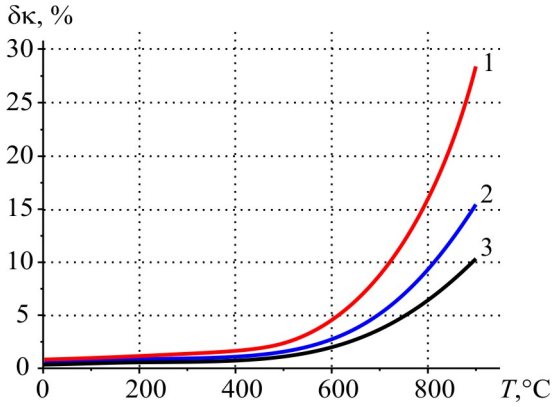

Fig. 3. Temperature dependences of the errors in measuring thermal conductivity for different thermal conductivity values of the sample (1 – κ_1 = 2 W/(m·K); 2 – κ_1 = 4 W/(m·K); 3 – κ_1 = 6 W/(m·K)).

The results obtained testify to low efficiency of radiation screens at such temperatures and the necessity to use additional measures for reduction of heat losses.

Using powder thermal insulating materials

A physical model for this case is given in Fig. 4. Unlike the previous case, there is no radiation screen and screen heater, and the space between the sample and the thermostat is filled with thermal insulation. Thermal switches are transferred from the screen to thermostat case.

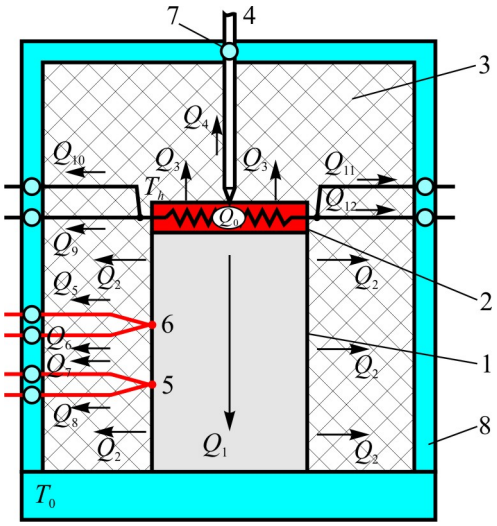

Fig. 4. Physical model of a device for measuring thermal conductivity by the absolute method with the use of powder heat insulating materials.
1 – sample under study, 2 – reference heater, 3 – powder heat insulating material, 4 – pressure mechanism, 5, 6 – thermocouples, 7 – thermal switches, 8 – thermostat.

Fig. 5 shows the temperature dependences of the error in measuring thermal conductivity for different thermal conductivity values of the sample under study obtained by computer simulation. As can be seen from the figure, the use of heat insulating powder materials for the reduction of heat losses from the surface of the samples becomes more efficient than radiation screens only at higher than 600 °C temperatures, however, the values of errors remain high – over 20 %. The reasons for this are residual losses due to thermal conductivity through heat insulating powder, as well as increasing losses in conductors when transferring thermal switches from the screen and the screen heater to the thermostat.

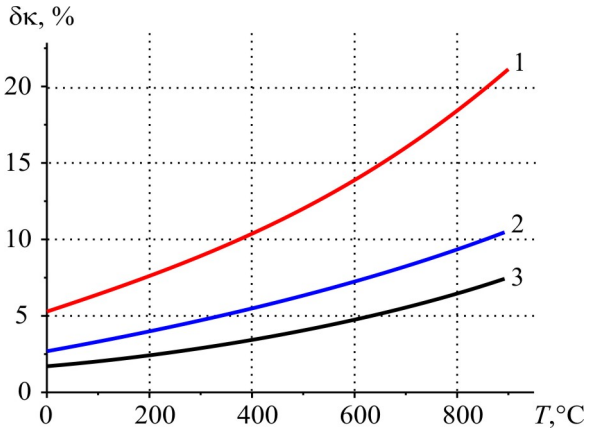

Fig. 5. The temperature dependences of the error in measuring thermal conductivity for different thermal conductivity values of sample under study ($1 – \kappa_1 = 2$ W/(m·K); $2 – \kappa_1 = 4$ W/(m·K); $3 – \kappa_1 = 6$ W/(m·K)).

To reduce the losses due to the use of heat insulating powder, it is reasonable to introduce a protective heater into the measuring cell (Fig. 6).

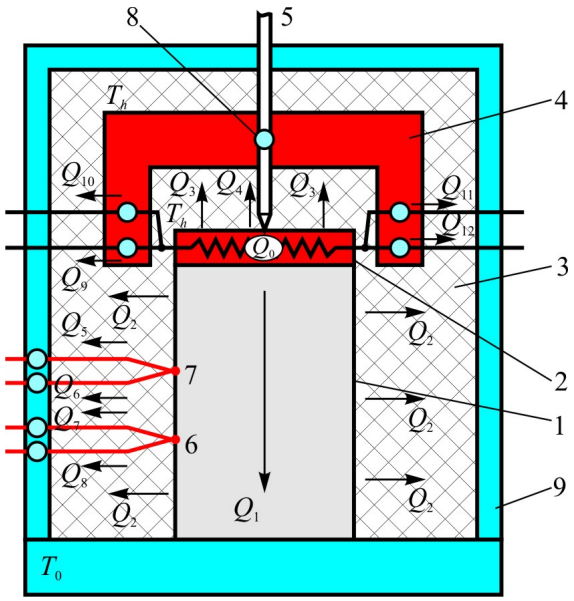

Fig. 6. Physical model of a device for measuring thermal conductivity by the absolute method with the use of powder heat insulating materials and protective heater. 1 – sample under study, 2 – reference heater, 3 – powder heat insulating material, 4 – protective heater, 5 – pressure mechanism, 6, 7 – thermocouples, 8 – thermal switches, 9 – thermostat.

The temperature dependences of the error in measuring thermal conductivity for this case are given in Fig. 7.

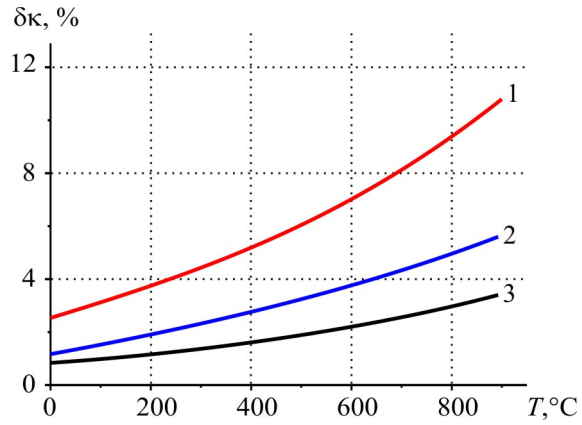

Fig. 7. The temperature dependences of the error in measuring thermal conductivity for the case of using heat insulating powder and protective heater (1 – κ_1 = 2 W/(m·K); 2 – κ_1 = 4 W/(m·K); 3 – κ_1 = 6 W/(m·K)).

The use of additional protective heater allows reducing measurement error to ~ 11 %.

The use of gradient thermal screens filled with heat insulation

The case is considered when heat insulating powder is filled into the space between the sample and gradient thermal screen (Fig. 8).

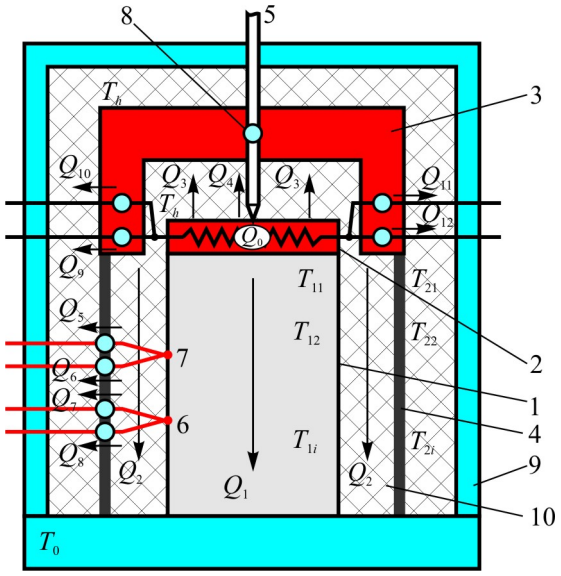

Fig. 8. Physical model of a device for measuring thermal conductivity by the absolute method with the use of gradient thermal screens filled with heat insulating powder materials. 1 – sample under study, 2 – reference heater, 3 – screen heater, 4 – gradient thermal screen, 5 – pressure mechanism, 6, 7 – thermocouples, 8 – thermal switches, 9 – thermostat, 10 – heat insulating powder.

The temperature dependences of the error in measuring thermal conductivity for this case are given in Fig. 9. As can be seen from the figure, at high temperatures the error in measuring thermal

conductivity for the sample with thermal conductivity 2 W/(m·K) does not exceed 5.5 %, which is the best parameter of those given above.

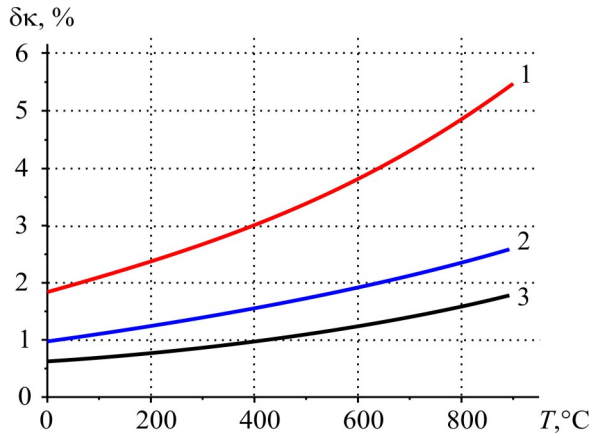

Fig. 9. The temperature dependences of the error in measuring thermal conductivity for the case of using gradient thermal screens filled with heat insulating powder materials (1 – κ_1 = 2 W/(m·K); 2 – κ_1 = 4 W/(m·K); 3 – κ_1 = 6 W/(m·K)).

Fig. 10 gives a comparison between the temperature dependences of the errors in measuring thermal conductivity for two cases, namely the use of a radiation screen and a gradient thermal screen filled with heat insulating powder (for sample with thermal conductivity 2 W/(m·K)). As is evident from the figure, at temperatures over 550 °C the lower values of errors are typical for the case of using a gradient thermal screen filled with heat insulating powder – the error in measuring thermal conductivity can be reduced to 5.5 %. However, at lower temperatures radiation screens remain more efficient.

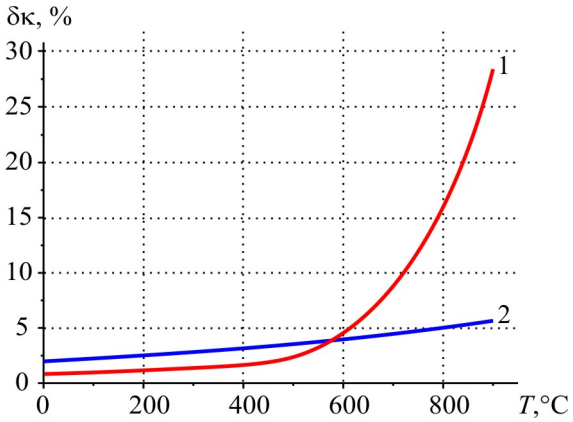

Fig. 10. Comparison of the temperature dependences of the errors in measuring thermal conductivity for the case of using a radiation screen (1) and a gradient thermal screen filled with heat insulating powder (2).

Therefore, in the temperature range of 30 – 550 °C the best will be measuring equipment that employs special radiation screens for the reduction of heat losses, and in the range of 550 – 900 °C – the equipment where these screens are additionally filled with heat insulation.

Conclusions

1. The errors in measuring thermal conductivity by the absolute method from room temperature to 900 °C were investigated. It was established that with the use of special radiation screens alone

for minimization of heat losses from the surface of the sample measurement errors at temperatures above 550 °C drastically increase and reach 30 %.

2. It was established that the use of heat insulating powder materials becomes efficient for reduction of thermal losses from the surface of the samples only at temperatures higher than 550 °C, however, the values of errors remain high – over 20 %. They can be reduced to ~ 11 % through use of additional protective heater.
3. It was established that at temperatures higher than 550 °C the efficient method for thermal losses reduction is the use of gradient thermal screens filled with heat insulating powder materials. The error in measuring thermal conductivity in this case can be reduced to ~ 5.5 %.

References

1. T.Caillat, A.Borshchevsky, J.-P.Fleurial, Search for New High Temperature Thermoelectric Materials, *SAE TechnicalPaper* 929424 (1992).
2. Jin-Cheng Zheng, Recent Advances on Thermoelectric Materials, *Front. Phys. China* **3** (3), 269 – 279 (2008).
3. J.R.Sootsman, D.Y.Chung, and M.G.Kanatzidis, New and Old Concepts in Thermoelectric Materials, *Angewandte Chemie International Edition* **48** (46), 8616 – 8639 (2009).
4. L.I.Anatychuk, M.V.Havrylyuk, and V.V.Lysko, Installation for Measuring Properties of Semiconductor Thermoelectric Materials, *J.Thermoelectricity* 3 (2010).
5. L.I.Anatychuk, M.V.Havryliuk, and V.V.Lysko, Absolute Method for Measuring of Thermoelectric Properties of Materials, *Materials Today: Proceedings* 2, 737 – 743 (2015).
6. L.I.Anatychuk, V.V.Lysko, Investigation of the Effect of Radiation on the Precision of Thermal Conductivity Measurement by the Absolute Method, *J.Thermoelectricity* 1, 67 – 76 (2012).
7. L.I.Anatychuk, V.V.Lysko, On Improvement to the Accuracy and Speed in the Process of Measuring Characteristics of Thermoelectric Materials, *Journal of ElectronicMaterials* 43 (10), 3863 – 3869 (2014).
8. A.V.Petrov, *Methods for Measuring Thermal Conductivity of Semiconductors at High Temperatures. Thermoelectric Properties of Semiconductors* (Moscow-Leningrad, AN SSSR Publ., 1963), P. 27 – 35.
9. A.S.Okhotin, A.S.Pushkarsky, R.P.Borovikova, and V.A.Simonov, *Methods for Measuring Characteristics of Thermoelectric Materials and Converters* (Moscow: Nauka, 1974).
10. H.Czichos, T.Saito, and L.Smith, *Springer Handbook of Metrology and Testing* (Springer, 2011), 1500 p.

Submitted 12.04.2016.

T.A. Ismailov, I.Sh. Mispakhov, O.V. Yevdulov, D.V. Yevdulov

Federal State Budgetary Educational Institution of Higher Professional Education "Dagestan State Technical University", 70, Imam Shamil avenue, Makhachkala, 367015, Russia

THERMOELECTRIC DEVICE FOR SHORT-TERM STORAGE AND TRANSPORTATION OF BIOLOGICAL MATERIALS

A design of thermoelectric device prototype for short-term storage and transportation of biological substances realized on the basis of multi-stage thermopile is considered. The specific feature of the device is possibility of simultaneous short-term storage and transportation of several types of biological objects having different storage temperatures. Dependences of temperature variation with time at device control points are represented for different values of thermopile supply currents, types of fillers for compartments with biological material and ambient temperatures. It is established that storage temperature requirements of biological material can be assured through use of standard thermoelectric modules. In so doing, it is advisable to fill in the compartment for storage of biological substance with high thermal conductivity filler.

Key words: thermoelectric device, biological material, short-term storage and transportation, prototype, experimental studies, measurement.

Introduction

Biological material, such as cells, blood, early embryos, tissue samples, etc. in normal conditions is subject to changes and degradation. Its long survival is possible only with the use of low temperatures. Large repositories of biological objects mainly employ equipment which is based on liquid nitrogen [1]. This fact allows providing stable level of biomaterial storage temperatures, the cost of maintenance of this equipment consisting only in regular replenishment of liquid nitrogen. However, in case of small storage spaces for biological substances the use of equipment based on liquid nitrogen is less advantageous. This is because while storing and freezing of a small amount of biological material the employed technical facilities have small volumes (several tens of liters). At the same time, nitrogen replenishment in the repository of biomaterials requires additional storage facilities for a large amount of liquid nitrogen or a regular purchase of small amounts thereof from relevant manufacturers.

The task of storing biological substances in medical institutions remote from large repositories of liquid nitrogen is solved with the aid of self-contained refrigerating plants [2]. As such, use is made of systems based on mixed-refrigerant Klimenko cycle, as well as cascade freon installations [3, 4]. One of essential drawbacks of such installations is the availability of a semihermetic compressor which leads to permanent leaks of working agent and the necessity of its periodic charging. Another weak point is the use of several compressors which reduces the reliability of such systems. Besides, the above systems require high maintenance costs and have high specific cost per unit of stored biological material.

The above discussed biological material storage systems have the limitations of period of service, since they require replenishment of the volume of liquid nitrogen used therein. Moreover, in

the cases under study simultaneous transportation in one system of biological substances with different storage temperatures is impossible (for instance, stem cells have storage temperature 223 K, blood – 281 K, specimens of liver, splin, lung – 277 K [5]). The above restrictions can be removed by using as the source of cold in biological material storage devices of thermopiles that can assure the required temperature conditions of the objects in transportation, are characterized by long service life, environmental friendliness, possibility of temperature control in the volume. However, the existing designs of thermoelectric devices of this type [6, 7] cannot assure simultaneous storage and transportation of several types of biological substances having different storage temperatures. Under these conditions it is reasonable to develop and thoroughly study a thermoelectric device which allows removing the above drawbacks of existing devices for storage and transportation of biological materials.

The purpose of the work is experimental study of thermoelectric device design for short-term storage and transportation of biological materials providing for possible simultaneous transportation of several types of biological objects with different storage temperature requirements.

Design of thermoelectric device prototype and experimental bench

Heat exchange processes were studied on a prototype model of thermoelectric device (Fig. 1) [8], comprising thermally insulated package 1 with cover 2. Inside the package there is a chamber divided into two thermally insulated from each other compartments 3 whose volume can be filled with various fillers (metal honeycomb structures, nets, chips, etc.). The bottom of each compartment is in good thermal contact with thermopile 4. The first compartment in is contact with single-stage thermopile of the type TURBO-1.3-Parallel, and the second compartment – with two-stage thermopile of the type TB-2-(127-127)-1.15 (both thermopile types manufactured by Open Joint-Stock Company “Cryotherm” (Saint-Petersburg) [9]).

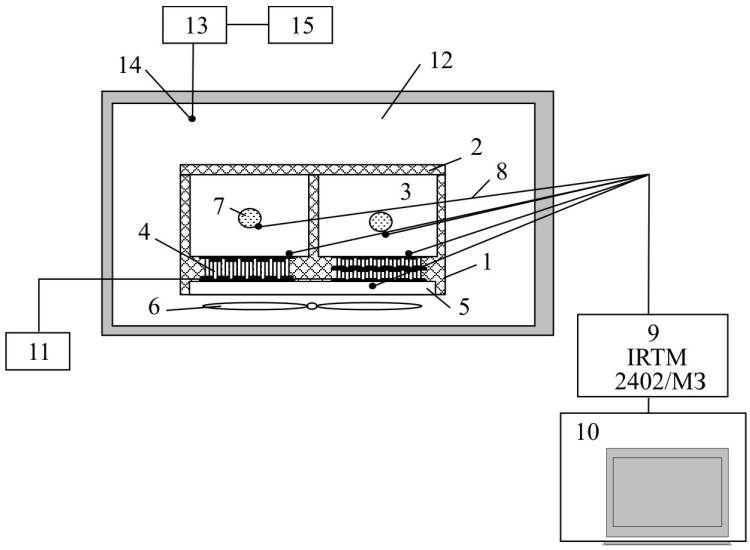

Fig. 1. Basic diagram of experimental stand.

Heat removal from the hot junctions was done by air heat sink comprising a plate heat exchanger system 5 and fan unit 6. In the experiment, each of the compartments was filled with biological material simulator 7, in which capacity gelatin was used. The appearance of prototype model of thermoelectric device is shown in Fig. 2.

Fig. 2. Appearance of thermoelectric device prototype for storage and transportation of biological material.

The values of temperature at design representative points were measured by means of copper-constantan thermocouples 8 whose reference junctions were placed in Dewar vessel filled with melting ice. Signals from the thermocouples through multichannel switch came to measuring system 9 from which the values of measured signal were passed to personal computer 10. The measuring system used was IRTM 2402/ M3 10.

Thermopiles were powered from controlled multi-channel electric power supply 11 whose current value and voltage drop were controlled by means of embedded voltmeter and ammeter.

When performing experimental studies, the thermoelectric device prototype was placed into thermally insulated climatic chamber 12 where the assigned temperature and relative humidity were regulated by control unit 13 related to temperature and humidity sensor 14 whose readings were displayed on digital panel 15.

The experiments were conducted in series, four experiments each, under identical conditions.

The main task when performing experimental studies of device prototype was to determine the time dependence of temperature variation at different points of object under study at fixed values of thermopile supply current, using various fillers for compartments with biological material, as well as variable ambient temperature values. It was important to compare the resulting experimental data to theoretical ones with a view to verify the adequacy of mathematical model.

Results of experimental studies

Fig. 3 presents temperature variation at control points of thermoelectric device prototype for supply current of single-stage thermopile 5 A and two-stage thermopile – 8 A. The control points considered were biological materials and thermopile cold junctions. From the presented data it follows that in the absence of any filler in the compartment with biological substance the difference in temperatures between this substance and the cold junctions of thermopile is significant. With the above values of supply current this difference is of the order of 8 K when thermoelectric device reaches the steady state. This fact necessitates the use of various fillers increasing the effective coefficient of heat transfer between compartment walls and biological material.

Characteristics of temperature variation of biological material simulator with time were obtained for various supply currents of single-stage and two-stage thermopiles. These dependences allow estimating possible temperature levels for storage of biological materials with the use of concrete type of thermopile.

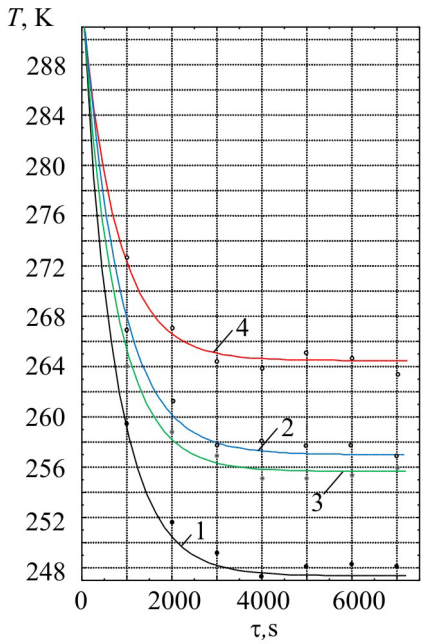

Fig. 3. Temperature variation at control points of thermoelectric device prototype with time for supply current of single-stage thermopile 5 A, two-stage thermopile – 8 A: 1 – cold junction temperature of two-stage thermopile, 2 – temperature of biological material simulator cooled by two-stage thermopile, 3 – cold junction temperature of single-stage thermopile, 4 – temperature of biological material simulator cooled by single-stage thermopile.

According to the results, increase in supply current of each thermopile to its maximum value reduces the temperature of biological substance. Thus, increase in supply current of two-stage thermopile from 4 to 8 A reduces the temperature of biological material from 266 to 257 K, increase in supply current of single-stage thermopile from 3 to 7 A reduces the temperature of biological object from 270 to 261 K. So, with the optimal value of supply current for each thermopile used, maximum reduction of biological object temperature is 257 K (compartment with two-stage thermopile) and 261 (compartment with single-stage thermopile). As previously stated, the temperature condition of biological substance is considerably affected by the heat exchange inside the corresponding storage compartment. In the absence of fillers, in the container for storage of biological material there is a natural convective heat exchange between the cooled walls of container and biological material. Exactly for this reason in thermoelectric device there is a considerable difference in temperatures between thermopile cold junctions and cooled biological substances. For its reduction it is reasonable to use various fillers making heat exchange in compartment more rapid. Variants when copper and aluminum honeycomb structures were introduced into compartment for storage of biological material were considered. The results obtained for a compartment with two-stage thermopile are represented in the plots of Fig. 4. In conformity with them, introduction of the aforesaid fillers into the space between biological material and compartment walls reduces considerably the difference in temperatures between them. Thus, introduction of aluminum honeycomb structure reduces the temperature of biological object by 4.5 K and copper honeycomb structure – by 6.5 K as compared to thermoelectric device operation without either of them.

In this case, where there are no restrictions for thermoelectric device structural weight, the most preferable variant is filling of space with narrow-meshed net or copper grit.

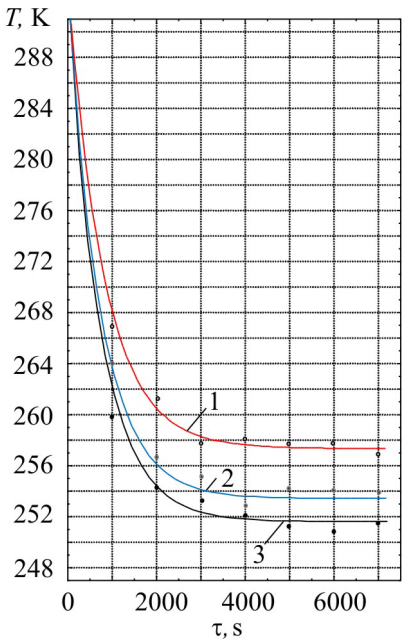

Fig. 4. Temperature variation of biological material simulator with time for supply current of two-stage thermopile 8 A and various types of fillers, 1 – no filler is used, 2 – filler of aluminum honeycomb structure, 3 – filler of copper honeycomb structure.

The reliable operation of thermoelectric device depends largely on the effective heat pickup from thermopile reference junctions. To estimate the possibilities of heat pickup from thermopile hot junctions, Fig. 5 presents the data on temperature variation with time of finned heat exchanger of thermoelectric device with cooling effect for different values of thermopile supply current.

From the plots it follows that the value of temperature of thermopile hot junctions is quite acceptable for the type used (for supply current of two-stage thermopile equal to 7 A, the hot junction temperature of the latter is about 312 K). This fact determines rather efficient heat pickup under conditions considered from thermopile hot junctions and is a good indicator of reliable operation of developed device at biological material transportation.

To estimate the influence of external conditions on the work of thermoelectric device, the dependences of biological object temperature variation with time were plotted for different values of ambient temperature (Fig. 6). From the presented data it follows that ambient temperature increase by 10 K raises the temperature of cooled biological object not more than by 1 K with selected type of thermal insulation. This fact suggests no need for using special measures for thermal insulation in thermoelectric device.

According to the results of experiments, correlation of calculated [10] and experimental data was performed. Apart from the experimental points, Fig. 3 – 6 also show the results of theoretical research.

There is a satisfactory agreement between calculated and experimental data, their maximum discrepancy not exceeding 7 – 7.5 °C. The greatest deviation of calculated data from the experiment is mainly observed during time interval related to the onset of regime by the system which is determined by the environmental effect and non-perfect thermal insulation of “device-target object” system, as well as by certain parameter spread of thermopile and measuring instruments. What is more, in case of reaching the lowest temperatures the experimental data show the greatest deviation from theory. This fact is mainly due to imperfection of thermal insulation, which does not satisfy conditions assumed in mathematical models, and, hence, heat inputs to device.

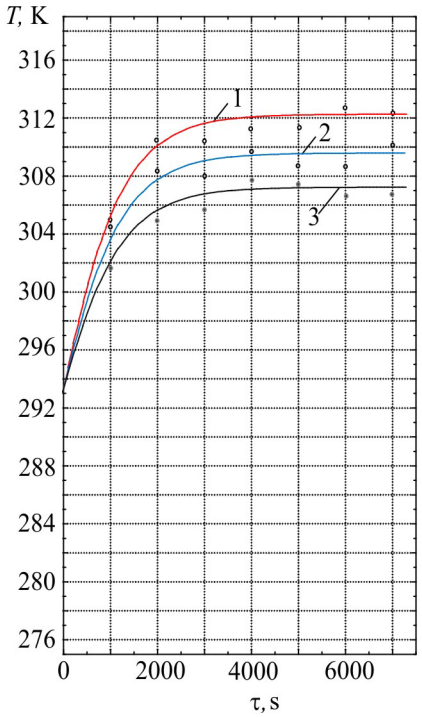

Fig. 5. Temperature variation of thermopile hot junction with time for various supply currents of two-stage thermopile, 1 – I = 3 A, 2 – I = 5 A, 3 – I = 7 A.

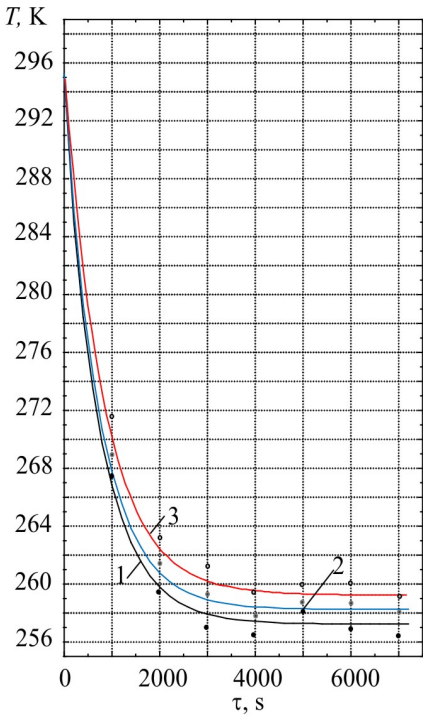

Fig. 6. Temperature variation of biological material simulator with time for supply current of two-stage thermopile 8 A and various ambient temperatures, 1 – Tamb = 293 K, 2 – Tamb = 303 K, 3 – Tamb = 313 K.

Conclusions

1. A thermoelectric device for short-term storage and transportation of biological substances is proposed which makes possible simultaneous transportation of several types of biological objects having different storage temperatures. In so doing, various storage temperature requirements of biological objects are maintained through integration of their compartments with different types of thermopiles, including multi-stage ones.
2. Dependences of temperature variation at control points of thermoelectric device prototype with time were obtained for different values of thermopile supply currents, types of fillers for compartments with biological material, ambient temperatures.
3. In conformity with the results, the increase in supply current of each thermopile to its maximum value reduces the temperature of biological substance. With the optimal value of supply current under experimental conditions it was established that for each thermopile used maximum temperature reduction of biological object is 257 K (compartment with two-stage thermopile) and 261 (compartment with single-stage thermopile).
4. For a more rapid heat transfer from thermopile to biological object it is advisable to fill its storage compartment with high thermal conductivity filler in the form of honeycomb structure, net, grit.
5. As a result of the experiments it was established that standard thermoelectric modules can be used to assure storage temperature requirements of biological material.
6. The results obtained suggest that ambient temperature increase has a slight influence on the temperature condition of biological object in proposed embodiment of thermoelectric device,

which enables one not to take special measures for thermal insulation of device.

7. The experimental results show a satisfactory agreement with calculated results, their maximum deviation from the theoretical values not exceeding 7 – 7.5 °C.

References

1. A.B.Smolyaninov, G.N.Kovan'ko, Sh.M.Bagautdinov, and O.G.Khurtsilava, Cryopreservation and Cryostorage of Stem Cells in Umbilical Blood and Bone Marrow Banks, *Vestnik of the International Academy of Refrigeration* 2 (2009) P. 38 – 43.
2. A.V.Nechotkiy, V.N.Vilyaninov, S.P.Kaleko, Sh.M.Bagautdinov, and G.I.Petrenko, Organizational Aspects of Using Low-Temperature Technologies of Modern Occupational Transfusiology, *Vestnik of the International Academy of Refrigeration* 2 (2005) P. 34 – 39.
3. D.A.Ivolgin, A.B.Smolyaninov, Sh.M.Bagautdinov, K.V.Korovina, K.V.Shun'kina, and A.V.Smirnova, Modern Methods of Cryopreservation of Stem Cells of Umbilical Blood for Social Register of Donors, *Vestnik of the International Academy of Refrigeration* 1 (2012) P. 36 – 39.
4. I.M.Kal'nin, K.N.Fadekov, Performance Evaluation of Thermodynamics of Cycles of Vapor Compression Refrigerating Machines and Heat Pumps, *Kholodil'naya Tekhnika* 3 (2006) P. 6 – 25.
5. A.V.Chechyotkin, V.N.Vilyaninov, and Sh.M.Bagautdinov, Low-Temperature Storage Technologies of Blood and Bone Marrow Cells, *Zdravookhraneniye i Meditsinskaya Teknika,* 18(4), (2005).
6. L.P.Bulat, Applied Research and Developments in the Field of Thermoelectric Refrigeration in Russia, *Kholodil'naya Tekhnika* 7 (2009) P. 34 – 37.
7. S.O.Filin, B.Zakshevsky, Current Status and Prospects for the Development and Manufacture of Stationary Thermoelectric Coolers, *J.Thermoelectricity* 2, 74 – 88 (2008).
8. *Patent RF for Invention №2416769*, Thermoelectric Thermostat for Storage and Transportation of Biomaterials// T.A.Ismailov, I.Sh.Mispakhov, O.V.Yevdulov, and Sh.A.Yusufov, Bul. №11 of 20.04.2011.
9. http://www.kryotherm.spb.ru.
10. T.A.Ismailov, I.Sh.Mispakhov, O.V.Yevdulov, and M.A.Khazamova, Study of Thermophysical Processes in the System of Short-Term Storage and Transportation of Biological Materials, *Vestnik of the International Academy of Refrigeration* 3 (2014) P. 74 – 88.

Submitted 05.05.2016.

NEWS
OF INTERNATIONAL THERMOELECTRIC ACADEMY

GRIGORIY ARAMOVICH ARAKELOV

On June 07, 2016, Grigoriy Aramovich Arakelov – a well-known expert in non-standard applications of thermoelectric cooling, a Corresponding Member of the International Academy of Refrigeration, a Corresponding Member of the International Thermoelectric Academy died in his 71 st year.

Grigoriy Aramovich Arakelov was born on September 22, 1945, in Baku city in the Azerbaijan SSR. After graduating from the Department of Machinery and Equipment of Chemical Plants of the Azerbaijan Institute of Oil and Chemistry (1968), he was directed to work at the Scientific - Research Institute of Applied Physics of the Ministry of Defence of the USSR (currently – Federal State Unitary Enterprise NPO Orion), where he was actively involved with the problems of thermoelectric cooling.

In 1983 he defended his thesis with assignment of the academic degree of the Candidate of Technical Sciences, and in 1988 taking into consideration the totality of scientific papers State Commission for Academic Degrees and Titles of the USSR awarded him the academic title of Senior Researcher in Solid-State Electronics and Microelectronics.

The main areas of research and practical developments of Grigoriy Aramovich Arakelov include creation of high-performance semiconductor infrared photoelectric detectors with their enhanced parameters implemented due to thermoelectric cooling of photosensitive elements; multi-pad photodetectors based on multi-stage thermoelectric coolers which provide under vacuum thermal insulation with minimum power consumption (≤ 8 W) the cooling temperatures of photosensitive elements 180…210 K at ambient temperature 300 K.

For a long period of time as an Academic Advisor (Chief Designer) in the framework of more than 30 research-and-development activities Grigoriy Aramovich Arakelov carried out the development and introduction of photodetectors with thermoelectric coolers into the industry. He validated the theory and practice of optimization of power modes for these devices as part of electrooptical equipment. He took part in the establishment of research and production base of the corresponding branch in the USSR and Russia. He conducted researches of galvanothermomagnetic and magnetothermoelectric coolers, including of cryogenic temperature levels; provided scientific - advisory services; reviewed articles and books; was an official opponent for theses. For many years, he was one of the heads of Narrow-Gap Semiconductors and Photodetectors Section at Scientific Council of the Academy of Sciences of the USSR on the problem of Physics and Chemistry of Semiconductors. Grigoriy Aramovich Arakelov was the author of over 100 scientific publications and more than 20 patents and copyright certificates in Thermoelectric Instrument Engineering.

The International Thermoelectric Academy bewails the death of a prominent scientist Grigoriy Aramovich Arakelov and expresses its condolences to his family members and close ones. His memory will remain forever in the hearts of his friends, colleagues and students.

LEV PETROVICH BULAT

On June 12, 2016, Lev Petrovich Bulat, Doctor of Physics and Mathematics, academician of the International Thermoelectric Academy, died in his 70 th year.

L.P. Bulat was born in 1947 in Chernivtsi (Ukraine). In 1970 he graduated from Chernivtsi State University with specialization in Physics, in 1973 he completed post-graduate course at the same university with a degree in Physics of Semiconductors and Dielectrics. PhD in Physics and Mathematics (1973), DSc in Physics and Mathematics (1989). The academic title of Associate Professor was granted in 1979, Professor - in 1990.

From 1975 to 1989 he worked as an Associate Professor at Lviv Polytechnic Institute; from 1989 to 1994 – as a Professor at Ternopil Instrument-Making Institute. In 1982 he organized Ternopil division of Phonon Design and Technological Bureau and headed it until 1994 and after its reorganization into Ternopil department of Institute of Thermoelectricity of NAS of Ukraine. Since 1994 – professor of St. Petersburg State Academy of Refrigeration and Food Engineering, since 1997 - Head of Electrical Engineering and Electronics Department at St. Petersburg State University of Low-Temperature and Food Technologies.

In 1998 – 1999 he was on academic mission as invited scientist at the Korea Institute of Energy Research (South Korea).

The prime area of research interests - thermoelectric method of direct energy conversion, including thermoelectric cooling; materials science and physics of semiconductors; transport phenomena in solids, including kinetic phenomena in composite materials; measurement of heat fluxes.

He was the author of about 200 scientific papers and inventions. He made more than 150 presentations at international and national scientific conferences, including in the UK, France, Germany, Poland, Czech Republic, Denmark, the USA, Mexico, China, Korea, Japan, and Australia. He was a member of the organizing committees of several international conferences. More than 30 research projects for the needs of machine engineering, aviation, ship building, instrument making, power engineering were conducted under his supervision.

He was the chief designer of a number of research and development works; under his supervision hundreds of prototypes and experimental samples of various products of emerging technology were successfully tested and highly appraised by the customers. His developments were marked by medals of the All-Union Exhibition of Achievements of National Economy and diploma of the All Russia Exhibition Centre.

He developed novel approaches to theoretical research of kinetic phenomena in condensed media under conditions of thermal effects and identified dozens of new effects. He developed a method for measuring heat flux density using high-sensitive thermoelectric converters and applied this method for the development of heat metering devices of medical and biological application, converters for geophysical research, for heat loss control, for non-contact measurement of liquid level, gas pressure in hermetically sealed shells, etc.

Lev Petrovich Bulat was well known to those skilled in the field of thermoelectric energy conversion and enjoyed international authority.

He was the organizer of Alternative Cooling Methods Section at the International Academy of Refrigeration; was academician of this Academy and its Presidium member.

He was academician of the International Thermoelectric Academy; a member of the International Thermoelectric Society; was elected a Bureau member of the Russian Thermoelectric Society. Was a member of the Section for Thermoelectric Conversion of Scientific Board of the Russian Academy of Sciences on a comprehensive problem "Methods for Conversion of Energy Types". Academician of the New York Academy of Sciences, a member of Materials Science Society (USA), a member of EuroScience Society (France); honorary member of the Trusteeship Council of International Biographical Centre (UK).

L.P. Bulat is listed in the "Who's Who of Intellectuals" encyclopedia, ed. by the International Biographical Center, Cambridge, U.K., 1997.

He held courses in "Electrical Engineering", "Fundamentals of Electronics", "Thermoelectric Power Converters", "Selected Divisions of Physics", etc. for students of Saint-Petersburg State University of Low-Temperature and Food Technologies. He was the author and editor of a cycle of training manuals on these courses.

The International Thermoelectric Academy bewails the death of a prominent scientist Lev Petrovich Bulat and expresses its condolences to his family members and close ones. The memory of Lev Petrovich Bulat will remain forever in our hearts.

OLEG BORISOVICH SOKOLOV

On January 22, 2016, Oleg Borisovich Sokolov, a Corresponding Member of the International Thermoelectric Academy, Candidate of technical sciences, died suddenly in his 79 th year.

O.B.Sokolov was born on August 09, 1937 in Moscow. He graduated from the Physics Department of Lomonosov Moscow State University.

He worked as a laboratory assistant at I.V. Stalin Mining Institute, and as an experimental mechanic at the aircraft factory. Since 1964 he was a junior and then senior researcher at Scientific and Production Enterprise "Quant", from 1992 to 1994- Director of Small-Scale Enterprise "Telviks", from 1994 to 1996 - Director of JSC "Telviks", from 1996 until his death he worked as the Director of thermoelectric material production at JSC "Specialized Design Technological Bureau Nord", which was renamed "Ferrotec Nord" in 2011.

The main lines of scientific research and practical developments pursued by O.B. Sokolov include the production of thermoelectric materials by hot extrusion method.

The results of research work conducted by Oleg Borisovich Sokolov allowed the quality of extruded thermoelectric material to be significantly improved, and industrial production process of such materials to be developed and implemented. O.B. Sokolov is the author of many scientific works and patents.

Every time this enthusiastic and talented person put his heart into everything he did.

International Thermoelectric Academy bewails the death of Oleg Borisovich Sokolov. His memory will remain forever in the hearts of all who knew him.

ARTICLE PREPARATION RULES

The article shall conform to the journal profile. The article content shall be legible, concise and have no repetitions.

The article shall be submitted to the editorial board in electronic version.

The text shall be typed in text editor not lower than MS Word 6.0/7.0.

Page setup: "mirror margins"- top margin – 2.5 cm, bottom margin – 2.0 cm, inside – 2.0 cm, outside– 3.0 cm, from the edge to page header – 1.27 cm, page footer – 1.27 cm.

Graphic materials, pictures shall be submitted in color or, as an exception, black and white, in .opj or .cdr formats, .jpg or .tif formats being also permissible. According to author's choice, the tables and partially the text can be also in color.

The article shall be submitted in English on A4 paper sheets; the number of pages shall not exceed 12. By agreement with the editorial board, the number of pages can be increased.

To accelerate publication of the article, please adhere to the following rules:

- the authors' initials and names are arranged in the centre of the first page at the distance of 1 cm from the page header, font Times New Roman, size 12 pt, line spacing 1.2;
- the name of organization, address (street, city, postal code, country) – indent 1 cm below the authors' initials and names, font Times New Roman, size 11 pt, line spacing 1.2, center alignment;
- the title of the article is arranged 1 cm below the name of organization, in capital letters, semi-bold, font New Roman, size 12 pt, line spacing 1.2, center alignment. The title of the article shall be concrete and possibly concise;
- the abstract is arranged 1 cm below the title of the article, font Times New Roman, size 10 pt, in italics, line spacing 1.2 ,center alignment;
- key words are arranged below the abstract, font Times New Roman, size 10 pt, line spacing 1.2, justified alignment. The title "Key words" – font Times New Roman, size 10 pt, semi-bold;
- the main text of the article is arranged 1 cm below the abstract, indent 1 cm, font Times New Roman. size 11 pt, line spacing 1.2, justified alignment;
- formulae are typed in formula editor, fonts Symbol, Times New Roman. Font size is "normal" – 12 pt, "large index" – 7 pt, "small index" – 5 pt, "large symbol" – 18 pt, "small symbol" – 12 pt). The formula is arranged in the text, centre aligned and shall not occupy more than 5/6 of the line width, formulae are numbered in round brackets right;
- dimensions of all quantities used in the article are represented in the International System of Units (SI) with the explication of the symbols employed;
- figures are arranged in the text. The figures and pictures shall be clear and contrast; the plot axes – parallel to sheet edges, thus eliminating possible displacement of angles in scaling;
- tables are arranged in the text. The width of the table shall be 1 cm less than the line width. Above the table its ordinary number is indicated, right alignment. Continuous table numbering throughout the text. The title of the table is arranged below its number, center alignment;
- references should appear at the end of the manuscript. References within the text should be enclosed in square brackets. References should be numbered in order of first appearance in the text. Examples of various reference types are given below.

– L.I. Anatychuk, *Thermoelements and Thermoelectric Devices: Handbook* (Kyiv: Naukova Dumka, 1979), p.766. (Book)
– T.M. Tritt, Thermoelectric Phenomena, Materials, and Applications, *Annual Review of Materials Research* **41**, 433 (2011). (Journal paper)
– U. Ghoshal, *Proceedings of the XXI International Conference on Thermoelectrics* (N.Y., USA, 2002), p. 540. (Proceedings Conference)

The article should be supplemented by:

• letter from the organization where the work was performed or from the authors of the work applying for the publication of the article;

• information on the author (authors): last name and initials; full name and postal address of the institution where the author works; academic degree; position; telephone number; E-mail;

• author's (authors') photo in color or, as an exception, in black and white. With the number of authors more than two their photos are not given;

• author's application to the following effect:

We, the undersigned authors, … transfer to the founders and editors of "Journal of Thermoelectricity" the right to publish the article…in Ukrainian, Russian and English. This is to confirm that the present publication does not violate the copyright of other persons or organizations.

Date Signatures